NTNU
Norwegian University of
Science and Technology

Optimization, Cellular Uptake and Cytotoxicity of Lipid Nanoparticles

Ida Sofie Jorstad

Abstract

Chemotherapy can potentially be greatly improved by using nanoparticles as drug carriers to deliver chemotherapeutic drugs specifically to cancer cells. Lipid nanoparticles can encapsulate hydrophobic drugs that have low solubility in water, and target tumor sites in the body either by active, passive or triggered delivery. In this thesis, nanoparticle stability and size is optimized from an already existing lipid particle formulation that is based on a mixture of solid (stearic acid) and liquid lipid (isopropyl palmitate). Systematic screening of the particle formulation and synthesis process parameters led to the development of a nanostructured lipid carrier particle stabilized by a combination of surfactants, Andean QDP Ultra and Phospholipon 80H. Zetasizer has been used to analyze size and stability of the monodisperse lipid nanoparticles.

In the second part of the project, flow cytometry was used to characterize cellular uptake of fluorescently labeled lipid nanoparticles. It was found that particle degradation extracellularly followed by release of dye and diffusion across the cell membrane is likely the main mechanism of fluorophore uptake. Both rate of uptake found from flow cytometry analysis, and stability analysis from the particle optimization process, indicates lipid particle degradation occuring over a time period of at least 48 hours in a physiological environment.

Lastly, cytotoxicity of lipid nanoparticles and nanoparticle encapsulated kinase inhibitor was investigated *in vitro*. The kinase inhibitor, Gefitinib showed time and concentration dependent cytotoxicity, while the nanoparticles had very high toxicity. Even at concentrations as low as $\approx 15 \mu g/ml$ empty nanoparticles in growth media, the cell viability was less than 80%.

Sammendrag

Dagens cellegiftbehandling kan potensielt forbedres betydelig ved bruk av nanopartikler med innkapslet cellegift som kan levere medisin spesifikt til kreftceller i kroppen. Lipid nanopartikler kan kapsle inn hydrofobe legemidler som har lav løselighet i vann og måltettet levere medikamentet til kreftsvulster, enten ved aktiv/passiv levering eller ved ekstern stimuli. I denne oppgaven har stabilitet og størrelse til lipid nanopartikler blitt optimert fra en allerede eksisterende lipidpartikkel formulering som er basert på en blanding av fast (stearinsyre) og flytende lipid (isopropylpalmitat). En systematisk utvelgelsesprosess av partikkel komponenter og synteseprosessparametre førte til utviklingen av en lipid partikkel stabilisert av en kombinasjon av to surfaktanter, Andean QDP Ultra og Phospholipon 80H. Zetasizer har blitt brukt til å analysere størrelse og stabilitet til monodisperse lipid nanopartikler.

I den andre delen av prosjektet, ble flowcytometri benyttet for å karakterisere cellulært opptak av fluorescensmerkede lipid nanopartikler. Det ble funnet at mulig hovedmekanisme for cellulært opptak av fluorofor er partikkel degradering ekstracellulært etterfulgt av frigjøring av fargestoff og diffusjon gjennom cellemembranen. Både cellulær opptakshastighet funnet fra flowcytometrianalyser, og resultater fra stabilitetsanalyse under partikkeloptimeringsprosessen, indikerer at nanopartikkel nedbrytning strekker seg over et tidsrom på minst 48 timer i et fysiologisk miljø.

Til slutt, cytotoksisitet av lipidpartikler og en nanopartikkel-innkapslet kinase inhibitor ble undersøkt *in vitro*, ved bruk av luminiserende cellevitalitets assay og mikroplate leser. Den inkaplede kinase inhibitoren, Gefitinib, hadde tids- og konsentrasjonsavhengig cytotoksisitet., mens lipidnanopartiklene var meget giftige. Selv ved konsentrasjoner så lave som ≈ 15 μg/ml av tomme nanopartikler i vekstmedium ble cellelevedyktigheten redusert til under 80%.

Preface

This thesis marks the end of a 5 year Master of Science program in Nanotechnology at the Norwegian University of Science and Technology. The last few years I have specialized in bionanotechnology. The work for this thesis has been carried out partly at Sintef Materials and Chemistry, and partly at the Department of Physics, NTNU, spring 2016.

I would like to give special thanks to several people who have helped me throughout this project. First of all, I would like to thank my supervisor, professor Catharina de Lange Davies for giving me the opportunity to work on a project related to nanoparticle mediated drug delivery for cancer therapy. I would also like to thank her for giving me useful suggestions and valuable feedback during the experimental work and writing of this thesis. Secondly I want to thank my co-supervisor professor Wilhelm Glomm for support and guidance throughout my project and masters thesis. I want to express my gratitude for how he has provided invaluable insight into properties of nanoparticles, and their synthesis.

A special thanks to PhD student, Einar Sulheim for training and assistance in the cell lab, as well as for giving me immensely valuable guidance for my experimental work and thesis writing. I would also like to thank research scientist Peter Molesworth at Sintef Materials and Chemistry for providing personal guidance with laboratory work at Sintef, and for always having time to discuss experimental results and share his knowledge in the field.

I want to thank all the participants on the nanoparticle group at biophysics, NTNU. The weekly meetings with discussion have been very helpful and the work environment has made me even more interested in the field. Thanks to Astrid Bjørkøy for assistance and training at the microplate reader and Kristin Grenstad Sæterbø for providing chemicals needed in this project. Lastly I would like to thank Anne Rein Hatletveit for giving me training and helping me getting started with experimental work at Sintef, and the rest of the group at the chemistry lab for always being friendly and helpful.

Ida Sofie Jorstad
Trondheim, June 2016

List of Abbrevations

ATP Adenosine triphosphate

CLSM Confocal laser scanning microscopy

DMEM Dulbecco's Modified Eagle Medium

DLS Dynamic light scattering

ECM Extracellular matrix

EDTA Ethylenediaminetetraacetic acid

EPR Enhanced permeability and retention

FBS Fetal bovine serum

FCM Flow cytometry

FS Forward scattering

IPP Isopropyl palmitate

LA Broth Luria Broth

NLC Nanostructured lipid carriers

NP Nanoparticle

PBS Phosphate-buffered saline

PDI Polydispersity index

PEG Polyethylene glycol

P80H Phospholipon 80H

SA Stearic acid

SD Standard deviation

SDS Sodium dodecyl sulfate

SNL Solid liquid nanoparticles

SOP Standard operating procedure

SS Side scattering

TKI Tyrosine kinase inhibitor

QDP Andrean QDP Ultra

ZP Zetapotential

ZS Zetasizer

Contents

1 Introduction

Cancer is one of the leading causes of death worldwide, the annual amount of new cancer cases is expected to rise about 70% within the next twenty years, according to World Health Organization (WHO) [1].

Treating cancer is a complex matter, as it is not one single disease, but rather a collection of diseases that have uncontrolled and abnormal cell proliferation in common. It arises from cells that through mutations acquire the ability to resist systematic cell regulations and begin growing and proliferating in an uncontrolled manner. These cells are often very similar to healthy cells and are therefore difficult to detect for both the immune system and developed drugs, thus making it difficult to fight the disease. Existing methods of therapy are often insufficient, re-occurring tumors and adverse side effects are common. There is intense research going into developing new methods of treatment. The major drawback of conventional chemotherapy is the systemic distribution of chemotherapeutic drugs, leading to unfavorable effects on healthy tissue. This calls for development of efficient treatments that are selective towards cancer cells.

Nanotechnology has the potential to create novel platforms for diagnosis and treatment of cancer. Biodegradable nanoparticles (NPs) have been studied extensively over the last few decades towards developing drug delivery systems that can potentially reduce drug dose released systemically and increase drug load to cancer cells [2]. Many systems have been proposed, but few have made it through trial stages. The concept of drug delivery is based on encapsulation or binding of pharmaceutical drugs to a nanocarriers that selectively delivers the loading compound at a targeted site in the body, often a tumor. Nanoparticles are known to passively target tumors by exploiting the enhanced permeability- and retention (EPR) effect, leading to accumulation in tumor tissue [3]. Triggered drug release [4] and surface functionalization for enhanced binding affinity (active targeting) [5] are other proposed methods of targeting.

Lipid nanoparticles provide a promising approach for site specific drug delivery and controlled drug release [6]. Lipid NPs are colloidal particles consisting of a biodegradable and biocompatible lipid matrix [6]. The lipid nanoparticles in this project are made through a one-step melt-emulsification process, where hydrophobic contrast agents and/or drugs can be incorporated in the same process. The particles are stabilized by surfactants organized on the lipid particle surface. Many drug candidates with high therapeutic efficiency have poor solubility in water, and

are therefore unsuitable for intravenous administration. By encapsulation of such drugs in lipid nanocarriers, solubility, bioavailability, targeting and absorption can be increased [7]. The lipid nanoparticle system that is evaluated in this project is nanostructured lipid carriers (NLC), which consist of a mixture of solid and liquid lipids [8].

To develop this lipid-based drug delivery platform further, it is important to gain knowledge of how the nanocarriers interact with cells. Many pharmaceutical targets are located intracellularly [9], thus the drugs must consequently be taken up by cells and reach the target to achieve a therapeutic effect. This uptake may occur through endocytosis followed by intracellular release, extracellular release followed by drug diffusion across the plasma membrane, or by contact-mediated transfer of drugs between NPs and the plasma membrane. Other important aspects that needs to be addressed of lipid NP-based drug delivery is particle cytotoxicity and circulation times. An increased understanding of the life cycle and interactions of NPs in a biological environment can result in improved knowledge on how to design a nanocarrier with optimal characteristics.

1.1 Purpose of this project

This thesis is part of a project aiming to develop a drug delivery system based on nanostructured lipid carriers. The work presented has been preformed at Sintef materials and chemistry and at NTNU Department of Physics, and can be divided into three main parts.

The purpose of the first part was further develop an already existing synthesis protocol for a lipid-based nanocarrier system, developed at Sintef. The goal was to find a formulation that would lead to particle improvements in terms of size and stability, making it better suited for drug delivery applications. In the second part, the motivation was to evaluate the cellular uptake of fluorescently labeled lipid NPs in human cancer cells, to get a better understanding of the fate of the NPs, uptake mechanisms and the interactions between nanocarriers and cells. Lastly, cytotoxicity of lipid NPs and a chemotherapeutic drug encapsulated in nanocarriers was to be analyzed *in vitro*.

2 Theory

In this project, lipid nanoparticles are developed with improved stability and size characteristics from an already existing lipid nanocarrier system. In addition, cellular uptake and cytotoxic effect of fluorophore/drug loaded nanoparticles are measured *in vitro*. In order to understand the results obtained from the experiments performed in this project, this section presents a basic introduction to cancer, treatments of cancer using nanocarriers, uptake of nanoparticles in cells, lipid nanoparticle composition and stability, as well as instruments and measurement techniques. This master's thesis has similarities in topic with my 5th year project thesis [10] written in the fall 2015, some of the theory has been adapted from that thesis.

2.1 Cancer

Cancer is collection of diseases, characterized by one or several uncontrolled, growing masses of cells that are capable of spreading throughout the body and can in many cases be life threatening. When cancer develops, old or damaged cells, that normally would die, can survive and new unneeded cells are formed. The resulting growing accumulation of cells is called a tumor ([11], ch.24). Cancerous tumors are malignant, meaning they can spread to other parts of the body through a process called metastasis. During metastasis, cells detach from the tumor and invade circulatory systems, allowing the cancer cells to reach distant tissues. Benign tumors on the other hand, grow in a confined area, do not spread to other tissues and are rarely dangerous.

Cancer cells differ from normal cells in many ways that allows them to grow uncontrolled and invade other tissues. In general, cancer cells are less specialized than normal cells, this is one of the reasons why cancer cells continue to divide whereas normal cells mature into distinct types of cells with specific functions. In addition, cancer cells are often able to evade the body's immune system. Normally, damaged, infected and dead cells are removed, but cancer cells are often able to "hide" from the immune system.

Cancer is a genetic disease, caused by changes to genes that are involved signaling pathways and control mechanisms for cell division and death ([11], ch.24). Genetic changes responsible for cancer can be inherited from our parents, or they can arise throughout a persons lifetime. Cell cycle controls do not function properly in cancer

cells, the cells do not respond appropriately to external or internal signals involved in cell cycle regulation. In addition, cancer cells have various ways of blocking signals that normally lead to apoptosis. By these mechanisms, cancer cells proliferate and survive under conditions that normal cells would not.

2.1.1 Cell cycle

A major difference between normal cells and cancer cells is the response to signals related to the cell cycle. The cell cycle are the stages involved in preparation and carrying out cell division. The cycle begins when two new cells are formed from the division of one parental cell, and ends when one of the new cells divide and give rise to another two cells ([11], ch.19).

The two main phases of the cell cycle is the M phase and the interphase. The M phase is the division phase, involving mitosis and cytokinesis where the nucleus divides first followed by the cytoplasm dividing the cell into two daughter cells. The growth phase in between cell divisions is the interphase, the events of the interphase accounts for a large portion of the total cell cycle. Cellular contents are synthesized during this phase. During cell division, each new daughter cell is left with one copy of each chromosome. Before the cells can divide again, the genetic material must be copied. This happens during the S phase of the interphase. The S phase is separated from the preceding M phase by time period called G_1, and from the next cell division by a time period called G_2 ([11], ch.19).

During G_1 the there is a checkpoint at which it is determined whether and when the cell should divide again. Cells that get arrested in G_1 enters state called G_0, where they await a signal to reenter the cell cycle and prepare for cell division. In animal cells, to pass the restriction point G_1, the cell must receive extracellular signals in the form of stimulating growth factors to proceed in the cell cycle. Other cells exit the cell cycle entirely and undergo terminal differentiation, meaning they are mature specialized cells that never will divide again [[11], ch.19]. For some cell types, a second arrest of the cell cycle can occur in G_2. These regulatory mechanisms makes sure the requirements of cells are met and prevent unneeded cells from forming. Cell cycle regulation mechanisms are interesting, not only to understand the behavior of different cell types, but also to understand how cancer can arise by escaping these control mechanisms.

2.1.2 Epidermal growth factor receptors and inhibitors

Tyrosine kinases are a family of enzymes that catalyzes phosphorylation of tyrosine residues of different proteins in the cell, using adenosine triphosphate (ATP) [12]. Tyrosine kinases are important mediators in different cellular signaling pathways involved in cell differentiation, apoptosis, metabolism and growth [12]. In normal cells, signaling pathways implicating tyrosine kinases can for example contribute to sensitivity towards apoptotic stimuli or be involved in preventing deregulated proliferation. These signaling pathways are have often been genetically altered in cancer cells [12].

One branch of the tyrosine kinase family is the receptor tyrosine kinase (RTK), which serves as a transmembrane cell surface receptor in addition to having enzymatic activity. The RTKs have an extracellular binding site for hormones, cytokines and growth factors, and an intracellular part involved in further downstream signaling [13].

The epidermal growth factor receptor (EGFR) is one type of RTK, it belongs to the ErbB family of receptor tyrosine kinases [14]. These receptors are activated by extracellular binding of peptide growth factors from the protein family of epidermal growth factors (EGF). Extracellular ligand binding induces dimerization of the transmembrane receptors, activating the intracellular parts of the kinases. Binding of ATP and autophosphorylation of intracellular parts of the receptors triggers further intracellular actions.

Mutations in the genes encoding tyrosine kinase receptors may lead to disturbance in the kinase activity. An example of this is overactive tyrosine kinases, which may lead to abnormal cell growth and eventually development of tumors. EGFR is involved in cell proliferation, and has been shown to be overexpressed in many types of cancer [14].

Inhibition of EGFRs is therefore a possible approach to inhibit abnormal cell growth and thereby development of tumors. This makes EGFRs targets of anti-cancer drugs [15]. There are several EGFR inhibitors already on the market, or in clinical trials [16].

The two main type of EGFR inhibitors, low molecular weight tyrosine kinase inhibitors (TKIs) and monoclonal antibodies, differ in binding site of the drug. TKIs usually act by diffusing through the cell membrane and binding to the intracellular kinase part of the receptor, blocking the binding site of ATP, while monoclonal antibodies block the extracellular binding site of the ligand [16] [17]. Both types of inhibitors prevent further downstream signaling from EGFRs.
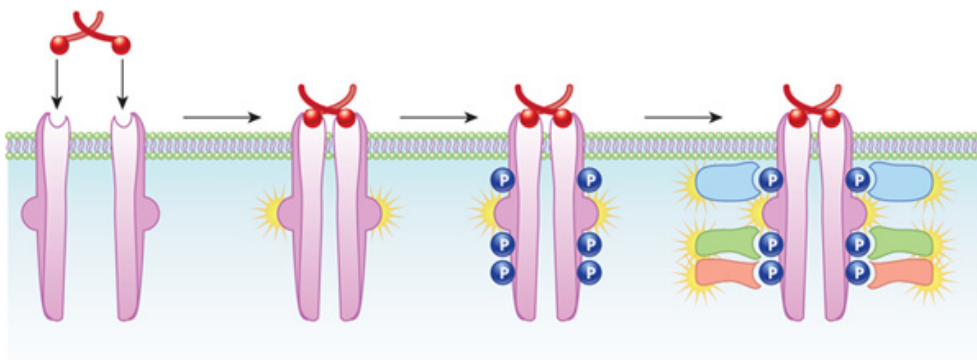
Figure 1: *Schematic of the activation of a receptor tyrosine kinase, including ligand binding, dimerizaton, autophosphorylation and activating internal signaling molecules [18]*

.

The TKIs used in this project are all low molecular weight tyrosine kinase inhibitors. Erlotinib (Tarceva®), Gefitinib (Iressa®) and Lapatinib (Tykerb®) are examples of commercially available low molecular weight TKIs [16], these were also used in this project. Erlotinib and Gefitinib are used for treatment of non- small cell lung cancer, while Lapatinib is used against breast cancer [19] [20] [21]. In addition to these three compounds, two other TKIs, that have been developed at the Department og Chemistry at NTNU, were used in this project. The chemical structure of all five compounds is shown in figure 2.

Development of new inhibitors is needed due to limitations of existing TKIs and to obtain a stronger platform for handling complex treatment issues [16]. Typical limitations to the existing TKIs are development of resistance towards the drug due to mutations in tumor cells, and lack of tumor response [16]. Cancer cells and cell growth is not only dependent on one signaling pathway, thus restraining growth might require a combination of treatments or multi-target drugs [22].

(a) *Erlotinib*

(b) *Gefitinib*

(c) *Lapatinib*

(d) *SB6-140-06 (BS-BL)*

(e) *JH08-096*
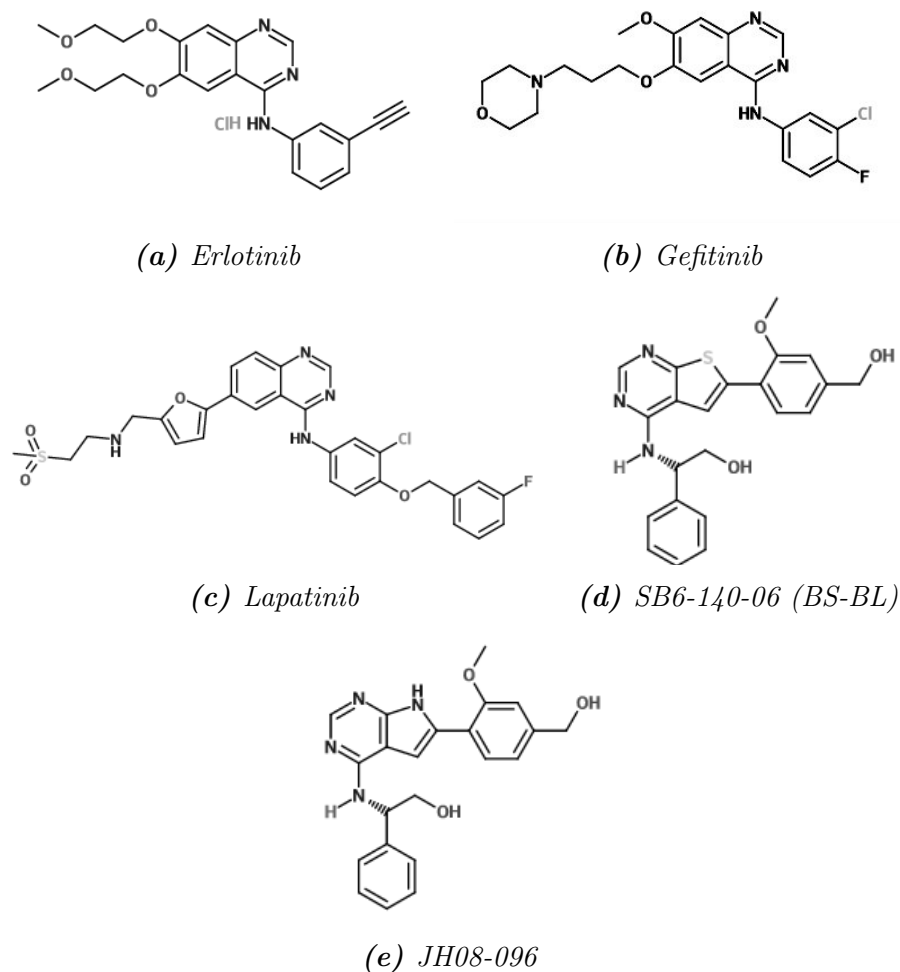
Figure 2: *Chemical structure of tyrosine kinase inhibitors used in this project. a-c) are comercially available d-e) have been developed at the Department of Chemistry, NTNU*

2.1.3 Cancer treatments

The most common types of cancer treatment are chemotherapy, surgery and radiation therapy. Often, a combination of these techniques are used to treat cancer. Chemotherapy involves the use of chemical substances to damage or stress cells, and it is most commonly used for metastasized tumors. Most chemotherapeutic drugs are cytotoxic and function by killing cells with high proliferation rate. Unfortunately, not only cancer cells grow and divide rapidly, some healthy cell types like cells in the bone marrow or hair follicles also have a high rate of proliferation. This means healthy cells are also affected by the cytotoxic drugs, and this causes side effects like hair loss and fatigue.

Surgery is often an efficient treatment method for tumors that have not spread, and are located at a superficial area. When tumors are very complex or located at areas

that are difficult to reach without endangering the health of the patient, like e.g. brain tumors, surgery can not be performed as the risks of complications are too high. In such complicated cases, radiation therapy is often used. Radiation is used to shrink or completely remove tumors. By applying radiation towards a tumor, the DNA of the cancer cells is damaged, leading to cell death [23]. The biggest disadvantage of radiation therapy is the risk of damaging healthy tissue surrounding the tumor. This is avoided to some extent by aiming the radiation beams from several different angles so that only the tumor area receives a high dose of exposure. Unfortunately, reoccurring tumors are common after radiation therapy [24].

Even with the treatments mentioned here and several other methods used today, cancer is still difficult to treat in many cases. The treatments often yield limited results and/or cause severe side-effects. With conventional chemotherapy, chemotherapeutic agents are distributed non-specifically throughout the body affecting not only tumor cells, but also healthy tissue. The dose actually ending up in tumor tissue no more than approximately 0.01-0.1% [25] [26]. Tissue selectivity is therefore a major topic in cancer therapy research. There is a need for development of cancer therapies that can fight cancer with more precision and potentially cause fewer side effects than the standard options. Examples of newer treatment regimes are immunotherapy and targeted cancer therapy. Immunotherapy involves using the body's own immune system to fight cancer, while targeted cancer therapy uses drugs or other substances to more precisely identify and attack cancer cells, without harming healthy tissue.

2.1.4 Tumor biology and the enhanced permability- and retention effect

Like all other cells, cancer cells need nutrients to grow and divide. A tumor mass receives necessary nutrients through passive diffusion, up until the size of the tumor reach about 2mm^3 [27]. At this point, new blood vessels must form for the tumor to continue to grow (angiogenesis). Angiogenesis is the process in which new blood vessels are formed from pre-existing ones [28]. Tumor angiogenesis is an important step in the development of tumors from a benign to a malignant state [28]. The new-formed tumor blood vessels develop rapidly and become abnormal in shape and branching [27] [28]. The vessels are leaky and tortuous, with much larger gaps (200nm-1.2μm) between endothelial cells than in healthy vessels (5-10nm) [29]. Because of these tumor tissue- and vessel characteristics, drug delivery systems can be designed to passively target tumor areas with drug carriers. This can be done by exploiting the Enhanced Permeability and Retention effect (EPR-effect). The

EPR-effect is an increase in permeability and ineffective lymphatic drainage occurring in solid tumors. The phenomenon leads to enhanced retention of nanoparticles in tumor tissue as the tumors are not able to eliminate extravasated nanoparticles, due to lack of functioning lymphatics and thus fluid retention [30]. Molecules of a certain size therefore tend to accumulate in tumor tissue due to the combined anatomical and physiological properties of tumor tissue and vessels [3]. This phenomena does not occur in healthy tissue, meaning that nanoparticles encapsulating drugs can passively target solid tumors.

However there are some problems related to exploitation of the EPR-effect for drug delivery purposes. Nanoparticles tend to accumulate around the leaky blood vessels, and are not distributed evenly throughout the tumor tissue due to high interstitial fluid pressure in tumors [31]. An other obstacle is low blood flow in immature vascular networks, making solid tumors less accessible for nanoparticle accumulation, and therefore making it difficult to obtain high enough concentration of NPs and drugs [32].

Non-tumor related obstacles

Getting drug-carrying nanoparticles to the targeted area intact, and at a high enough concentration to have therapeutic effect is challenging. When intravenously administered, nanoparticles may be recognized by the immune system and be cleared from the circulatory system by phagocytes. Both particle size and hydrophobicity are important factors in determining the level of opsonins (blood proteins) that binds to the particle surface and lead to clearance by phagocytes [2].

Once the nanoparticle leave the circulatory system, the extracellular matrix (ECM) presents challenges for transport of drugs into tumor tissue. The ECM is a structural network of molecules, fibrous proteins and highly viscous fluids.

Many chemotherapeutic drugs must enter the cells to function. Internalization of NPs encapsulating drugs often occur by endocytosis which renders the nanoparticle inaccessible for the cytoplasm. If the endocytotic vessels enters the endolysosomal pathway the drug must withstand the low pH inside the vesicle, ranging from 5 to 7.4 [33]. Only if the early endosome bursts, the nanoparticles will enter the cytoplasm, where the drug needs to be released in order to have an effect [33].

2.1.5 Nanoparticles and cancer targeting

As mentioned in the previous section, there is a demand for development of tumor-selective drug delivery in order to avoid systemic side-effects as a consequence of chemotherapeutic drugs affecting healthy tissue. Targeted therapy is a relatively new branch within cancer therapy, where therapeutic agents interfere specifically with cancer cells. In traditional chemotherapy, a large problem is the effect the cytotoxic drugs have on healthy rapidly dividing cells. The dose in the tumor cells, and thereby the therapeutic effect, is restricted by these side-effects. By encapsulation of the chemotherapeutic agent in nanoparticles targeted for solid tumors, side-effects can be reduced, as can the total dose due to the increased concentration of particles in tumor tissues.

A drug delivery system is in short a formulation or device that enables introduction of a pharmaceutical compound in the body, safely transports the drug and delivers it in a controlled way to a target site in the body for local pharmaceutical action. In this project, the system consist of a lipid carrier structure that encapsulates a chemotherapeutic drug, and potentially can transport and release the drug at the site solid tumors for cancer treatment. During transportation, it is important for the drug-carrying system to avoid clearance by the immune system and to be stable enough to reach the targeted area before degradation starts. The goal of targeted drug delivery is to deliver medication to specific areas of the body and obtain a higher dosage of medication there relative to other areas. Besides targeting, drug-carriers can also be used to deliver substances that are not suitable for traditional chemotherapy due to adverse side-effects, poor solubility in water etc.

The three main groups of targeting strategies are passive targeting, active targeting and triggered drug delivery. In passive targeting, the physiological and anatomical characteristics of tumor tissue and vessels are exploited for particle accumulation in tumor tissue (EPR-effect, see section 2.1.4). Due to the low-effectiveness of the process, NPs must have long circulation time to achieve a high enough concentration in the tumor tissue before they start to degrade. In the case of active targeting, nanocarriers have a functionalized surface with molecules that binds specifically to cancer cells. Lastly, triggered drug delivery uses external stimuli to either direct the NPs to the right area, or to trigger the release of drugs from nanocarriers. This stimuli can be a change in the local environment, like pH or temperature, or it may be an external signal like ultrasound or a magnetic field.

2.2 Nanoparticles as drug delivery systems

NPs are small enough to travel into capillaries, and diffuse through the walls of tumor blood vessels, but are too big to diffuse across endothelial layers in healthy blood vessels. How well NPs travel through the extracellular matrix when diffusing from the blood vessels, towards cancer cells depends on properties like charge and pegylation (pegylation is presented section 2.2.3). The actual uptake of particles in cells varies with different types of particles. Some particles are actively taken up through endocytosis, while others are not taken up at all. NPs may degrade or be leaky outside the cells leading to release of drugs followed by diffusion into cells, or they can engage in contact-mediated transfer of drugs into the cells [34]. The topic of cellular uptake of drugs and/or NPs will be further introduced in section 2.3.

The particles used for drug delivery are usually solid spherical structures in the size range of 50-200nm in diameter [30]. Due to the high surface to volume ratio, NPs show improved biodistribution of chemotherapeutic agents, and minimize toxicity to the rest of the body by accumulating at the target site [35].The physical and chemical properties of NPs can be varied significantly by surface functionalization. The nanocarrier must be biocompatible, meaning it should not be taken up by phagocytes of the immune system, and the particle should not be toxic. An other aspect of biocompatibility is that particles should be degraded or removed by the kidneys to avoid accumulation in the body [36].

Medication that can not be used in traditional chemotherapy due to hydrophobic properties or harmful side-effects may be encapsulated in nanocarriers and used for cancer therapy [35]. In addition, the carrier structure may protect medication and thereby increase its stability intravenously. The circulation time of the nanoparticles should be high enough for the particles to accumulate at the targeted site before degradation starts.

The drug may be dispersed throughout the particle, entrapped inside one or several local cavities of the particles, or be attached the to particle surface [30]. A wide range of NPs have been developed, with differences in size, shape, composition, surface chemistry etc., some of which have been approved by the Food and Drug Administration (FDA) for use in humans, while others are currently undergoing clinical trials [37].

Some of the most common groups of nanocarriers are micelles, emulsions, liposomes, polymeric nanoparticles and solid lipid nanoparticles.

2.2.1 Lipid-based nanocarriers

An essential factor for drug delivery vehicles pertains to low toxicity of the carrier itself, both *in vivo* and in the environment as a by-product. Therefore, nanocarriers consisting of natural biomolecules such as lipids and proteins have gained a lot of interest [38]. Limitations of poorly water soluble drugs may be reduced by encapsulation in lipid nanocarriers [39]. Lipid carriers have potential applications within cosmetics, research, drug delivery etc, and are generally easy to prepare, nontoxic and biodegradable [40] [41]. Common disadvantages for many types of lipid nanoparticles are tendency to gelate, unfavorable polymorphic transitions, and lipid particle growth [41]. The particles used in this project are based on lipids.

Liposomes

Among many variations of lipid carriers, liposomes are the most common. Liposomes are closed vesicular structures composed of amphipathic phospholipids forming a bilayer [39]. Due to the alternating hydrophilic and hydrophobic structure of liposomes, they have the ability to enclose compounds of different solubility. In addition, liposomes offer versatility in chemical and physical properties by modification of the simple structure [39]. The surface can be functionalized with polyethylene glycol (PEG) to avoid being removed by the immune system and to maintain steric stability [42]. A great deal of liposomal formulations are already in clinical applications, and more are coming with many in clinical trials [43]. A common drawback with liposomal formulations is low stability under physiological conditions leading to uncontrollable drug release [44].
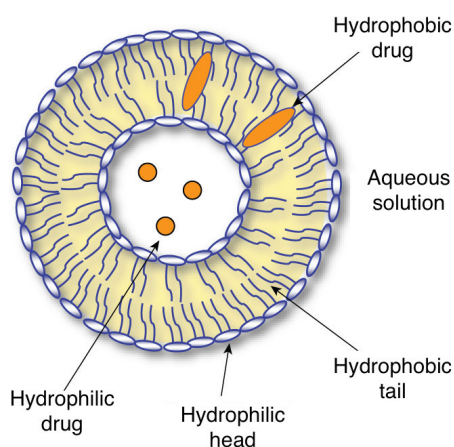
Figure 3: *The figure illustrates a model liposome nanocarrier for drug delivery. [45]*

Solid lipid nanoparticles

Solid lipid nanoparticles (SLN) has over the years emerged as an alternative system to more traditional carriers like emulsions, liposomes and polymeric nanoparticles [46]. SLNs offer incorporation of hydrophobic drugs, increased drug release control, stability and targeting efficiency [41] [39]. Compared to polymeric nanoparticles, solid lipid based nanoparticles posses some important advantages, such as low toxicity due to use of non-toxic system components, inexpensive materials, and easier scale-up of production with the simple synthesis process of high pressure homogenization [47]. SLNs are composed of one or several solid lipids dispersed in an aqueous surfactant solution [46]. Some common disadvantages of SLNs are low drug loading capacity due to the crystalline structure, particle growth and drug expulsion after recrystallization during storage [46] [39]. A wide range of SLNs have been developed with variations in composition.
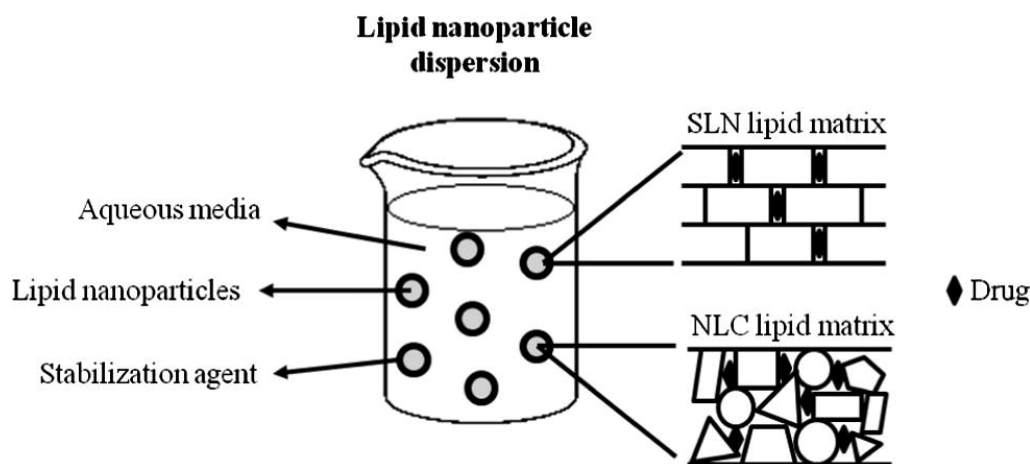
Figure 4: *The figure illustrates the two types of lipid nanoparticles, solid lipid nanoparticles (SLN) and nanostructured lipid carriers (NLC). They differ in composition and structure of the lipid matrix. SLNs has a crystal structure of one or more solid lipids, while NLCs consist of a mixture of solid and liquid lipids giving more room for drug accomodation. Both particle types have a stabilization agent at the interface of the aqueous media and the lipid core. [48].*

Nanostructured lipid carriers

The nanoparticles used in this project falls under the category of nanostructured lipid carriers (NLC). NLCs were developed as a modification of SLNs to potentially overcome difficulties with low loading capacity and to prevent drug expulsion [41]. The particle matrix of NLCs consists of a blend of solid and liquid lipids. The matrix of NLCs is less ordered than SLNs, this property typically improves drug load capacity and stability [41]. In addition, the less ordered structure leads to reduced/avoided drug expulsion [41]. The conventional method of NLC synthesis

involves mixing of solid lipid(s) and oil(s), resulting in a matrix that is still solid at body temperature, but shows melting point depression compared to the original solid lipid(s) [39].

2.2.2 Emulsions

The lipid nanoparticles used in this project were all produced through a miniemulsion process. An emulsion is a mixture of two (or more) immiscible liquids, where one of the liquids is dispersed in the other as micro or nanosized droplets [49]. The system is stabilized by a third component, a surfactant.

A pure mixture of immiscible liquids will separate into distinct phases to minimize the interface between the liquids. When a surfactant is added to the mixture, it will organize itself at the interface, and reduce the surface tension due to its amphiphilic nature. With the surfactant present in the solution, the system can be mixed into an emulsion where one of the liquids is dispersed in a continuous phase of the other liquid. The hydrophilic head of the surfactant will be situated in the water, while the hydrophobic tail will be situated in the oil phase. Even with the surfactant stabilizing the system, over time the emulsion will separate back into distinct phases of each liquid.
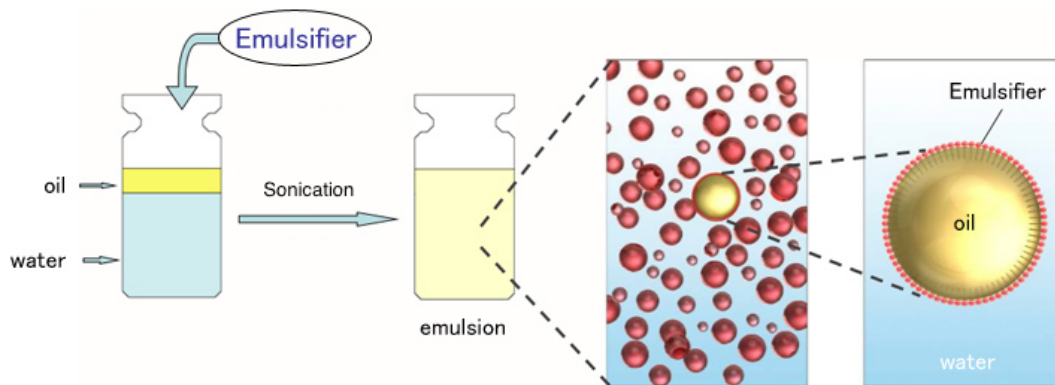
Figure 5: *The figure illustrates an emulsification process, where sonication is used to create micro/nano-sized oil droplets stabilized by emulsifier/surfactant at the oil-water interface. In this project, a solid lipid is used in addition to a liquid lipid in the oil phase. Figure adapted from [50].*

Drugs, dye or other materials to be incorporated in the lipid nanoparticles, are solubilized in the oil phase before the two phases are mixed. By applying a high frequency ultrasonic field to the solution, the oil droplets will split into smaller ones and droplet size will be reduced to the nanometer range. At this point, the mixture is a nanoemulsion where the droplets have an oily core of lipids and loading

material, and an outer layer of surfactants. During sonication, the oil droplet area increases rapidly. There must be excessive surfactant in the solution as the process of surfactant covering new surfaces competes with agglomeration of uncovered lipid surfaces [51].

2.2.3 Particle stability

One of the main issues in the search of new nanoparticles for drug delivery is developing particles with optimal stability, both in terms of shelf-life and circulation time in biological systems [52].

During storage, lipid nanoparticles are subject to several destabilizing mechanisms, such as aggregation and Ostwald ripening. Ostwald ripening is a phenomena in which larger particles grow on the expense of smaller ones in order to reach a thermodynamically more favorable state. Aggregation is simply clustering of particles. These destabilizing mechanisms must be avoided to keep the particle size stable, and maintain functionality and safety of the drug delivery system. Too large particles can block capillaries ($>5\mu$m), resulting in particles not even reaching the targeted area [53]. Degradation of large particles may lead to drug leakage leading to harmful effects on healthy cells [53].

In solution, charged particles are mainly affected by electrostatic repulsive forces, and attractive Van der Waals forces [54]. This is a dynamic interaction due to Brownian motion. Particles of the same charge will repel each other, but for particles in solution the net charge at the particle surface is screened by ions of the opposite charge in the surrounding media. An electric double layer is built up on the particle surface. The inner layer, called the Stern layer, consist of immobilized ions. In the outer layer, the ions are less firmly associated [54]. The effective surface potential also called zeta potential is measured at the surface of the outer layer, the slipping plane. A high zeta potential generally indicates stable particles. In biological environments, particles are exposed to various proteins and high concentrations of electrolytes. The electric double layer surrounding the particles will be reduced due to the high electrolyte concentration. Proteins and other substances can therefore come closer to the particle surface [55]. Proteins adsorbing to the particle surface may change several properties of the NP, such as size, shape and surface properties. Some blood proteins are part of the innate immune system, and can by adsorbing to NP surface facilitate particle recognition by phagocytes of the immune system [55].
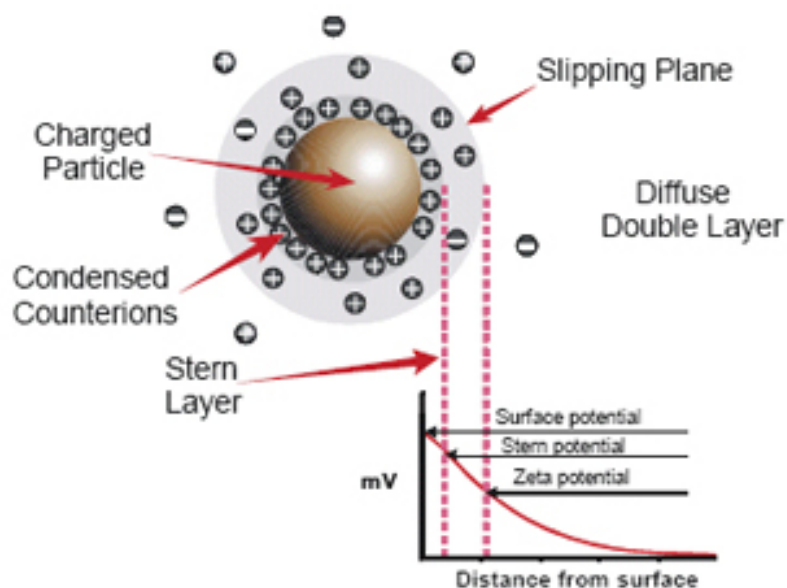
Figure 6: *Illustration of the elctric double layer on a particle with negative surface charge in dispersion medium. Adapted from [56]*

Steric stability can be significantly improved for lipid nanoparticles by coating the particle surface with steric stabilizers, known as stealth agents [57]. Particle properties like size, charge and hydrophobicity are important factors in the recognition of nanoparticles by phagocytes of the immune system. To decrease hydrophobicity, and thus increase circulation time of the particles, stealth agents such as polyethylene glycol (PEG) are used for surface coating [57]. The PEG chain is usually part of a molecule that also has a non-polar part, making the molecule amphipathic so it will organize on the particle surface and act as a surfactant.

In addition to providing steric hindrance, coating with PEG increases particle biocompatibility. Pegylation is important to avoid protein adsorption to particle surfaces, thus reducing particle uptake by phagocytes of the immune system [55].
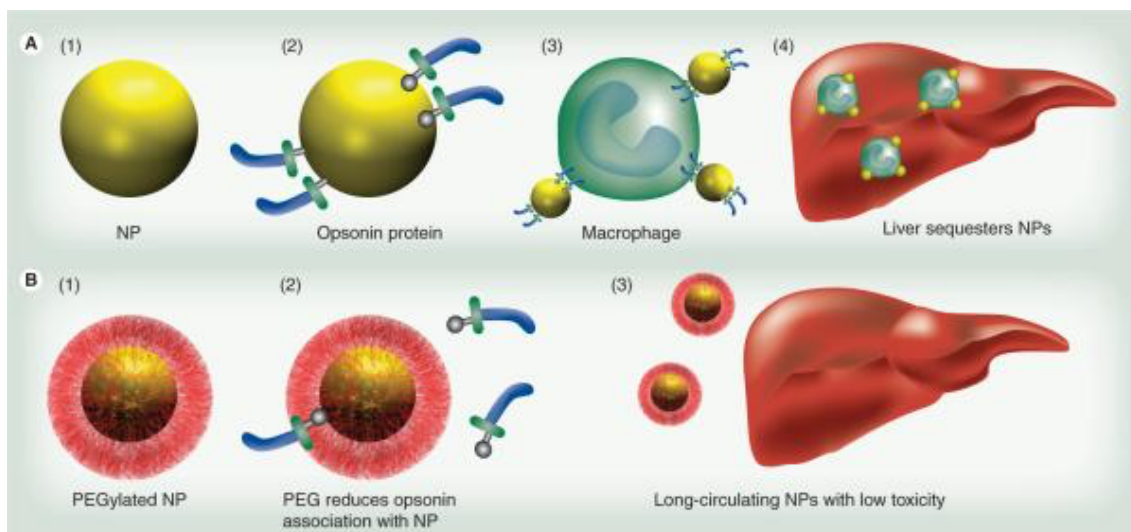
Figure 7: *The figure illustrates how pegylation of NP prevent uptake by the reticuloendothelial system. In A(1-4) NP without PEG are coated with opsonin protein, taken up by macrophages, and transported to the liver. In B(1-3) NPs coated with PEG are prevented from opsonization and liver accumulation [55]*

2.3 Cellular uptake of nanoparticles

For a drug to have a biochemical reaction leading to a therapeutic effect, it must reach its target. Molecular targets of chemotherapeutic agents are typically located inside cancer cells. This means that either nanoparticles must cross the cell membrane and release the drug inside the cell, or the drug must be released from the particles outside the cell and cross the cell membrane. It is essential to understand the mechanism of drug delivery to optimize nanoparticle properties in terms of release profile, circulation time etc.

The release of drugs from lipid nanoparticles has been poorly studied at the cellular level. Possible mechanisms of drug delivery that do not require cellular uptake of nanoparticles are: release of drugs outside the cell followed by diffusion of across the membrane, and contact-mediated transfer of drugs [34].

The mechanism of drug delivery for some nanocarrier systems is release of drugs outside the target cell membrane, followed by diffusion across the plasma membrane directly into the cytoplasm. The process of release of drug/dye from the lipid carrier may employ various mechanisms such as burst release, matrix swelling, particle degradation [34]. Solute diffusion is highly dependent on size, polarity and charge, and is a relevant means of transport only for small, relatively non-polar molecules. Diffusion is movement toward equilibrium, and is a spontaneous, passive transport mechanism.

Contact-mediated drug delivery is a unique mechanism for transferring highly hydrophobic agents from nanoparticle carriers to cells [58] [59]. The mechanism is dependent on close apposition between the carrier and the targeted cell membrane. It involves particle binding to the cell surface, and it is highly dependent on the particle composition and properties. Drugs/dye along with other nanoparticle lipid components are transferred directly into the cytoplasm of the target cell [58] [60] [61]. This is a relatively rapid process compared to e.g. diffusion [34] [62].

The nanoparticles are too large to cross the cell membrane by passive transport, such as simple diffusion. Uptake of nanoparticles occurs by mechanism of endocytosis, which is a form of active transport where the cell membrane internalizes molecules by forming a vesicle around them. The two main categories of endocytosis is phagocytosis and pinocytosis. Phagocytosis is mainly performed by specialized cells of the immune system to internalize and degrade bacteria and damaged cells. Pinocytosis occurs in all cell types and is mainly used for uptake of extracellular fluids [11]. Pinocytosis can be divided into four different uptake mechanisms; clathrin-mediated endocytosis (CME), caveolae-mediated endocytosis (CvME), macropinocytosis and

other clathrin- and caveolae-independent mechanisms [11]. The two most common mechanisms, CME and CvME will be explained in detail here, as they will be studied as possible uptake mechanisms of lipid nanoparticles in this project.
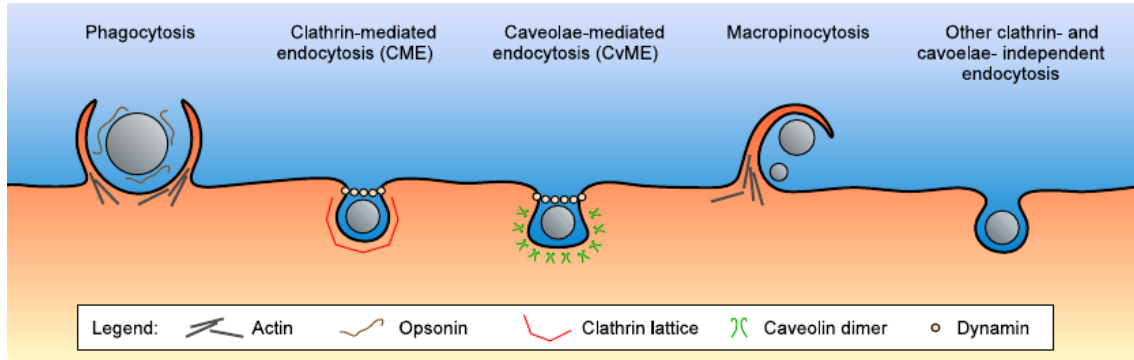
Figure 8: *The illustration shows the principal pathways of endocytosis. The two main groups of endocytosis is phagocytosis and pinocytosis. Pinocytosis is further subdivided into clathrin-mediated endocytosis, caveolae-mediated endocytosis, macropinocytosis and other mechanisms independent of clathrin and caveolae. Figure adapted from [63].*

Clathrin-mediated endocytosis

Clathrin-mediated endocytosis, also called receptor-mediated endocytosis, is the primary mechanism for specific internalization of macromolecules [11]. To initiate this process, ligands bind to specific receptors located on the outer surface of the plasma membrane. The receptor-ligand complex diffuse to membrane regions called coated pits, where there is an accumulation of such complexes. Invagination of the plasma membrane is facilitated by adaptor protein, clathrin and dynamin on the cytosolic side of the membrane [11]. Eventually a vesicle will be formed and pinched of the plasma membrane.

Clathrin-independent endocytosis

The two most important types of clathrin independent endocytosis is caveolin mediated endocytosis and macropinocytosis.
Caveolin mediated endocytosis, is the second most common process of pinocytosis. Invaginations in the plasma membrane are formed due to oligomerization of the coat protein caveolin [64]. Oligomerization leads to local caveolin-rich areas on the cytosolic side of the plasma membrane. The resulting invaginations called caveolae, eventually turn into caveolin coated flask-shaped vesicles that are pinched off the membrane by dynamin 2 proteins [64]. Once internalized, caveolar vesicles are

mainly directed to the ER and Golgi complex [64].

Macropinocytosis is called cell drinking, as it is a mechanism cells use to internalize large volumes of extracellular fluid, as well as any material present in the fluid. The uptake mechanism is based on cell surface lamellipodia extending out of the plasma membrane, bending and sealing back onto the membrane, forming vesicles called macropinosomes [65]. This mechanism is not selective, and does therefore not depend on stimuli from the internalized material.

Endocytosis inhibitors

To study what mechanisms are involved in cellular uptake of drug/dye/NPs, different pathways of endocytosis can be selectively inhibited. This can be done by blocking specific steps of the various vesicle formation processes.

For caveolin-mediated endocytosis, a tyrosine-kinase inhibitor, Genistein, can be used to cause local disruption of the actin network positioned at the site of endocytosis. In addition genistein inhibits recruitment of dynamin 2 to the site of uptake. Both actin network and dynamin 2 are crucial for caveolin-mediated endocytosis [66].

Chlorpromazine is an inhibitor for formation of clathrin-coated pits, and thus an inhibitor of clathrin-mediated endocytosis [66]. Chlorpromazine is believed to inhibit by reversible translocation of clathrin and adaptors from the plasma membrane to vesicles [66].

All forms of endocytosis can be blocked by cultivating cell samples at 4°C [67].

2.4 Instruments

In order to understand and be able to interpret the results, one must know how measurements are performed and understand the basic principles of experimental techniques. A short introduction to the instruments used in this project is presented here.

2.4.1 Dynamic Light Scattering (DLS)

DLS is a technique that is used for analyzing particles in the size range of a few nanometers to several microns. In this thesis DLS was used to determine average particle size and polydispersity index for particles suspended in a liquid. The technical instrument, used for this project, employing DLS is called a Zetasizer (ZS) nano particle analyzer. It can be used to perform measurement within a wide range of concentrations and temperatures for molecules and particles in a liquid medium [68]. When nano-sized particles suspended in a liquid medium are hit with laser light, Rayleigh scattering occurs. Rayleigh scattering is the elastic scattering of light by particles that have much smaller diameter than the wavelength of the radiation [69]. Measurements of fluctuations in the scattered light can be analyzed to determine particle size. Smaller particles lead to more fluctuations in intensity than larger particles, see figure 9.
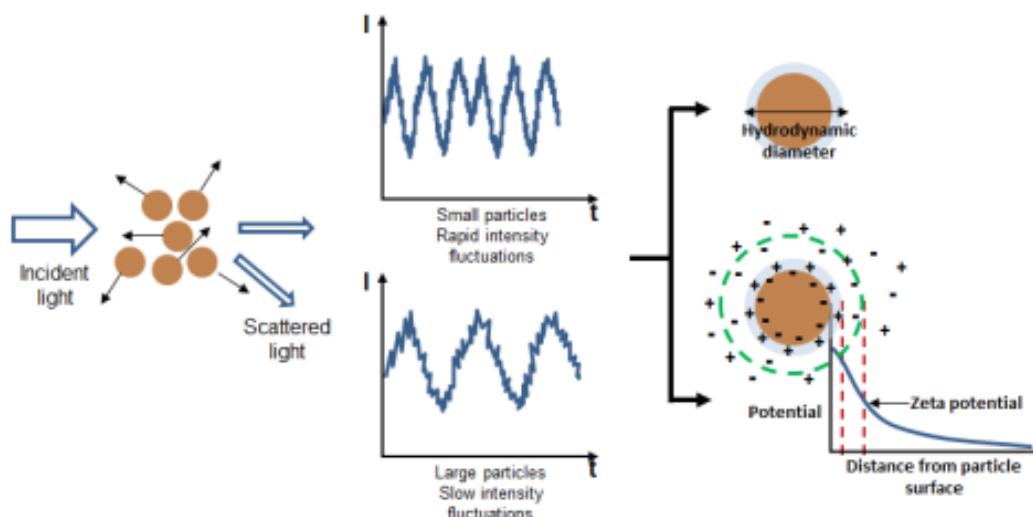
Figure 9: *Dynamic light scattering (DLS) prinicle (left) and measurement of zetapotential using DLS (right). Image adapted from [70]*

.

The intensity I of the scattered light is dependent on particle diameter d, refractive index n, wavelength of laser light λ, and initial light intensity I_0, and it is given by equation 1 [71].

$$I = I_0 \frac{1 + cos^2\theta}{2R^2} \left(\frac{2\pi}{\lambda}\right)^4 \left(\frac{n^2 - 1}{n^2 + 2}\right)^2 \left(\frac{d}{2}\right)^6 \tag{1}$$

The measured scattering intensity is based on the average scattered light from the sample, and not from single particles. The intensity of Rayleigh scattered light is proportional to the sixth power of the particle diameter, as seen in equation 1, the determination of average particle size is therefore greatly affected by the presence of larger particles or aggregates. For this reason, it is essential that the particle suspension is relatively monodisperse, to obtain trustworthy results. Polydispersity index (PDI) is calculated when doing DLS measurements. The PDI varies between 0 and 1, and indicates to which degree the sample is polydisperse. A low PDI, typically less than 0.1 indicates that the sample is monodisperse [54]. PDI is correlated with standard deviation (SD) of measured particle diameter, as shown in equation 2 [68].

$$PDI = \left(\frac{\sigma}{d}\right)^2 \tag{2}$$

Here, σ is the SD, and d is the measured average particle diameter. PDI is important not only for characterization of particles, but also to ensure equal amount of drugs is loaded into each particle.

DLS exploits diffusion of particles moving under Brownian motion, as well as Rayleigh scattering to determine average particle size in a particle suspension. Brownian motion is a result of random bombardment of neighboring particles in the suspension, leading to particle diffusion. The reported results of particle size measurements are given as hydrodynamic particle diameter. Hydrodynamic diameter is the size of a hypothetical hard sphere moving in the same fashion and having the same translational diffusion coefficient as the particle being measured, assuming there is a hydration layer surrounding the particles in the suspension [72].

2.4.2 Fluorescence

Several experimental techniques used in this project exploit the properties of fluorescent molecules. Fluorescence is the emission of light from a substance that has absorbed energy from electromagnetic radiation. An electron is excited to a higher energy state by absorption of energy from incoming radiation. During the process of relaxation, some thermal energy is lost and so the wavelength of emitted light

is typically longer and has lower frequency of vibrations than that of the absorbed radiation. This shift in photon energy is called *Stokes shift* and is illustrated in figure 10. Stokes shift is essential for measurements as it gives rise to a difference in absorption and emission spectra of the fluorophores, which makes it possible to separate the excitation laser and the emitted light using spectral filters.
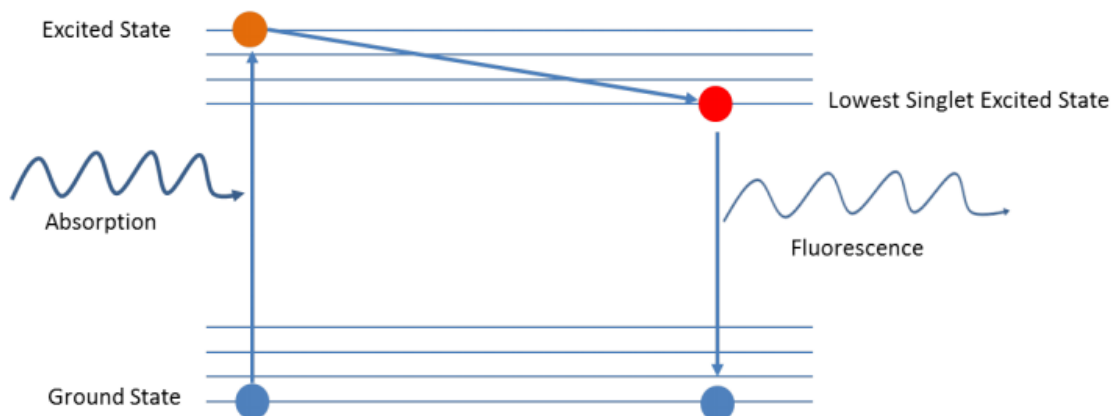
Figure 10: *An energy level diagram of a molecule. Energy absorbation leads to excitation, followed by stokes shift (the arrow between the orange and the red dot), and emission of fluorescence [73].*

NR668-modified nile red

Fluorescence is often exploited in biological research, because it enables imaging of living organisms, cellular structures and can be used to study specific cellular events. A variety of tagging methods are used to make visible specific cellular components. In this project, a fluorescent dye called NR668 was used for labeling nanoparticles, the dye is a modified version of nile red. Nile red is a lipophilic stain, mostly used to stain intracellular lipid droplets [74]. NR668 was used mainly due to its hydrophobic nature, which makes it possible to encapsulate in lipid nanoparticles. Conventional nile red is also lipophilic, but has been shown to leak out of lipid particles [40]. The chemical structure of both conventional nile red and NR668 can be seen in figure 11. The alkane chains of NR668 makes the molecule more hydrophobic than conventional nile red.
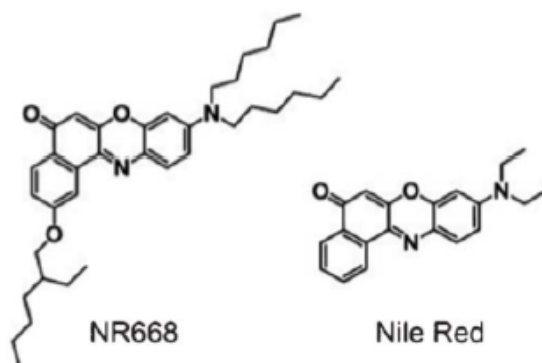
Figure 11: *Chemical structure of NR668 and nile red [40]*

.

2.4.3   Flow cytometry

In this project flow cytometry (FCM) has been used to quantify uptake of fluorescent dye (NR668) within cells, and thereby quantifying the uptake of dye-containing nanoparticles or free dye in cells. FCM is a powerful tool for the analysis of multiple parameters of individual cells within a heterogeneous populations. The flow cytometer performs analysis by passing cells in solution through a laser beam and detecting the light that emerges from each cell as it passes through. The data gathered can be analyzed statistically by FCM software, to report cellular characteristics, such as size, complexity, phenotype and health of cells [75]. Figure 12 shows a schematic of the primary systems of a flow cytometer.

Fluorescent tagged cells are passed through a laser beam, one at a time. This is performed using a mechanism called hydrodynamic focusing where a stream of sheath fluid carries and focuses the cells, leaving room for only one cell at a time to pass the laser beam. As a cell passes through the laser it will scatter light at all angles. Forward scattering (FS) is the amount of light that scatters in the forward direction, as laser light strikes the cell. The magnitude of forward scatter is roughly proportional to the size of the cell [75]. FCM is mostly used to analyze cells in the size range of 1 to 15 microns in diameter [75]. The scattered light received at the detector is translated into a voltage pulse. A histogram of the forward scattered data is a graphical illustration of the size distribution of cells within the population.

Side scattering (SS) is caused by granularity and structural complexity inside the cell [75]. The signals detected from side scattering can also be plotted in one dimensional histograms as for forward scattering, only in this case showing population

24

complexity. A specific cell type with great internal complexity or a cell undergoing apoptosis (rough cell) will have high side scattering signals.
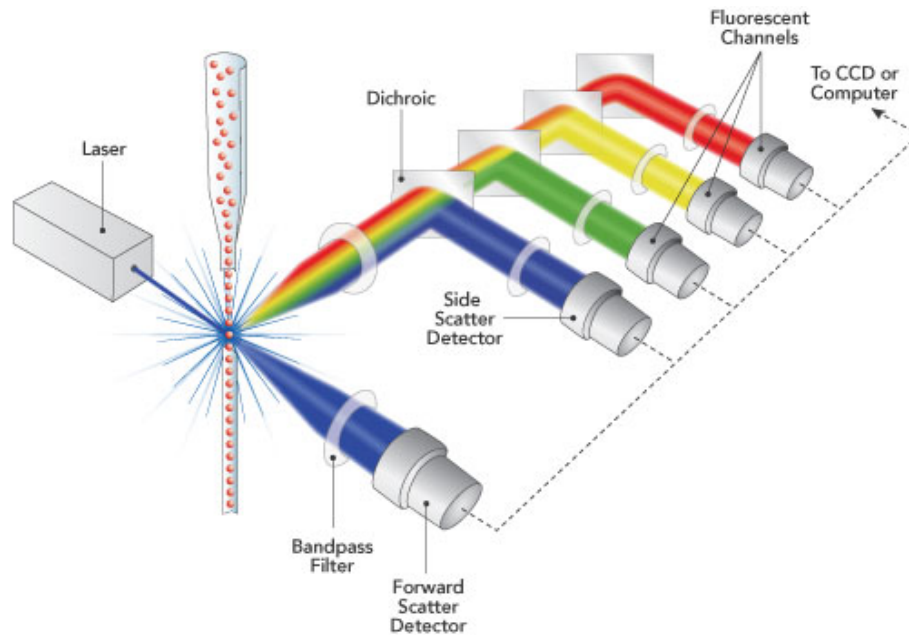
Figure 12: Schematic of the primary systems of a flow cytometer, including fluidics system, lasers, optics, detectors, electronics and peripheral systems [76]

.

Two dimensional scatter plots can be used to distinguish populations of cells, that in one dimensional plots appear as a single population. For example, side scatter and forward scatter can be plotted against each other to create a two dimensional scatter plot. This multi-parametric analysis is a great advantage of flow cytometry. Another parameter that can tell us a lot about cell structure and function is fluorescence. One of the most common ways to study cellular characteristics, using FCM, involves the use of fluorescent molecules. In this project, nanoparticles encapsulating a fluorophore (NR688) are used to study the uptake of lipid nanoparticles in cells. In FCM, when laser light of a specific wavelength strikes the fluorophore, a fluorescent signal is emitted and detected. The emitted fluorescent signal travels along the same path as the side scatter. Light is directed through a series of filters and mirrors, so that light with particular ranges of wavelength are delivered to the appropriate detectors. The fluorescence signal is translated into a voltage pulse, proportional to the amount of fluorescence emitted.

In order to perform multiple fluorophore experiments at once, different fluorophores must have absorption spectras that include the wavelength of the laser light in order to be excited, and their emission peaks must be far enough apart so that discrete

emission data can be collected [75]. Multiple fluorescence parameters are necessary to dissect complex biological systems.

In order to avoid dominance of small irrelevant particles in the sample, a threshold is set for scatting intensity, such that a certain pulse size must be exceeded for the instrument to collect data.

The data obtained in FCM measurements are relative, so control experiments must be included in each analysis. In this project where uptake of fluorescently labeled nanoparticles is analyzed, a control sample is a sample of cells that has been incubated under the same conditions, but without NPs. This way, autofluorescence of the cells can be detected and the data can be compared with cells incubated with NPs.

2.4.4   Multimodal microplate reader

Multimodal microplate readers are instruments that are used for detection of various biological, chemical and physical events of samples in multiwell plates. Plate readers are widely used in quality control, manufacturing processes, academic, medical and biotechnological research. Many measurements can be performed in a short amount of time, with low cost and labor. Typical functionalities are spectral-based measurements of absorbance, fluorescence and luminescence [77]. Absorbance mode is commonly used for measuring enzymatic activity and quantifying protein and nucleic acid concentration in a sample [78]. Luminescence and fluorescence modes are important for reading samples with specific components tagged with fluorescent or luminescent molecules [78].

A multimodal plate reader was in this project used for fluorescence detection and fluorescence spectral analysis of a fluorophore encapsulated in lipid nanoparticles, compared to free fluorophore in solution. The technique is based on excitation of fluorophores in the sample by illumination with a laser beam of a specific wavelength. The light emitted from the fluorescent molecules is separated from the laser light, detected and presented as intensity of fluorescent light. The intensity of the signal is proportional to the amount of fluorophores in the sample.

Luminescence

In addition to fluorescence measurements, luminescence detection was in this project used to study nanoparticle toxicity and toxicity of a tyrosine kinase inhibitor. Luminescence is the emission of light by materials not resulting from heat, as opposed to burning wood or coal that require heat to emit light **??**. Luminescence can occur in some materials as a result of energy absorption from an electron beam, photon-

rays, chemical reactions, crystallizations, mechanical action and more. This energy absorption lifts the material to an unstable excited state, followed by a transition back to its ground state during which light and/or heat is emitted. Fluorescence (see section 2.4.2) is one type of luminescence that occurs as a consequence of absorption of photons.

For cell viability studies in this project, luminescence is detected as a result of a chemical reaction (chemiluminescence) in cells. The molecule that emits light is called a luciferin, while the oxidative enzyme that catalyzed the reaction is called a luciferase.

CellTiter Glo cell viability assay

The technique used for viability studies in this project is called CellTiter-Glo luminescent cell viability assay. Cell viability assays, like the CellTiter Glo, are commonly used to assess the effect of chemotherapeutic drugs on cells. CellTiter Glo is a multiwell plate format where cells are incubated with a thermostable luciferase (Ultra-Glo^{TM} recombinant luciferase) generating a luminescent signal proportional to the amount of ATP available in the cells [79]. The amount of ATP present in a cell culture signals the presence of metabolically active cells, indicating whether a cell is living or dead.
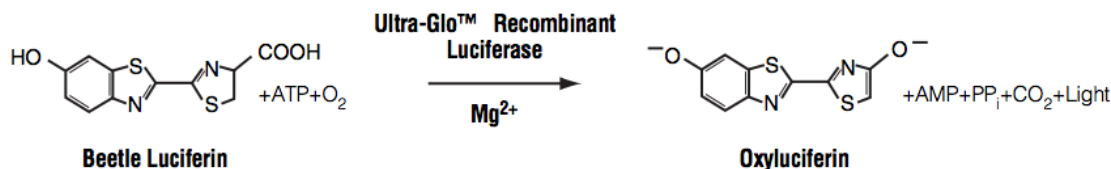
Figure 13: *Chemical reaction resulting in luminescence. Oxygenation of a luciferin catalyzed by a luciferase, in the presence of oxygen, ATP and Mg^{2+}. Figure adapted from [79]*
.

3 Materials and methods

The experimental work performed as part of this thesis was carried out at Sintef Materials and Chemistry and at the Department of Physics, NTNU. An overview with basic chemical and physical information about the materials used for this project can be found in appendix A.1.

3.1 Nanoparticles

The nanoparticles that have been used for all the experiments are lipid-based, and produced through a miniemulsion process.

3.1.1 Synthesis of lipid nanoparticles

- An oil phase and a water phase are mixed in a miniemulsion process. The oil phase consists of a liquid lipid, isopropyl palmitate (IPP), a solid lipid, stearic acid (SA), and whatever molecules that are to be encapsulated in the nanoparticles. The water phase contains water and one or several surfactants, either Tween 80 or Phospholipon 80H (P80H) and/or Andean QDP Ultra (QDP). Each phase is prepared in a 40ml vial. The exact concentration of surfactants, IPP, SA, and loading compounds of each particle batch produced in this project is listed in table 6 found in appendix B.1.

- A magnetic stir bar is added to the water phase, which is placed in a water bath on a combined hot-plate magnetic-stirrer device. The temperature and duration of the water bath varies with surfactant type in the water phase. For particle batches with Tween 80, the water bath temperature was set to 80°C and duration was until the water phase reached the set temperature. For Phospholipon 80H (P80H) and Andean QDP Ultra (QDP) the water bath temperature was 90°C and duration was 30 minutes. Towards the end of the water-phase heating, the lipid phase is heated in a separate water bath at 80°C until the stearic acid has melted. The water phase is added to the lipid phase.

- Before sonication of the water/oil solution, the sonication probe is kept in a water bath of 80-90°C to prevent any fat in the sample from sublimating on the probe. Nanometer oil droplets are created by sonication (Branson Ultrasonics Corporation Digital sonifier model 450). Surfactants adsorb at the water-oil interface and thereby stabilize the droplets.

28

- The physical state of the nanoparticles changes from liquid to solid by cooling the sample solution in cold tap water after sonication. Directly after cooling, the particle size is determined. The procedure for particle characterization is presented in section 3.1.2.

The exact procedure for making lipid particles is developed throughout this project, and has therefore been changed as the project moved forward. The protocol from which later experiments have evolved from is listed in table 1, and will be referred to as lipid particle synthesis protocol #1. The latest developed protocol is also listed in table 1 and will be referred to as lipid particle synthesis protocol #2. The resulting particles of the two protocols will be referred to as NLC#1 and NLC#2.

Table 1: *Lipid nanoparticle synthesis protocol*

Synthesis protocol #1	**Synthesis protocol #2**
Lipid phase: 0.6g SA + 0.4g IPP+drug/dye	Lipid phase: 0.8g SA + 0.2g IPP+drug/dye
Water phase: 20ml of distilled water + 0.25g Tween 80+ magnetic stir bar	Water phase: 20ml of distilled water + 0.24g QDP+ 0.06g P80H+ magnetic stir bar
Water phase in 80°C water bath for ≈10 min, oil phase in 80°C water bath until SA has melted	Water phase in 90°C water bath for ≈30 min, oil phase in 80°C water bath until SA has melted
Water phase added to lipid phase	Water phase added to lipid phase
Probe preheated in 80°C water bath	Probe preheated in 80°C water bath
Sonication 3 minutes 60% intensity	Sonication 3 minutes 60% intensity
Immediately cooled under tap water	Immediately cooled under tap water

The standard particle synthesis procedure is as listed earlier. However, a few batches of particles were made with minor adjustments to the standard procedure.

- In this project a batch of nanoparticles (particle batch PHAT 116) was homogenized using ultra-turrax instead of sonication, for comparison of the resulting particles with particles made by sonication. The ultra-turrax was set at 24000 rpm for 2 minutes.

- In addition, the ultra-turraxed batch (PHAT 116) as well as a standard sonicated batch (PHAT 115) of particles were each split into four samples and cooled down in alternative ways to the cold water tap cooling as stated in the standard procedure. The four different ways of cooling after sonication/ultra-turraxing were as follows: ice bath for one hour, 90°C water bath for one hour followed by cooling under cold tap water, standard tap water cooling and lastly room temperature cooling. Directly after cooling, the particle size is determined, see section 3.1.2.

3.1.2 Characterization of nanoparticles

Particle size and degree of polydispersity (PDI) is determined by DLS using a Malvern Zetasizer nanoparticle analyzer (Nano ZS 90) at isothermal measurement mode in room temperature. Prior to the measurements, all samples are diluted in distilled water by adding $\approx 40\mu l$ sample solution and 1 ml water to a disposable zetasizer cuvette. Dilution of the original particle solutions in water is necessary to obtain suitable scattering intensity from DLS measurements. Zetasizer measurements are performed immediately after particle synthesis for all particle batches produced in the project.

To monitor particle size and polydispersity over time, DLS measurements are repeated after 1,2, (3) and 4-6 days after synthesis. Particles are normally stored at 4°C in between measurements. Some of the particle batches were stored at 37°C for the purpose of stability studies . A complete overview of zetasizer measurements in this project including storage temperature conditions and time of measurement can be found in appendix C.1.

3.1.3 Particle stability in various media

In addition to monitoring size and PDI of particles diluted in water, the stability of lipid nanoparticles was also investigated for particles suspended in various other media. This was done to get an understanding of what kind if environments the

nanoparticles are stable in and thus may applicable to. Lipid nanoparticles that are to be used for cancer treatment must be stable in biological media for at least long enough for the chemotherapeutic drugs to be reach the targeted area in the body. In this project, five different medias were used for particle stability analysis, the medias are listed below:

- Phosphate buffer saline (PBS), pH 7.4. PBS is commonly used in biological research due to its osmolarity and ion concentration matching physiological values.

- Luria Broth media (LB), pH 7. LB is a widely used bacterial culture media, and is commonly used to cultivate E.coli [80]. Many slightly different recipes for LB media exist. The media used for this project contains 1g tryptone, 0.5g yeast extract, 0.5 g sodium chloride and 100ml water. No protein serum was added to the media.

- Deionized water, pH 7.

- 0.2M Glycine solution, pH 9. Glycine is the smallest of the 20 amino acids that are found in proteins. Glycine buffer solution is commonly used for enzyme studies [80].

- Dulbecco's Modified Eagle's Medium (DMEM), with 1% penicillin streptomycin and 10% fetal bovine serum (FBS). DMEM is the same media as used for cell cultivation in this project, see section 3.2.

Each solution was filtered to exclude any particles with a diameter larger than 0.2μ. Two samples were made with each type of media, each sample containing 9ml media and 1 ml nanoparticle solution (PHAT 122). One parallel was stored at 4°C, the other at 37°C. Size measurements were performed after 0, 1, 2, 3, 5, 24 and 48 hours for the particles stored at 37°C, while after 0, 3, 5, 24 and 48 hours for the particles stored at 4°C. The size measurements were performed using zetasizer, by addition of 0.2ml sample and 0.8ml DI water to each zetasizer cuvette. As for normal particle size measurements (see section 3.1.2), isothermal measurement mode in room temperature was also used for size measurements of particles in various media. The resulting PDI values, size distributions and variations is mean size over time are evaluated in order to determine the stability of the systems.

3.2 Cell cultivation

3.2.1 A-431 cells

In the experimental work of this thesis, epidermoid carcinoma cells (A-431, ATCC No. CRL-1555) provided by the Department of Physics were used for all of the cell experiments.

A-431 is a hypertriploid human cell line, originating from an 85-year-old female patient. The cells grow attached to a surface in a monolayer structure. A-431 cells are well suited for studies on cancer cell-signaling pathways since they have abnormally high levels of expression of a cell surface receptor, epidermal growth factor receptor (EGFR). EGFRs are related to DNA synthesis, cell proliferation and apoptosis.

The growth medium used for cell cultivation was Dulbecco's Modified Eagle's Medium (DMEM 11995-065, Gibco Life Technologies) mixed with 10% fetal bovine serum (FBS, Sigma Aldrich), and 50mg streptomycin penicillin (Sigma Aldrich). The cells were cultivated in 75 cm^2 cell culturing flasks with 15 ml of growth medium and incubated at 37°C with 5% carbon dioxide, CO_2.

Splitting of cells was performed every third or fourth day when the cells were approaching confluency. During cell splitting, old growth medium was first removed, before 5 ml sterile phosphate buffered saline (PBS, Sigma Aldrich) was used to wash away any proteins that might inhibit the protein trypsin. PBS was furthermore removed before 3 ml 0.25% trypsin/0.02% EDTA (Ethylenediaminetetraacetic acid) solution (Sigma Aldrich) was added and the flask was incubated at 37°C for 5-7 minutes. The effect of adding trypsin/EDTA solution is cell detaching from the incubation flask, this could be seen in a phase-contrast microscope. If the cells are incubated with trypsin for too long, trypsin will damage the cells leading to cell death. To stop the effect of trypsin after cells had detached, 7 ml of growth medium was added to the flask. 10 ml of the cell suspension was transferred to a falcon tube and centrifuged (Heraeus Megafuge 1.0) at 1500 rpm for 5 minutes. 10 μL of cell suspension left in the incubation flask was furthermore used to determine concentration of living cells with the help of a cell counter (Countess, Invitrogen) and 10μl Trypan blue stain. Trypan blue is a vital stain used to selectively color dead cells blue. After centrifugation, the supernatant was removed and the cell pellet was resuspended in growth medium to a concentration of 1 million cells/ml. 1-2 million cells were transferred to a new incubation flask together with 14ml DMEM, and placed in an incubator. The remaining cell solution was used for experiments or was discharged. The growth medium was changed once during every passage.

3.3 Flow cytometry analysis

A flow cytometer (Gallios, Beckman Coulter) was used to study cellular uptake of fluorescently labeled nanoparticles in A431 cells. Modified nile red (NR668) was encapsulated in the nanoparticles used for the FCM experiments. A green laser with wavelength $\lambda=561$nm was used to excite the fluorescent particles, while emission was detected for $\lambda=630$nm with a 30nm bandpass filter.

Plotting forward scatter versus side scatter enabled separation of dead and alive cells. Detection limit was set to 10000 counts for each sample. A single parameter histogram was obtained from these events, with cell count vs fluorescence intensity. The voltage of the system was set so that the peak fluorescence of the control samples were positioned between 0 and 1 on a logarithmic scale. Kaluza flow cytometry analysis software (Beckman Coulter) was used for data analysis and for making overlay histograms. A marker was applied in the overlay histograms, including all events with fluorescence intensity above $\approx 3\%$. These events were defined as positive detection.

The protocols used for uptake studies using flow cytometry were from previous studies performed at the biophysics department, and were suggested by PhD student, Einar Sulheim. Sample preparations were as follows:

For each experiment, cells were seeded two days prior to incubation with nanoparticles in order to reach approximately 80% confluency in growth wells. The solution with cell concentration 1E6 cells/mL from the splitting process was diluted to a concentration of 150 000 cells/ml, by addition of DMEM. 1ml of the diluted solution was added to each well of a 12 wellplate (COSTAR). The cells were incubated at 37°C for 2-4 days before they were used for flow cytometry experiments.

To study uptake of nanoparticles in cells, solutions of nanoparticles and DMEM were made with a NP concentration of 20μg/ml. The solutions were added to the wells in volumes of 1ml per well. The chosen concentration of NPs were based on protocols with other particle types at the biophysics department, as well as literature values for studies of SLNs *in vitro* [81] [82]. 2-3 wells were used as controls, and therefore contained cells in DMEM, but no nanoparticles. The samples were incubated for a specific time period and stored at 37°C, duration varying with different experiments (1, 3, 6, 24 or 48 hours).

After incubation, the samples were washed and harvested for FCM. Cell medium was removed before the samples were washed with 1mL prewarmed sterile PBS two times, the PBS was removed after each rounds of washing. Furthermore, 300μL of prewarmed trypsin/EDTA solution was added to each well. The cells were incubated at 37°C for about 5 minutes before 700μL of DMEM was added to each well to stop

the trypsinization. The cell solutions were transferred from the wells into separate falcon tubes and centrifuged at 1500 rpm for 5 minutes. Cell solution was removed from the falcon tubes, before the cell pellet was washed two times by adding 400μL of cold PBS to each tube, centrifugate at 1200 rpm for 3 minutes, and removing the PBS between each wash. Finally, 400μL of cold PBS was suspended with a pipette to each tube until the cells were well dispersed in the liquid. The tubes were stored on ice. Right before FCM analysis, the samples were transferred to FCM tubes.

3.4   Spectral analysis of NR668

In order to interpret results from FCM in a correct way, spectral properties of the fluorescent dye NR668 inside lipid nanoparticles vs free dye was analyzed. In addition, the dependence of NR668 spectral properties on temperature and time of incubation were investigated. Spectral analysis were performed using SpectraMax i3x Multi-Mode microplate. Fluorescence mode was used for both point analysis and spectral analysis. 521nm was used as excitation wavelength, while emission detection was in the range of 550-700nm for spectral analysis and 610nm with a 25 nm bandwidth for end point analysis. 10nm increments of wavelength selection was used. Sample preparations were as follows:

- A batch of nanoparticles encapsulating NR668 was made as described in section 3.1.1 (particle synthesis protocol#2), with a concentration of 0.5wt% NR668 in the oil-phase, giving a concentration of 0.02347wt% in the particle solution in total.

- 5mg NR668 was dissolved in 21,3g of IPP, giving the same concentration of NR668 as a 0.5% NR668-particle batch in total, 0.02347wt%.

- Two solutions were made; one containing 4ml DMEM and 20μg/ml lipid nanoparticles, the other containing 4ml DMEM and $1.4\mu l$ of IPP/NR668-solution. Both solutions have the same total concentration of NR668.

- Each solution was split in two, one part placed in an incubator at 37°C, the other in a fridge at 4°C.

- After 1, 3, 6, 24 and 48 hours, a small amount of each solution was transfered to a black costar 96- well microplate. 3 parallel wells were tested for each of the four solutions, each well containing $150\mu l$ solution. Analysis was performed by use of a microplate reader.

3.5 Inhibition of endocytosis

To better understand what mechanism underlies the uptake of fluorescent dye in A431 cells, two inhibitors of endocytosis were used. The two inhibitors each inhibit a specific mechanism of endocytosis, as there are more than one possible (see section 2.3). Stock solutions of inhibitors, Chlorpromazine and Genistein, were made with the following contents and concentrations:

- 5mg/mL Chlorpromazine in FBS

- 10mM Genistein in dimethyl sulfoxide (DMSO)

The protocols for inhibition in A431 cells using Genistein [83] and chlorpromazine [84] was found in the literature. Before experiments where cells were incubated with nanoparticles and endocytosis inhibitors, the cells were allowed to attach and grow in growth wells for two days.

To prepare cells for incubation with Chlorpromazine and Genistein, a small volume of each stock solution was diluted in DMEM, reaching a concentration of $10\mu g/mL$ for Chlorpromazine and $50\mu M$ for Genistein. Old DMEM was removed from twelve growth wells and washed with PBS, 1 ml in each well. PBS furthermore was removed, 1ml of diluted Genistein solution was added to three wells and 1 ml of Chlorpromazine solution to three wells. The cells were placed in incubator for one hour before the cell media was removed and DMEM containing fluorescently labeled nanoparticles was added in the manner described in section 3.3. NPs were added to nine wells. Thus, out of the twelve wells, three contained Genistein + NPs, 3 chlorpromazine + NPs, 3 only NPs, and 3 no NPs (control samples). After three hours of incubation with nanoparticles, flow cytometry analysis was performed.

3.6 Cell viability testing

Cell viability studies were performed to determine toxicity of both empty and kinase inhibitor loaded nanoparticles. Two EGFR inhibitors were provided by the Department of Chemistry at NTNU (SB6-140-06 and JH08-096), while three were commercially available (Gefitinib, Erlotinib and Lapatinib). Before any of there kinase inhibitors could be used in nanoparticle encapsulation and cell toxicity studies, solubility in IPP was tested to determine which of the five substances was most suitable for encapsulation in lipid particles. Cell toxicity was furthermore analyzed with CellTiter Glo Luminescent cell viability assay.

3.6.1 Solubilitytesting of kinase inhibitors

In order to encapsulate any substance in a lipid nanoparticles, the loading compound needs to be hydrophobic. As described in section 3.1.1, solid lipid nanoparticles are made in a miniemulsion process with a water phase and a lipid phase. The actual nanoparticles consist of all the components in the lipid phase, plus the surfactant dissolved in the water phase. It is therefore important that any loading compound is lipophilic, or it will not be included in the nanoparticles. The solubility test procedure is based on attempting to dissolve powdered kinase inhibitors in liquid lipid, in order to determine which inhibitor is most suitable for encapsulation in lipid nanoparticles.

The solubility was determined in a step-wise procedure that involved attempting to dissolve kinase inhibitors in IPP at relatively high concentrations using a sequence of mechanical procedures (listed below). If the kinase inhibitor was not dissolved, the volume of the IPP was increased so as to decrease the concentration by a factor of 2, and then the sequence of mechanical procedures were repeated in an attempt to solubilize the inhibitor at the decreased concentration. Determination of whether an inhibitor has dissolved was based on visual observation. If a solution appeared clear and no grains of powder could be seen, the kinase inhibitor was considered dissolved. Table 2 shows the end concentrations of each of the five kinase inhibitors in IPP.

Preparation of solutions

- Five solutions were made, containing 0.4g IPP and 0.01g kinase inhibitor, giving a starting concentration of 2.5wt%. The kinase inhibitors were the following substances: Gefitinib, Erlotinib, Lapatinib, SB6-140-06 and JH08-096.

- A reference solution containing 1mg NR668 in 40 mg IPP (2.5wt% NR668) was made for comparison of solubility with the solutions containing kinase inhibitors.

Mechanical procedures

- The samples were placed on a roller mixer (Stuart roller mixer SRT9) overnight to ensure proper mixing.

- Samples were sonication for 10 minutes in a 20°C ultrasonic bath to dissolve any aggregates of kinase inhibitors.

- Samples were kept in a water bath at 80°C for 30 seconds.

Table 2: End concentrations of kinase inhibitors in IPP

Kinase inhibitor	*End concentration in IPP [wt%]
Erlotinib-HCl	0.625
Gefitinib	1.25
Lapatinib	1.25
SB6-140-05	0.625
JH08-096	1.25

*The end concentration of each kinase inhibitor was not actually measured, but assuming the kinase inhibitor is dissolved in the total amount added IPP, these concentrations were obtained.

3.6.2 Luminescent cell viability assay

Cell viability experiments were performed by CellTiter-Glo Luminescent Cell Viability Assay and plate reader luminescence measurements. Cellular viability was measured with plate reader (SpectraMax i3x), endpoint luminescence detection and 600ms integration time.

Viability was studied for cells that had been incubated with blank nanoparticles,

kinase inhibitor loaded nanoparticles, as well as non encapsulated kinase inhibitor. The protocols used for viability studies were had been used for viability studies performed with other NP types at the biophysics department and were suggested by PhD student, Einar Sulheim. The procedure of the experiment was as follows:

- A431 cells were seeded out in three 96-well plates (black costar 96- well microplate) at a concentration of 8000cells/100μl growth medium. The microplates were incubated at 37°C with 5% carbon dioxide, CO_2 for 24 hours.

- On the same day as cell seeding, six solutions were made for toxicity testing. Four of them were batches of lipid nanoparticles, all following nanoparticle synthesis protocol#2. One particle batch with no loading material, the three other with 5wt%, 2.5wt% and 1wt% Gefitinib. The last two solutions produced were dimethyl sulfoxide (DMSO) mixed with Gefitinib, and pure DMSO solution. The concentration of Gefitinib in DMSO was 0.117wt%. This concentration is the same as the total concentration of Gefitinib in a particle batch with 2.5wt% Gefitinib (concentration in the oil phase).

- One day after cell seeding, a 96-well source plate was prepared with the six solutions diluted in growth medium. The six solutions were diluted in the source plate in growth medium at 2 fold serial dilutions along each row of the source microplate, starting at 1000μg/ml of nanoparticles, and 1v/v% of DMSO solutions. 2ml of diluted solution was added to each or the wells in the first column, the two top wells of the column containing blank nanoparticle solution, followed by particles encapsulating 1wt%, 2.5wt%, repetition of 2.5wt% and 5wt% Gefitinib. The last two wells of the first column were filled with DMSO containing Gefitinib and pure DMSO respectively. The serial dilutions were carried out until 11 out of the 12 columns of the source plate were filled. End volume in each well was 1ml. The last column was filled with 1ml of growth medium per well. Table 3 shows an overview of the microplate setup.

- A 8-channel pipette was used to transfer the various dilutions of solutions from the source plate to the three cell-containing 96-well plates. 100μl were transfered to each well of the three 96-well plates by pipetting one column at a time from the source plate. The three plates were incubated at 37°C with 5% carbon dioxide, CO_2.

- After 1, 2 and 3 days of incubation, a 96-well plate was taken out of the incubator and left in room temperature before the last sample preparation for

luminescence measurements could take place.

- 100μl of solution was removed from each well, before 80μl of CellTiter Glo luminescent reagent was added to each well.

- The microplate was covered with alumni foil and left on a benchtop shaker set to 200 rpm for 10 minutes before cell viability was measured with luminescence recording, using a microplate reader.

Table 3: *96-well plate setup for toxicity experiment. Each well contains cells, DMEM and one of the six prepared solutions.*

	Column											
	1	**2**	**3**	**4**	**5**	**6**	**7**	**8**	**9**	**10**	**11**	**12**
Blank NPs $[\mu\text{l/ml}]$	1000	500	250	125	62.5	31.25	15.6	7.8	3.9	1.95	0.98	0
Blank NPs $[\mu\text{l/ml}]$	1000	500	250	125	62.5	31.25	15.6	7.8	3.9	1.95	0.98	0
NPs 1% gef $[\mu\text{l/ml}]$	1000	500	250	125	62.5	31.25	15.6	7.8	3.9	1.95	0.98	0
NPs 2.5% gef $[\mu\text{l/ml}]$	1000	500	250	125	62.5	31.25	15.6	7.8	3.9	1.95	0.98	0
NPs 2.5% gef $[\mu\text{l/ml}]$	1000	500	250	125	62.5	31.25	15.6	7.8	3.9	1.95	0.98	0
NPs 5% gef $[\mu\text{l/ml}]$	1000	500	250	125	62.5	31.25	15.6	7.8	3.9	1.95	0.98	0
DMSO w/gef **[v/v%]**	1	0.5	0.25	0.125	0.062	0.031	0.016	0.008	0.004	0.002	0.001	0
DMSO **[v/v%]**	1	0.5	0.25	0.125	0.062	0.031	0.016	0.008	0.004	0.002	0.001	0

4 Results

In this chapter the results are given with a brief description of the aim and method for the experiment. The results are presented in three separate sections. The first is about optimization of nanoparticles with respect to stability and size. The second deals with cellular uptake of lipid nanoparticles. Lastly, the third section is about cytotoxicity of kinase inhibitors and lipid nanoparticles.

4.1 Optimization of nanoparticle stability and size

Particle size and stability are essential features in a nanoparticle drug delivery system. The particles must be large enough to ensure high drug payload, but at the same time be small enough to travel in capillaries, across biological barriers and accumulate in tumor tissues as a result of the EPR-effect, section 2.1.4. And with respect to stability, the particle must have sufficient shelf life in solution, as well as stability in biological environment.

To optimize these parameters, particle synthesis was repeatedly performed while systematically varying subcomponents, composition and preparation protocol, all the while monitoring particle stability, particle size and degree of polydispersity by zetasizer measurements. Only one parallel was measured for each particle batch at each time point throughout the optimization process, as the purpose of the experiments were to screen particle properties. The end NP formulation (NLC#2), was measured with ZS several times, statistical results will therefor be presented for only that formulation in section 4.1.4.

4.1.1 First generation lipid nanoparticles (NLC#1)

Sintef materials and chemistry have prior to this project worked with synthesizing lipid nanoparticles that have potential applications in drug delivery and medical imaging. At the start of the project, lipid nanoparticles were made following the general protocol used at Sintef was produced (synthesis protocol#1). This was done to create a basis for further work and improvement of the NPs. First generation lipid particles consist of an oil phase with 6:4 ratio of stearic acid and IPP stabilized by Tween 80 in a water phase. Zetasizer measurements were performed to monitor the particle size and PDI of the particle solutions over time.

Figure 14 show the mean particle size as a function of time for NLP 1 and NLP 3. These particles differ in presence of loading material (see table 6 in appendix B.1). NLP1 were empty, while NLP3 contained 0.5wt% curcumin. Average particle diameter for both batches was in the rage of $\approx$230-240nm immediately after synthesis, while after two days of storage at 4°C it had increased about 14-15% to 260-280nm. PDI values were between 0 and 0.2 for all measurements, indicating relatively monodisperse solution. Exact PDI values and particle diameter can be found in appendix C.1.
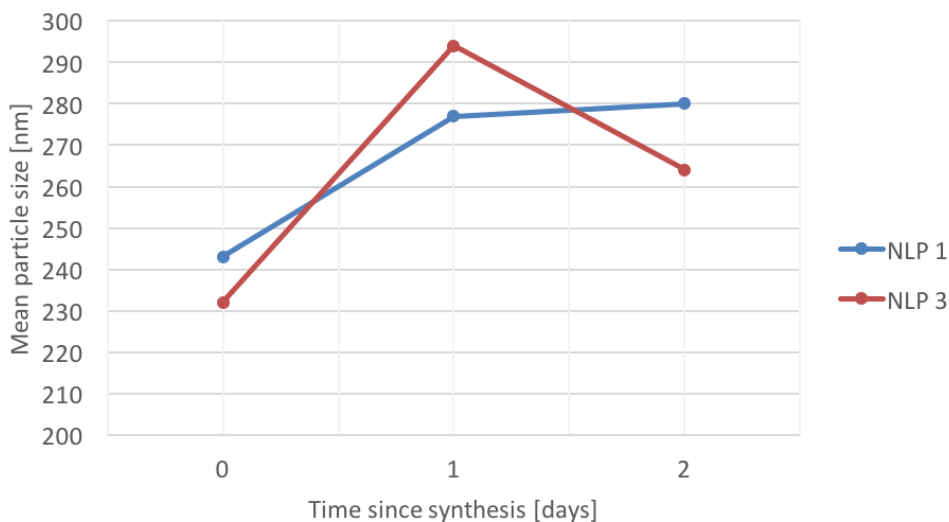
Figure 14: *Mean particle size after 0, 1 and 2 days since synthesis for particle batches NLP 1 and NLP 3, made with synthesis protocol #1, stored at 4°C. NLP1 are empty, while NLP3 contains 0.5% curcumin (model drug).*

4.1.2 Second generation lipid nanoparticles

Systematic changes were done to the particle synthesis protocol of first generation particles to produce improved nanoparticles with respect to particle size and stability.

The parameters that were varied in the NP optimization process were: surfactant type and concentration, amount and ratio of SA and IPP, particle storage temperature, instrument used for emulsification, and lastly particle cooling method.

Selection of surfactant system and SA:IPP ratio and amount

Figure 15 shows the mean diameter found by zetasizer measurements for particle batches PHAT 95-PHAT 98, where amount and ratio of SA and IPP was varied, and Phospholipon 80H (P80H) was used as surfactant instead of Tween 80 (see table 6
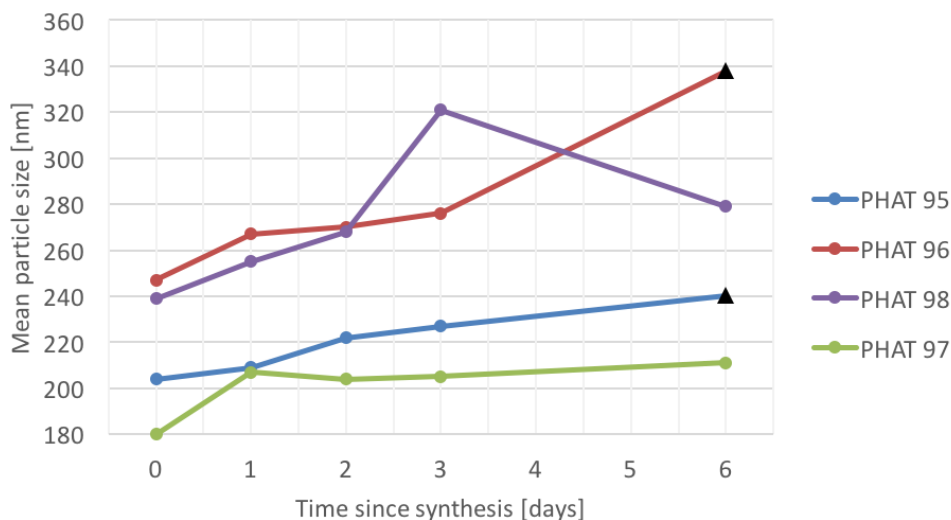
in appendix B.1).

PHAT 95 has high SA:IPP ratio, but low amount of SA, IPP and P80H.

PHAT 96 has high SA:IPP ratio, and high amount of SA, IPP and P80H.

PHAT 97 has low SA:IPP ratio, and low amount of SA, IPP and P80H.

PHAT 98 has low SA:IPP ratio, but high amount of SA, IPP and P80H.

Figure 15: *Mean particle size after 0, 1, 2, 3 and 6 days since synthesis for particle batches PHAT 95-98, where amount and ratio of SA and IPP was varied, and the amount of surfactant Phospholipon 80 varied. Particle solutions were stored at 4°C between measurements. Black triangles in the figure represent less reliable ZS measurements due to high PDI or presence of large/sedimenting particles.*

The results show a decrease in particle size for PHAT 95 and PHAT 97 compared to first generation particles. PHAT 95 and 97 have the same concentration of P80H, but differ in SA:IPP ratio. PHAT 96 and 98 on the other hand, have higher amounts of both SA, IPP and P80H than PHAT 95 and 97, but as the results show the particle size is approximately the same in for those batches as for first generation particles. The particle size increase over the first 2 days was $\approx$9% and $\approx$13% for PHAT 95 and 97, respectively. PDI values increased for all four batches over a time period of 6 days, from around 0.185 up to 0.22-0.32, indicating a slight increase in polydispersity. Out of the four batches, PHAT 95 had the lowest increase in PDI. The exact values of PDI and mean size can be found in appendix C.1.

After interpreting the results of zetasizer measurements of particle batches PHAT 95-98, the formulation of batch PHAT 95 was used in subsequent experiments for synthesis of dye and drug encapsulating nanoparticles (PHAT 99-102). Figure 16 shows the increase in mean size for particle batch PHAT 99-PHAT 102, where cur-

cumin and NR668 were encapsulated at two different concentrations (0.5% and 1%). PDI measurements resulted in values in the range of 0.15-0.24 for all measurements, indicating a slight increase in polydispersity.
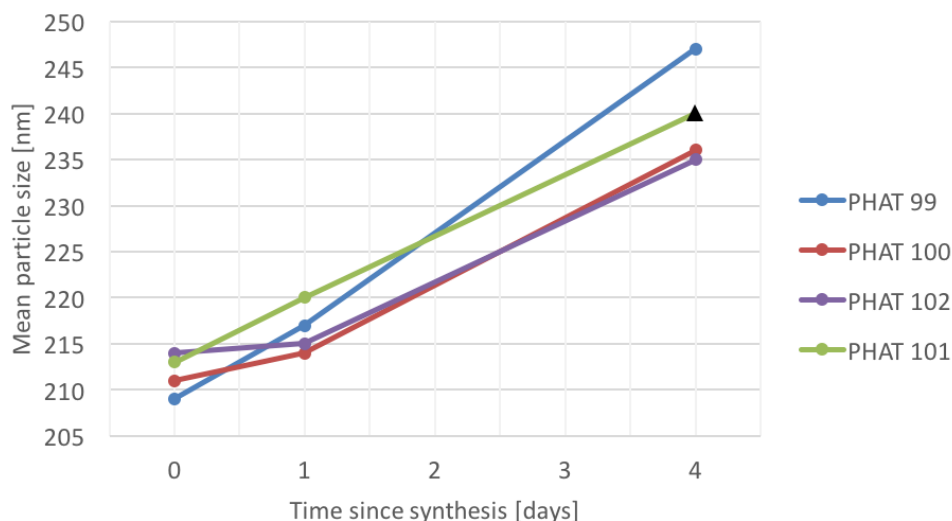
Figure 16: *Mean particle size after 0, 1 and 5 days since synthesis for particle batches PHAT 99 (with 0.5% curcumin), PHAT 100 (with 1% curcumin), PHAT 101 (with 0.5% NR668) and PHAT 102(with 1% NR668). Particle solutions were stored at 4°C between measurements. Black triangles in the figure represent less reliable ZS measurements due to high PDI or presence of large/sedimenting particles.*

The results of particle size measurements for PHAT 99-102 show slightly larger diameter of particles encapsulating either dye or drug, compared to empty particles (PHAT 95). All four batches have almost the same mean size and stability over a time period of four days.

Due to limitations in the synthesis protocol of particles stabilized by P80H alone, a third surfactant, Andean QDP Ultra (QDP), was introduced for particle optimization testing. Figure 17 show the results of zetasizer measurements of particle batch PHAT 106-109, stored at 4°C. The four batches differ in ratio used of surfactants P80H and QDP (see table 6 in appendix B.1). In addition to monitoring particle size and distribution for particles stored at 4°C, a small volume of all four batches were stored at 37°C and analyzed with dynamic light scattering measurements, particle size as function of temperature is shown in figure 18.
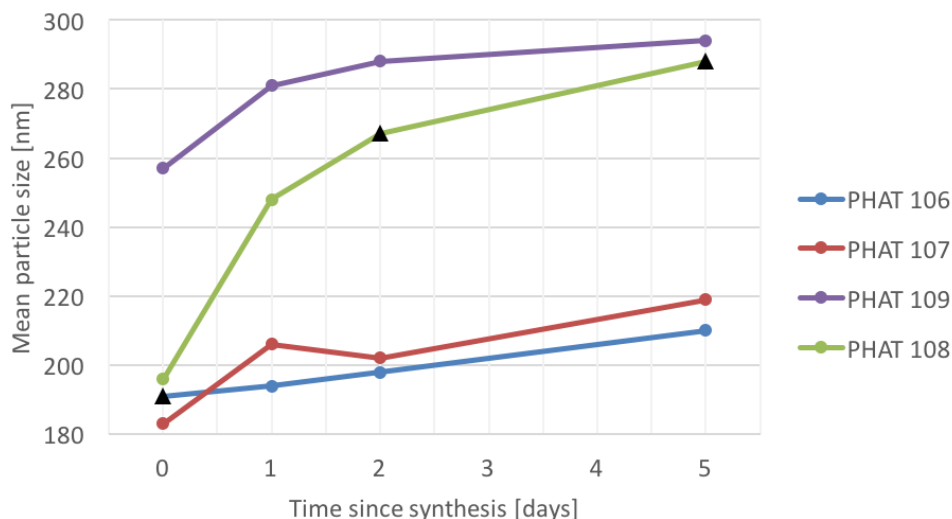
Figure 17: *Mean particle size after 0, 1, 2 and 5 days since synthesis for particle batches PHAT 106 (with 3g QDP), PHAT 107 (with 0.24g QDP and 0.06g P80H), PHAT 108 (with 0.15g QDP and 0.15g P80H) and PHAT 109 (with 0.06g QDP and 0.24g P80H). Particle solutions were stored at 4°C between measurements. Black triangles in the figure represent less reliable ZS measurements due to high PDI or presence of large/sedimenting particles.*

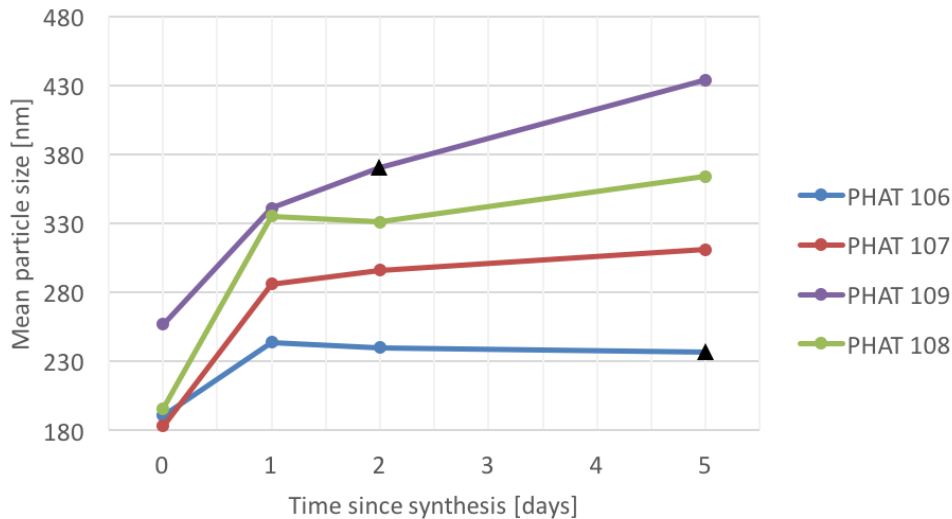***Figure 18:*** *Mean particle size after 0, 1, 2 and 5 days since synthesis for particle batches PHAT 106 (with 3g QDP), PHAT 107 (with 0.24g QDP and 0.06g P80H), PHAT 108 (with 0.15g QDP and 0.15g P80H) and PHAT 109 (with 0.06g QDP and 0.24g P80H). Particle solutions were stored at 37°C between measurements. Black triangles in the figure represent less reliable ZS measurements due to high PDI or presence of large/sedimenting particles.*

In the four batches, the ratio of QDP:P80H decreases with increasing batch number. The results of zetasizer measurements of the four batches generally show smaller particle diameter and higher stability for particles with higher QDP:P80H ratio (PHAT 106-107). This is especially evident in the particle solutions stored at 4°C. PDI values ranged from 0.03-0.2 for all four batches, except for PHAT 109 at 37°C where a slightly higher polydispersity was measured (PDI around 0.2-0.24). In addition, after 1-5 days of storage the average diameter was larger for particles stored at 37°C compared to those stored at 4°C.

Selection of method for emulsification and cooling

Based on the results of particle size and PDI measurements of all previous particle batches produced in the project, the protocol used for particle batch PHAT 107 was used for the remaining experiments of the particle optimization process. The protocol used for PHAT 107 is referred to as lipid nanoparticle synthesis protocol#2, and can be found in table 1 in section 3.1.1. Table 4 shows the results of zetasizer measurements of particle batch PHAT 115 and 116, where particle composition was the same as for PHAT 107 (8g SA, 2g IPP, 0.24g QDP and 0.06g P80H), while ultra-turraxing (for PHAT 116) and sonication (for PHAT 115) as method of emulsification was compared. In addition, four different particle cooling methods were tested.

Table 4: *Results of zetasizer particle size and PDI measurements for particle batches PHAT 115 (sonicated) and PHAT 116 (ultra-turraxed), where both method of emulsification and cooling were varied for particles stored at 4°C and 37°C.*

Sample ID	Storage temperature [°C]	Particle cooling	Time since synthesis [days]	PDI	Average diameter
	4	Ice bath	0	(0.238)	(215.1)
			1	(0.255)	(217.6)
			2	0.125	213.6
			6	0.178	218.3
	4	Tap	0	0.230	225.9
			1	0.157	210.8
			2	0.181	212.2
			6	0.198	217.5
	4	Room tempera- ture	0	0.236	292.9
			1	0.092	234.1
			2	0.150	240.2
			6	0.150	241.0
PHAT 115	4	90°C water bath	0	0.256	279.4
			1	0.207	265.9
			2	(0.178)	(275.5)
			6	0.182	271.3
	37	Ice bath	1	0.147	253.9
			2	0.122	259.4
			6	-	-
	37	Tap	1	0.123	280.9
			2	0.109	285.6
			6	-	-
	37	Room tempera- ture	1	(0.234)	(430.8)
			2	0.216	426.5
			6	0.223	480.1
	37	90°C water bath	1	0.213	332.4
			2	0.121	349.0
			6	-	-

	Fridge 4°C	Ice bath	0	(0.659)	(535.9)
			1	(0.665)	(840.9)
			2	-	-
			6	-	-
	Fridge 4°C	Tap	0	(0.630)	(892.1)
			1	(0.517)	(576.9)
			2	-	-
			6	-	-
	Fridge 4°C	Room temperature	0	(0.333)	(1366)
			1	(0.471)	(676.8)
			2	-	-
			6	-	-
PHAT 116	Fridge 4°C	90°C water bath	0	(0.435)	(495.0)
			1	-	-
			2	-	-
			6	-	-
	Oven 37°C	Ice bath	1	-	-
			2	-	-
			6	-	-
	Oven 37°C	Tap	1	-	–
			2	-	-
			6	-	-
	Oven 37°C	Room temperature	1	-	-
			2	-	-
			6	-	-
	Oven 37°C	90°C water bath	1	-	-
			2	-	-
			6	-	-

All table cells marked with "-" represent samples that were either separated into two phases (oil/water) or had too much aggregates of fat/lipids for zeta measurements to be performed.

All table cells enclosed by parenthesis gave unreliable zeta measurements, indicating a increased polydispersity and poor stability.

Zetasizer measurements showed wide particle size distributions, high degree of poly-dispersity and generally large particles in the particle batch emulsified by ultra-turraxing (PHAT 116). In all four cases of cooling methods for PHAT 116, particles stored at 37 degrees had separated into an oil and a lipid phase within the first 24 hours. This indicates low particle stability, which can also be seen from the high and increasingly growing PDI values ($\approx$0.3-0.6). Ultra-turraxing as a method of emulsification was discarded. Sonicated particles, batch PHAT 115, had more gaussian particle distribution in addition to much smaller average particle size and higher stability at both 4 and 37°C.

For sonicated samples, cooling in ice bath or 90°C water bath resulted in particle solutions with visible lumps and aggregates of fat. Both cooling methods were therefore discarded. Particles cooled under cold tap water or in room temperature, resulted in more stable solutions with no visible aggregates or particles. NPs made with tap water-cooling had the smallest average particle size, both immediately after synthesis, over time, and at both storage temperatures. Tap water-cooling was therefore chosen as method of particle cooling in synthesis protocol#2.

### 4.1.3   Particle stability in various media

As a continuation of optimization and characterization of lipid nanoparticles, particles produced by the new synthesis protocol (protocol#2) were subjected to five different medias in order to analyze particle stability in various environments over time. Zetasizer measurements were performed for particles stored at 4°C and 37°C, the results are shown in figure 19 and 20, respectively.

The orange line in figure 19 shows the change in average diameter of particles in pure particle solution, where no dilution has been made until the sample preparation for ZS measurements. These results are therefore used as a reference for comparison with particles dispersed in various types of media.

An immediate increase in particle size after dilution in media can be observed in all five cases. This increase is very small for dilution in DI water, only about 8%, while it is relatively high for solution with glycine and DMEM, 28% and 20% respectively. This size increase is mainly due to the choice of instrumental procedure, as the same standard operating procedure (SOP) on the zetasizer is used for all measurements. A SOP measurement uses predefined parameters, including specifications of the type of solution being tested. Small variations in refractive index of the different medias will affect the calculations of average size and distribution [85], see section 2.4.1.

The reference particles increase about 9% in average particle size over a time period of 48 hours (original particle solution). In comparison, particles dispersed in PBS, LA Broth, DI water, Glycine and DMEM, and stored at 4°C increase about 5%, 6%, 9%, 13%, 7% respectively over the first 48 hours, indicating a relatively similar particle stability in all medias including the pure particle solution.

When comparing the two figures (figure 19 and 20), it is found that higher storage temperature generally leads to larger average particle size, and a higher rate of size increase. Over 47 hours of storage at 37°C the average diameter of particles diluted in PBS, LA Broth, DI water, Glycine and DMEM increased 33%, 18%, 11%, 15% and 35% respectively. (The first measurement at t=0 has not been included in the calculations due to the SOP-related size effects, the percent values of size increase are thus based on 47 hours of storage instead of 48). Only stability of particles diluted in DI water was not affected by the increased storage temperature. Measurement of PDI generally resulted in low values (<0.2), indicating high degree of monodispersity for all solutions at both temperatures. Only DMEM stored at 37°C showed a slight increase in PDI and thus increase in polydispersity. The exact values of particle size and PDI for each measurement can be found in appendix C.1, table 11.
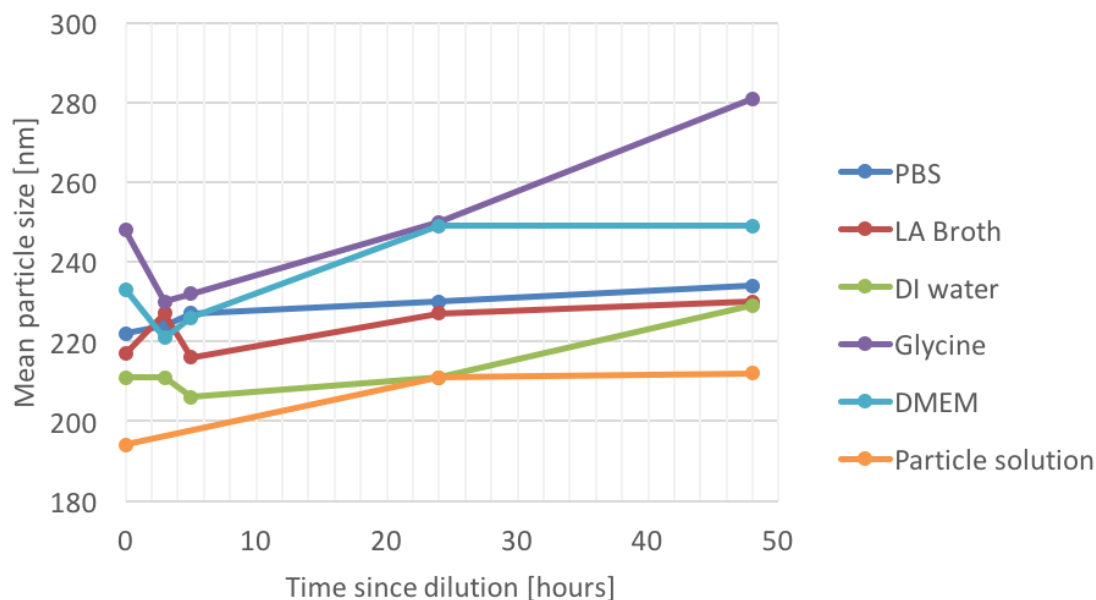
Figure 19: *Mean particle size plotted for PHAT 122 after 0, 2, 3, 5, 24 and 48 hours after dilution in various media. The orange line represent a refrence sample of the original particle solution. Particle solutions were stored at 4°C between measurements.*
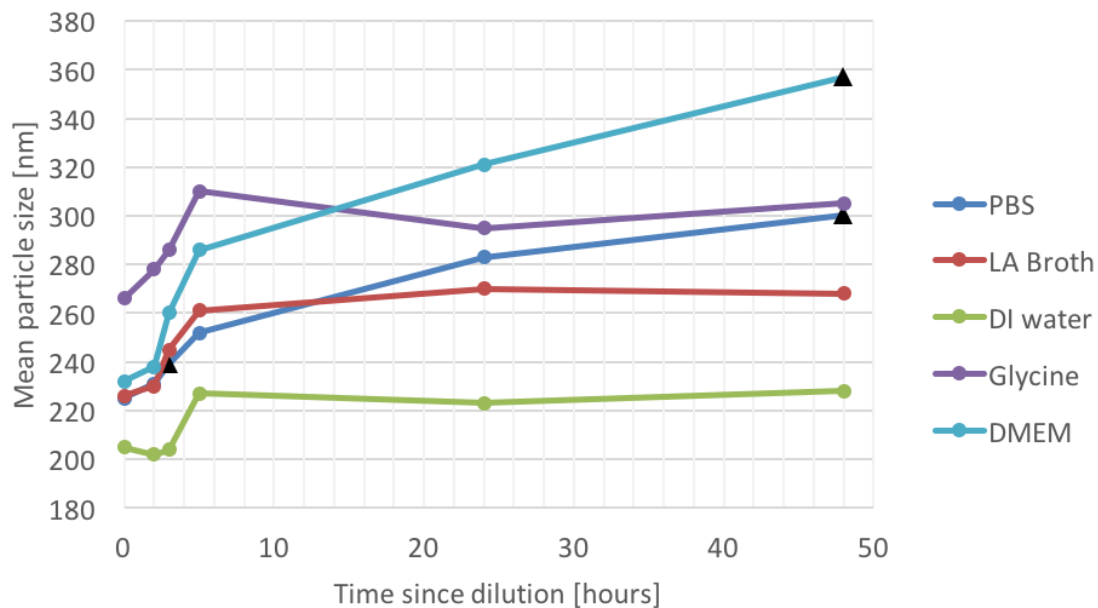
Figure 20: *Mean particle size plotted for PHAT 122 after 0, 2, 3, 5, 24 and 48 hours after dilution. Particle solutions were stored at 37°C between measurements. Black triangles in the figure represent less reliable ZS measurements due to high PDI or presence of large/sedimenting particles.*

After 24 and 48 hours at 37°C, small amounts of lipid clusters was observed in four of the particle solutions, not in the original particle solution, and the DI water-solution.

The media that is of most interest for this project is DMEM, as it was the same media used for cultivating A431 cells, and used in all cell experiments. In DMEM at 37°C, particle size increase during the first two hours was 2%, while after 5 hours the average particle size has increased by 22%. Figure 21 shows the change in size distribution over time for particles in DMEM, stored at 37°C. The size distribution becomes wider with time, eventually two separate intensity peaks can be seen.
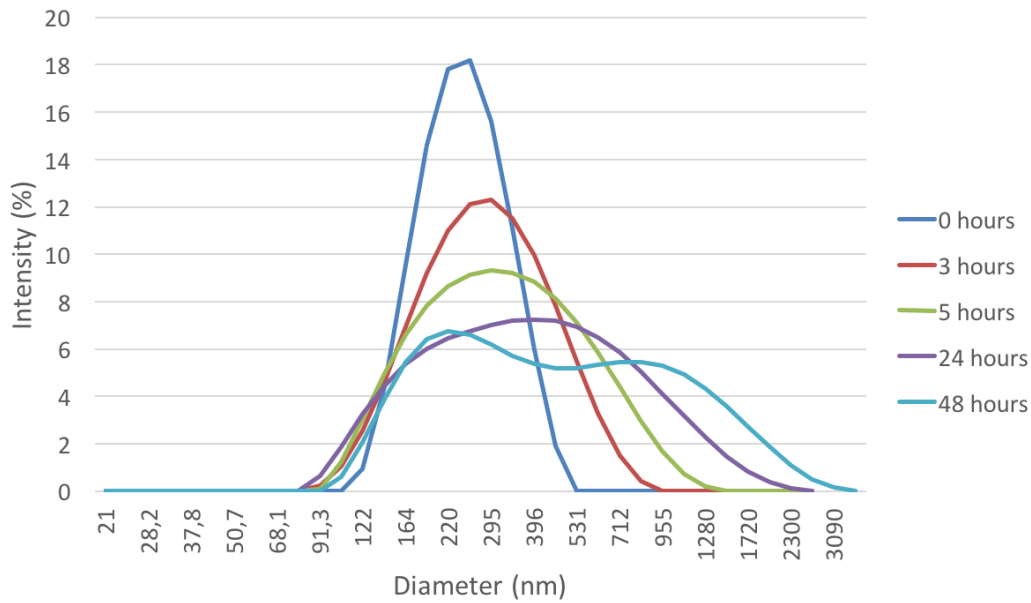
Figure 21: *Particle size distribution over time for lipid particle batch PHAT 122 in growth media DMEM. Particles were stored at 37° C between measurements.*

Because of a desire to find the underlying mechanisms leading to increased particle size as a function of time, the fit of experimental data with criteria of Ostwald ripening were investigated. Size measurements performed with ZS on particle batches PHAT 122 were used for plotting the cube of the mean particle radius against time, see figure 22. A linear regression line was applied to determine the linearity of the experimental data.
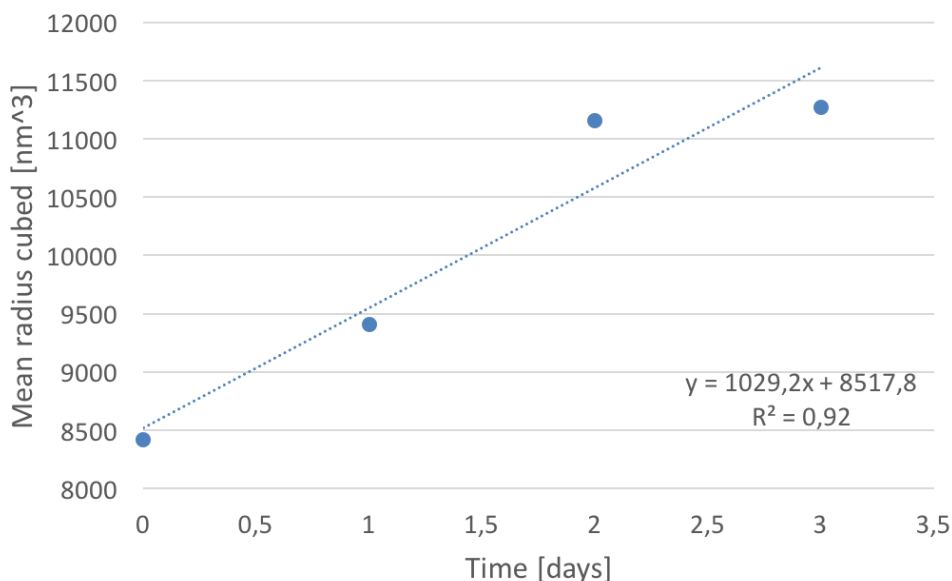
Figure 22: *The figure shows a plot of the cube of the mean particle radius (PHAT 122) for four time points since synthesis of ZS measurement. A linear regression model is used for determining the linearity of the experimental data.*

4.1.4   Lipid nanoparticle optimization summarized

Systematic variations in surfactant system, SA and IPP ratio and amount, method of emulsification and cooling were performed in the preceeding particle synthesis experiments. The lipid NP formulation, showing the highest stability and lowest particle size was found for particles containing 0.8g SA, 0.2g IPP, 0.24g QDP, 0.06g P80H (was used in PHAT 107, PHAT 122 and PHAT 115). This formulation will be referred to as NLC#2 particles throughout the rest of this thesis. NLC#2 was produced multiple times for use in cell experiments, with and without the presence of loading material. Figure 23 shows particle size increase during the first 3 days after synthesis, for NLC#2 particles. The standard deviations are calculated from three independent experiments.
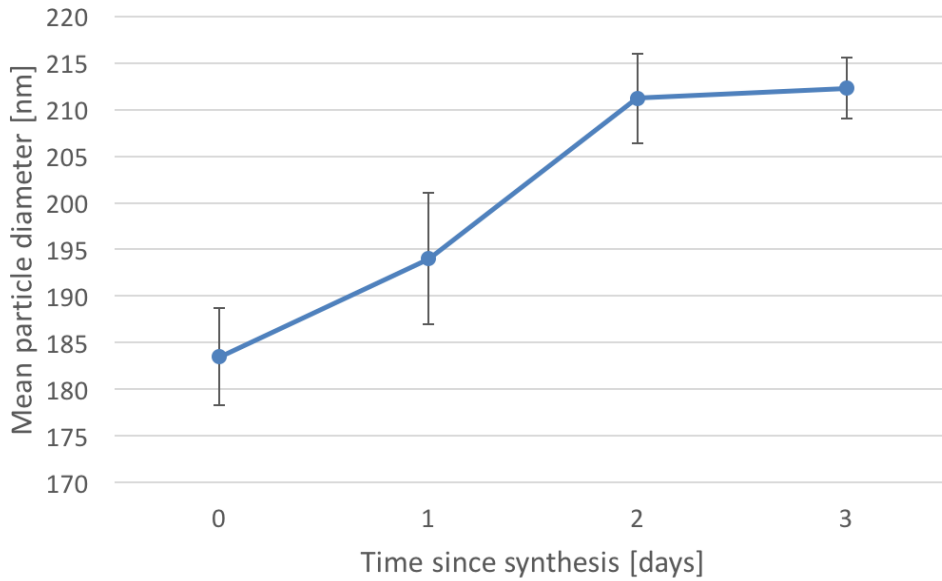
Figure 23: *Zetasizer results of mean particle size measurements of NLC#2 particles at four time points. The standard deviation is calculated from three independent experiments.*

Differences between old and new synthesis protocol is shown in table 1 found in section 3.1.1. Particle size distribution for NLC#1 and NLC#2 are shown in figure 24. The average particle size has been reduced from about 250-270nm to 180-190nm in initial particle diameter.
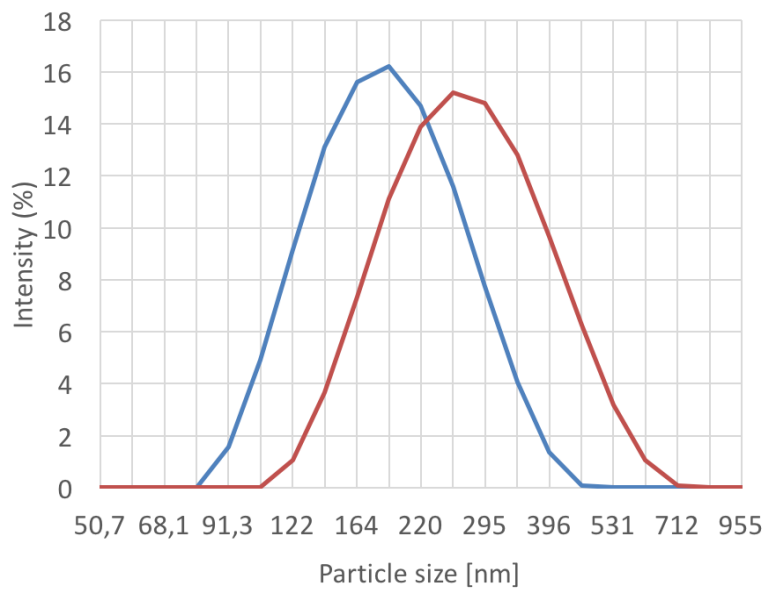
Figure 24: *Typical particle size distribution for NLC#1 particle (red graph) and NLC#2 particles (blue graph)*

53

NLC#2 particles developed throughout this project has a significantly higher stability in various media compared to NLC#1 particles. Prior to this project, stability tests on NLC#1 particles had been conducted at Sintef Materials and Chemistry (unpublished results). The particles were subjected to various different types of media, a few of these were also used for stability testing of batch PHAT 122 in this project. The results generally showed low stability for NLC#1 particles dispersed in media. NP solutions stored in fridge were stable for 3-24 hours, but swelled constantly, while at 37°C all NP solutions showed visual signs of degradation within 3 hours.

Mean size and distribution of all particles involved in cell experiments of this project was only measured directly after synthesis, and not monitored over time as in the previous particle optimization experiments. The results of these measurements can be found in appendix C.1.

4.2 Uptake studies

4.2.1 Cellular uptake of fluorescent dye encapsulated in lipid nanoparticles

Uptake of fluorescent dye encapsulated in lipid nanoparticles made with synthesis protocol#1 and #2 (NLC#1 and NLC#2)were measured with flow cytometry. Both particle types tested had the same amount of NR668 encapsulated. For all uptake studies, A431 cells were incubated with nanoparticles for either 3,6,24 or 48 hours at 37°C.

Initially, NLC#1 particles encapsulating NR668 (0.5wt% of the oil phase), were incubated with cells for 1, 3, 6, 24 and 48 hours. A histogram with one of the three parallels from each time point is seen in figure 25. Shift in mean fluorescence after each time point can be seen in figure 26. The mean fluorescence is calculated from three parallels of each experiment. Standard deviation between parallels of each experiment is also included in the chart. It can be seen that the uptake of dye in the cells is almost linear during 48 hours of incubation with fluorescently labeled NPs (NLC#1). The linear regression line in figure 26 has a slope of ≈ 0.16. Compared to uptake after 1 hour of incubation, cellular uptake after 24 and 48 hours is 20 and 40 times higher, respectively.
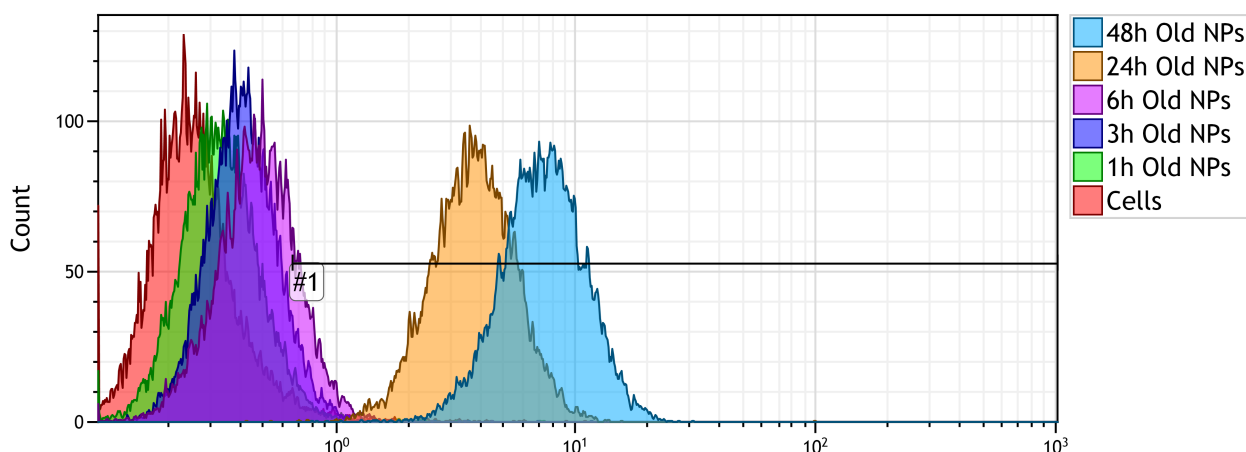
Figure 25: *Logaritmic FCM histogram of uptake of NR668 by cells incubated for 1, 3, 6, 24 and 48 hours with NLC#1 particles. The gate (labelled #1) is set at approximately 3,3% false positive cells and captures 100%, 99.98%, 18.28%,7.84% and 3.67% of the cells incubated with NPs for 48, 24, 6, 3 and 1 hour(s) respectively.*
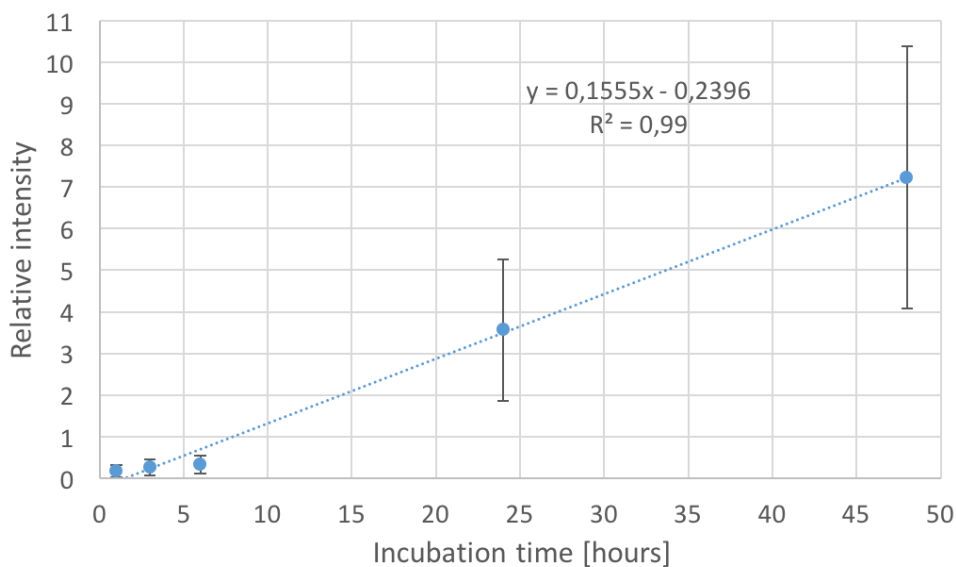
Figure 26: *Relative mean fluorescence intensity for cells incubated with NLC#1 particles for 1, 3, 6, 24 and 48 hours. The values and standard deviations are calculated from 3 parallels in one experiment. Autofluorescence has been substracted.*

Equivalent FCM measurements were performed on cells incubated with particles made with synthesis protocol#2. A histogram with one of the three parallels from each time point is seen in figure 27. Already here it can be seen that fluorescence intensity is a lot higher for all time points equivalent to the FCM performed on cells incubated with NLC#1 particles.

Shift in mean fluorescence after each time point can be seen in figure 28. The mean fluorescence is calculated from three parallels of each experiment As was seen in FCM with the NLC#1 particles, uptake of dye in the cells is almost linear during 48 hours of incubation with fluorescently labeled NLC#2 particles too. But here, the slope of the linear regression line is almost three times steeper ($\approx$0.42) than for NLC#1 particles, indicating a higher rate of cellular uptake.
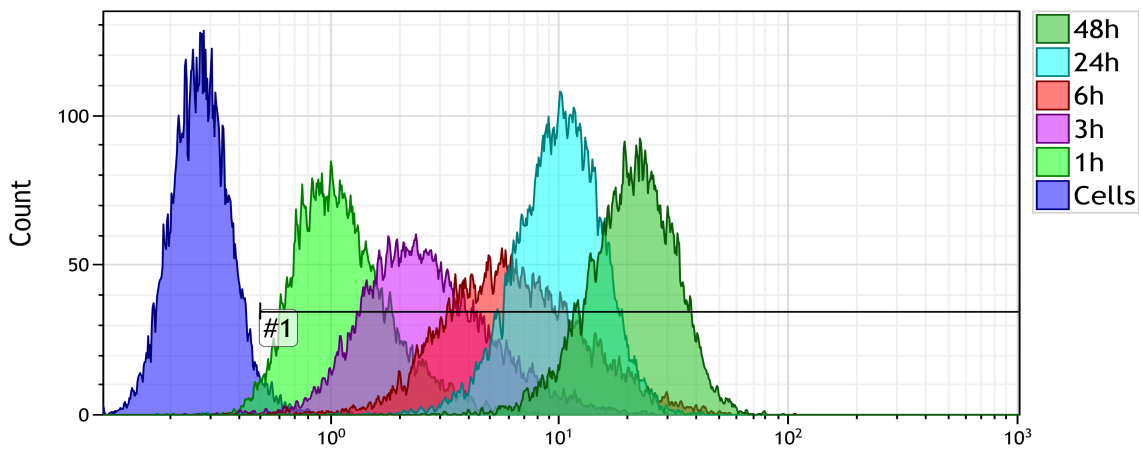
Figure 27: *Logaritmic FCM histogram of uptake of NR668 by cells incubated for 1, 3, 6, 24 and 48 hours with NLC#2 particles. The gate (labelled #1) is set at approximately 3% false positive cells and captures 100%, 99.9%, 99.9% and 99.7%, 98.3% of the cells incubated with NPs for 48, 24, 6, 3 and 1 hour(s) respectively.*
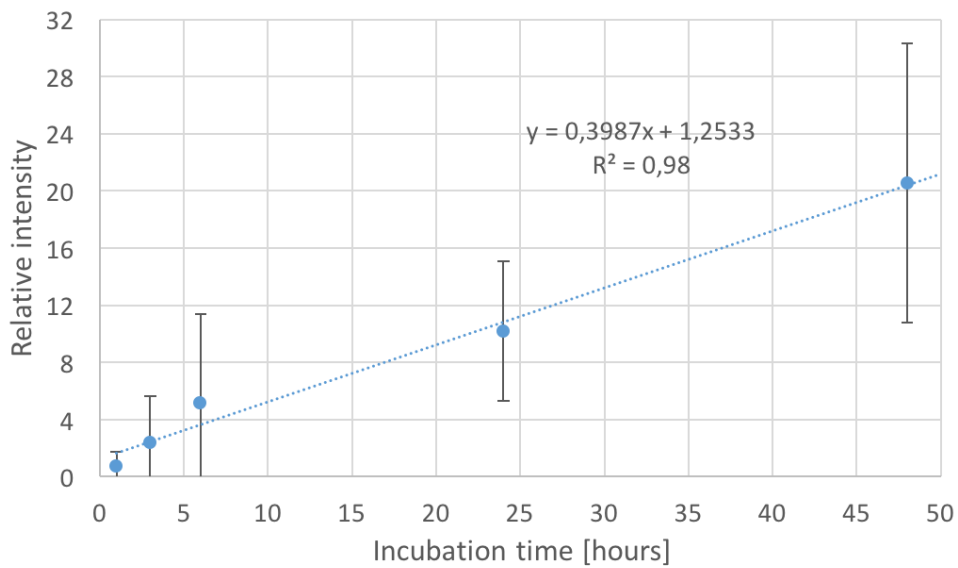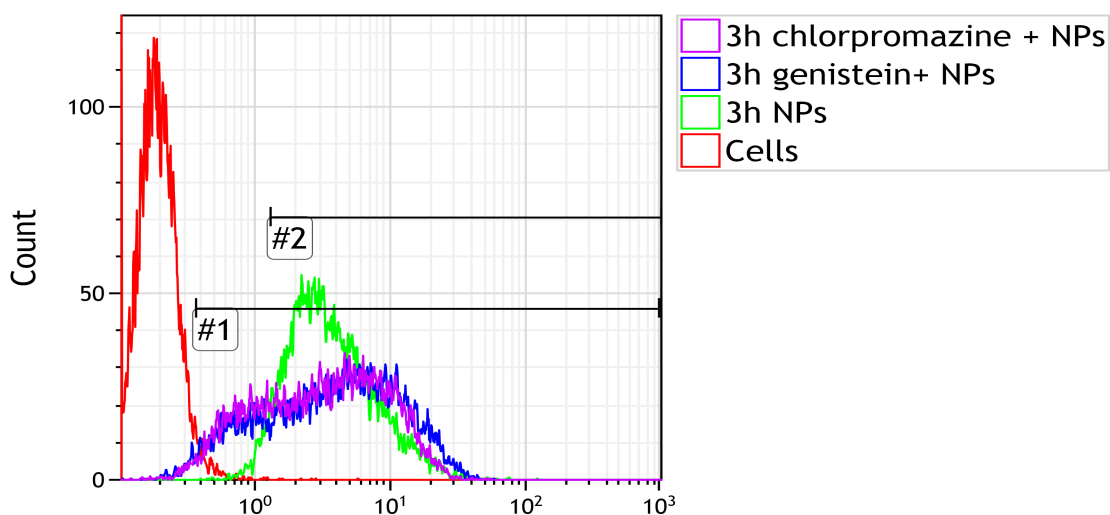

Figure 28: *Relative mean fluorescence intensity for cells incubated with NLC#2 particles for 1, 3, 6, 24 and 48 hours. The values and standard deviations are calculated from 3 parallels in one experiment. Autofluorescence has been substracted.*

4.2.2 Uptake mechanism

To better understand the cellular uptake mechanism of NR668, cells were incubated with endocytosis inhibitors prior to uptake experiments with NPs. The two inhibitors, Chlorpromazine and Genistein, inhibit CME and CvME respectively. NPs produced with synthesis protocol#2 were used for these measurements.

Figure 29 shows the resulting histograms of uptake under suppression of inhibitors. For both samples with endocytosis inhibitors, the fluorescence intensity is significantly higher than the cells autofluorescence, indicating cellular uptake has not been inhibited to a very large degree. Gate#1 is set to ≈3% positive cells (autofluorescence), and includes the percentage value of each population with fluorescence intensity above the gate starting point. The data from cells with suppressing inhibitors do not overlap completely with the cells that have been incubated only with NPs. CME and caveolin mediated endocytosis are thus not main mechanisms of cellular uptake. A dip in both graphs of suppressed cells can be seen in figure 29. Gate #2 includes all cells with fluorescence intensity above the area of the observed dip. Figure 30 shows the percentage of cells in each population with fluorescence intensity values in the area of gate#1 - gate#2. The area entraps approximately 3%, 5%, 20% and 24% of the four populations treated with only DMEM, NPs, NPs + Genistein and NPs + Chlorpromazine, respectively. In the FCM measurements of this project, 10000 cells are recorded in each parallel of each experiment, further gating reduces the amount of cells to approximately 8000-9000 cells. Assuming the measured cell populations have the same size, about 15% and 19% of the cells pretreated with Genistein and Chlorpromazine respectively, have been affected by the endocytosis inhibitors.

Figure 29: *Relative mean fluorescence intensity for cells pretreated with endocytosis inhibitors Genistein and Chlorpromazine. The gate (labeled #1) is set at approximately 3% false positive cells and captures 100%, 98.2% and 997.8% of the cells incubated with NPs, NPs + Genistein and NPs + Chlorpromazine respectively. Gate #2 captures 0.06%, 94.7%, 77.2% and 74.0% of cells autofluorescence, cells incubated with NPs, NPs + Genistein and NPs + Chlorpromazine respectively.*

.
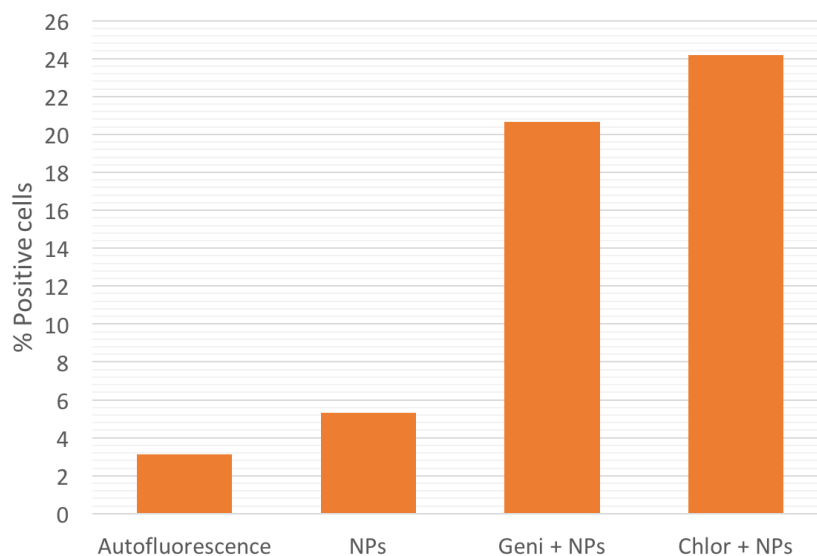
Figure 30: *Flow cytometric analysis of cells incubated with (I) only growth media (autofluorescence), (II) NLC#2 nanoparticles, (III) Genistein and NPs and (IV) Chlorpromazine and NPs. The percentage value refers to the percent positive cells out of 10,000 cells analyzed that have fluorescence intensity in the area of gate#1-gate#2, marked in figure 29.*

4.3 Spectral analysis of NR668

In order to properly interpret the results of FCM, emission spectra of the fluorescent dye NR668 was recorded using a multi-modal plate reader. In flow cytometry experiments performed in this project, the dye is initially encapsulated in lipid nanoparticles and incubated with cells before fluorescence intensity measurements are performed at various time points after NP/cell incubation. From start to end of each experiment the dye is exposed to storage at 4°C, incubation at 37°C, encapsulation in NPs and release into growth media or cytosol. The effect of changes in media and temperature were to be investigated by spectral analysis of NR668. The setup for spectral analysis of NR668 therefore included both dye encapsulated in lipid NPs (NLC#2) and free dye, both with parallels stored at 4 and 37°C, giving four different samples. Potential changes in spectral properties over time were also taken into account, by recording emission after 1, 3, 6, 24 and 48 hours of storage. Three parallels of each sample were made, the results presented in this section is based on the average of three parallels from each recording.

Emission spectra recorded at various time points for the four solutions are presented graphically below in four separate figures.
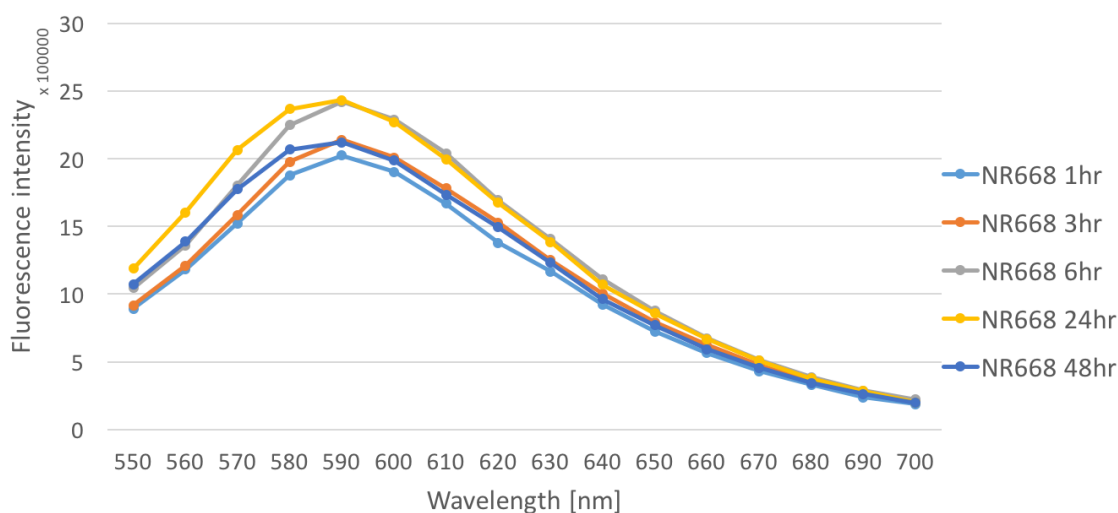
Figure 31: *Emission spectra of free NR668 in growth media, stored at 4°C. There recordings from different time points are almost overlapping, the intensity peak occurs around 590nm in wavelenth for all recordings.*
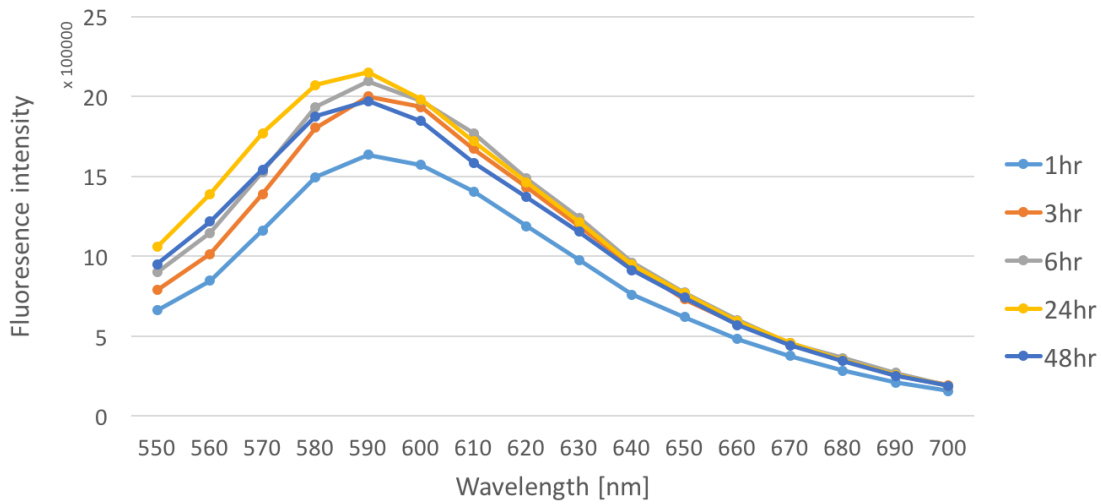
Figure 32: *Emission spectra of free NR668 in growth media, stored at 37°C. There recordings from different time points are almost overlapping, the intensity peak occurs around 590nm in wavelenth for all recordings.*

Figure 31 show the emission spectra of free NR668, stored at 4°C, in DMEM at different time points of recording. The peak fluorescence intensity occurs around 590nm in wavelength for all five time points. The spectra of the five measurements are almost overlapping, indicating that spectral properties of free NR668 in DMEM does not change significantly during 2 days of storage at 4°C. For free NR668, stored at 37°C, the results are very similar, shown in figure 32. Recordings from all time points nearly overlap, and intensity peaks occur around 590nm wavelength.
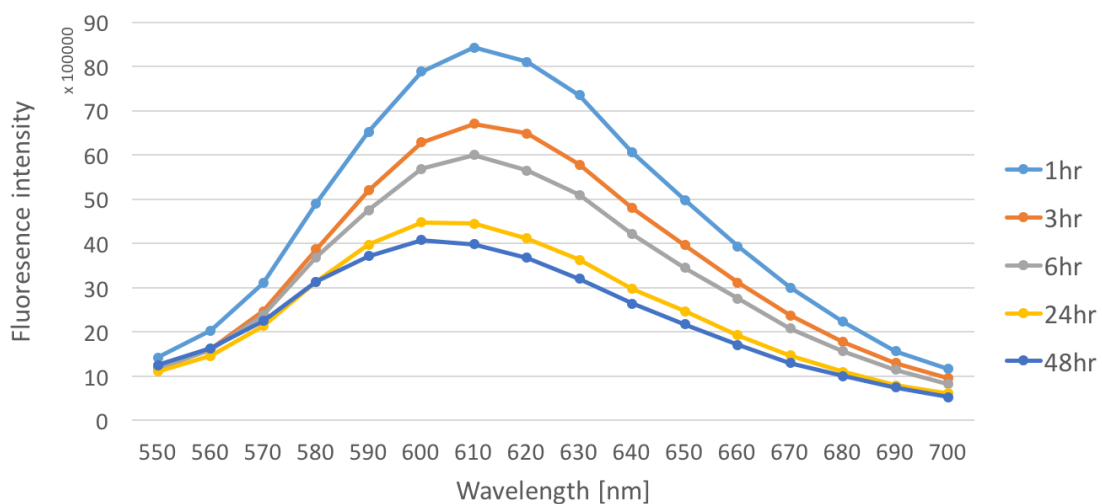
Figure 33: *Emission spectra of NR668 encapsulated in lipid nanoparticles, stored at 4°C. Fluorescence intensity decreases with time and a blueshift in emission peak is observed.*

61
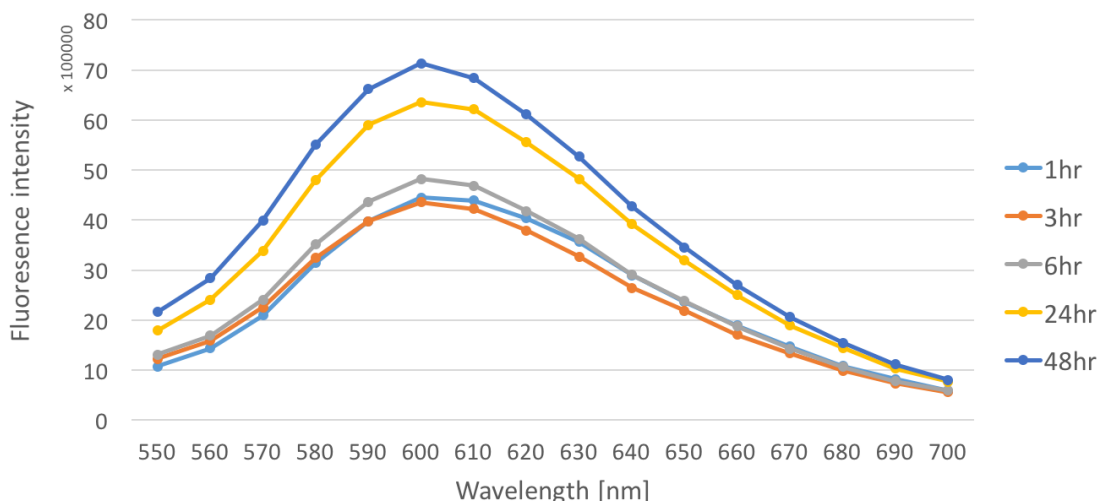
Figure 34: *Emission spectra of NR668 encapsulated in lipid nanoparticles, stored at 37° C. Fluorescence intensity increases with time, while the emission peak occurs in the same wavelenght area for all recordings*

Figure 33 and 34 show emission spectra of NR668 encapsulated in lipid particles, stored at °C4 and 37°C respectively. For particles stored at 4°C, the fluorescence intensity decreases over time. While peak in fluorescence intensity shifts from about 610nm to 600nm in wavelength over a time period of 2 days, see figure 33.

The opposite effect in fluorescence intensity occurs for particles stored at 37°C. As figure 34 shows, the intensity increases as a function of time, while the emission peak occurs around 600nm in wavelength for all recorded time points.
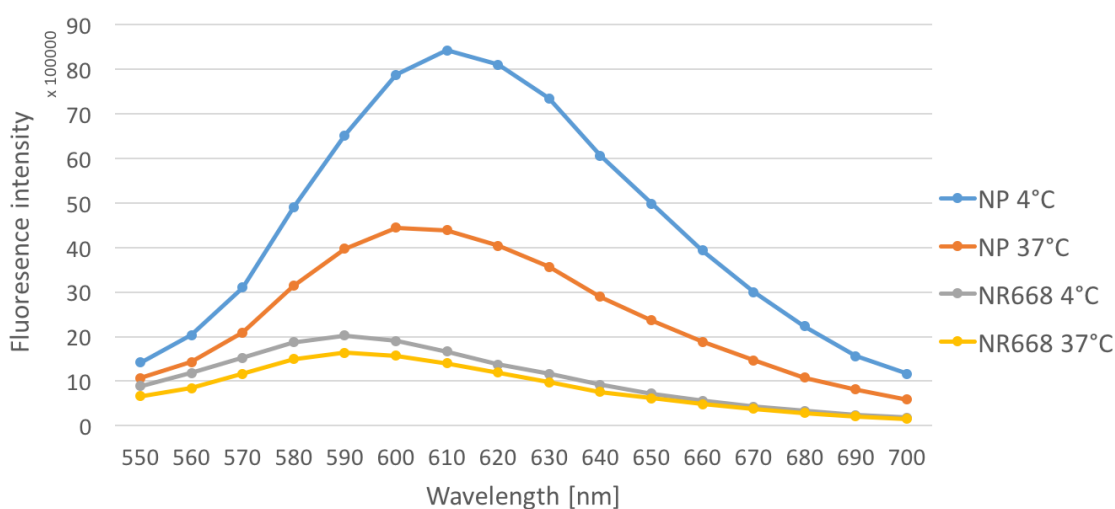
Figure 35: *Emission spectra of free and encapsulated NR668, stored at 4° C and 37° C for 1 hour.*
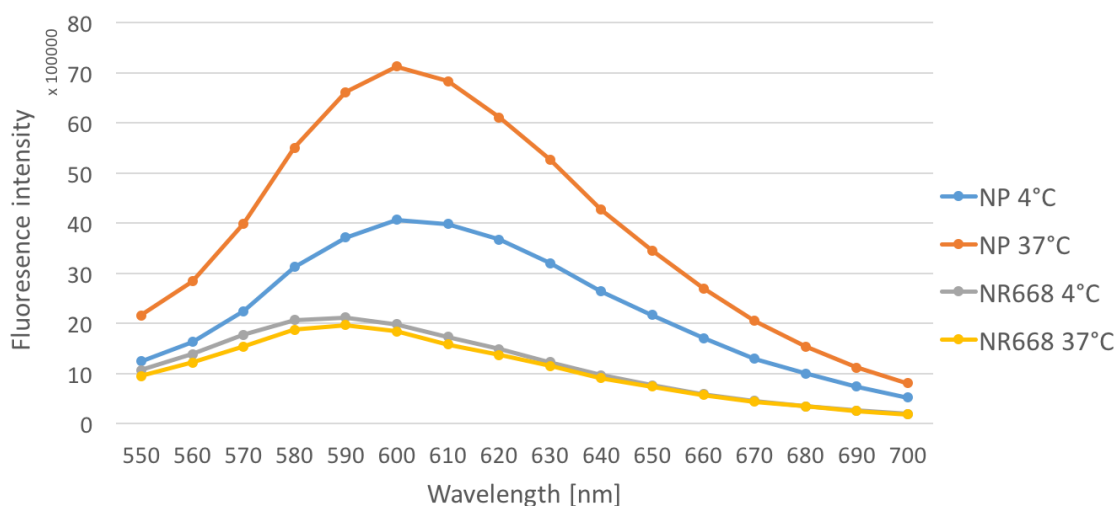
Figure 36: *Emission spectra from free and encapsulated NR668, stored at 4°C and 37°C for 48 hour.*

.

In figure 35 and 36 the emission spectra of all four solutions are plotted at time points 1 and 48 hours respectively. The emission spectra for free NR688 is relatively invariant after both 1 and 48 hours, at 4 and 37°C. The emission peak occurs around 590nm in wavelength for all four recordings. While for encapsulated NR668, after 1 hour (figure 35), the fluorescence intensity is almost twice as high for particles stored at 4°C compared to those stored at 37°C. And as seen earlier, the intensity peak occurs at shorter wavelengths (around 600nm) for particles stored at 37°C, than for those stored at 4°C (610nm).

After 48 hours the opposite fluorescence intensity of NPs can be seen (figure 36). NPs stored at 37°C have almost twice as high intensity as those stored at 4°C.

4.4 *In vitro* EGFR inhibition- and NP toxicity testing

The effect of EGFR tyrosine kinase inhibitors and lipid NPs on cell viability was tested using CellTiter Glo luminescent cell viability assay. Prior to the toxicity testing, solubility of five different kinase inhibitors in IPP was investigated in order to determine which were most suitable for encapsulation in lipid nanoparticles.

4.4.1 Solubilitytesting of kinase inhibitors

In order to encapsulate a substance into lipid nanoparticles in an emulsion process, it is essential that the loading compound is lipophilic for it to end up inside the particles, not in the surrounding media. Solubility-testing of five substances, that were all types of TKIs, was performed in this project. In short solubility was determined in a step-wise procedure that involved dissolving powdered kinase inhibitors in IPP using a sequence of mechanical procedures. The start concentration of kinase inhibitor in IPP was 2.5wt% in all five solutions, but further dilution was necessary in all cases to dissolve the compounds.

- Erlotinib-HCl in IPP: At a concentration of 0.625wt%, the solution looked cloudy, some small particles were visible. Further dilution was not performed as such a low concentration of kinase inhibitor in NPs would not have efficient therapeutic effect.

- Gefitinib in IPP: At a concentration of 1.25wt%, the solution looked clear, no particles visible.

- Lapatinib in IPP: At a concentration of 1.25wt%, the solution looked clear, no particles visible.

- SB6-140-05 in IPP: At a concentration of 0.625wt%, the solution looked cloudy, with only a few particles visible.

- JH08-096 in IPP: At a concentration of 0.625wt%, the solution looked cloudy, with only a few particles visible.

- The reference solution of the hydrophobic dye NR668 (2.5wt%) in IPP looked clear immediately, no mixing or dilution was necessary for the dye to dissolve.

Out of the five solutions containing TKIs, Gefitinib and Lapatinib reached dissolution at the highest concentration and with the lowest number of process steps. Due to cost and availability, Gefitinib was chosen out of the two substances for use in further toxicity tests.

4.4.2 Effect of EGFR inhibitor and NPs on cell viability

In vitro EGFR inhibition activity was tested for the most oil soluble compound (Gefitinib) out of the five TKIs, both in free and NP encapsulated form (NLC#2). In addition, toxicity of empty NLC#2 particles were analyzed. All viability tests were performed using CellTiter Glo luminescent cell viability assay, analyzed by SpectraMax i3x Multi-mode microplate reader.

The three microplates used in the experiment all had the same experimental setup, but different incubation times. The eight rows of each microplate contained solutions of A431 cells in DMEM with either empty NPs, NPs encapsulating Gefitinib (at three different concentrations), DMSO with Gefitinib, or pure DMSO. The concentration of cells were the same in all microplate wells, while the concentration of the compounds of interest deceased along each row, ending in the last column containing only cells in growth media, DMEM (see section 3.6.2 for setup and concentration of samples in the microwells).

Table 13, 14 and 15 found in appendix D.1 show percent cell viability in each well of the three microwell plates. The value describing viability, seen in both the mentioned tables and in the following figures, is based on comparison with a reference consisting of the average luminescence signal intensity originating from cells incubated in only growth media. The last column of all three microplates contain only cells and growth media, the reference viability value is calculated from luminescence signal from the eight microwells in the last column of each microplate in each experiment.

Figure 37 and 38 show viability of cells incubated with DMSO or DMSO+Gefitinib for 24 and 72 hours, respectively. The DMSO was diluted in DMEM in a 2-fold serial manner along the row in the microwell plate, thus Gefitinib dissolved in DMSO was also diluted to the same degree.

After 24 hours of incubation, viability of cells incubated with DMSO remains relatively stable around $100\%\pm20\%$ for all concentrations of DMSO. The lowest viability value ($\approx80\%$) is recorded at low concentrations of DMSO, which is most likely due to small variations in cell concentration, and is not a result of DMSO toxicity. Cells incubated for 24 hours with DMSO and Gefitinib have a decreasing viability from $\approx80\%$ to $\approx13\%$ for increasing concentrations of DMSO/Gefitinib-solution, indicat-

65

ing a concentration dependent toxicity of Gefitinib on A431 cells, figure 37.

After 72 hours of incubation, viability of cells incubated with DMSO decreases from about 100% to 20% with increasing concentrations of DMSO (figure 38). While cells incubated with DMSO and Gefitinib has a decreasing viability from 80% to $\approx$2% for increasing concentrations of DMSO/Gefitinib-solution. These results show that Gefitinib has a toxic effect on A431 cells. In addition, cultivation of cells with high concentrations of DMSO for 72 hours also reduces the cell viability significantly. Similar results were found after 48 hours of incubation with DMSO and DMSO/Gefitinib, these can be found in appendix D.1, figure 45.
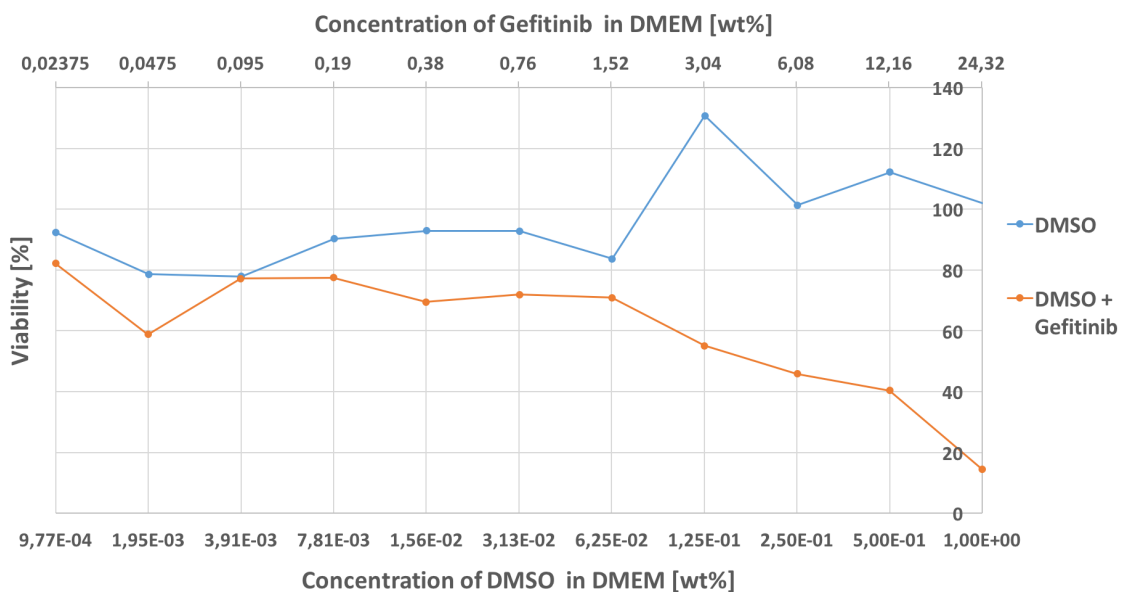
Figure 37: *Luminescence recording showing viability of cells that have been incubated for 24 hours with DMSO and DMSO w/ Gefitinib. The concentration of DMSO was reduced in a 2-fold serial dilution manner, with 1% DMSO as starting concentration. Gefitibib dissolved in DMSO was thus diluted to the same degree, with starting concentration of 24,5μg/ml. NB: notice there are two x-axes, and neither is not linear. They are based on the concentration of DMSO and Gefitinib from 2-fold serial dilution i DMEM.*
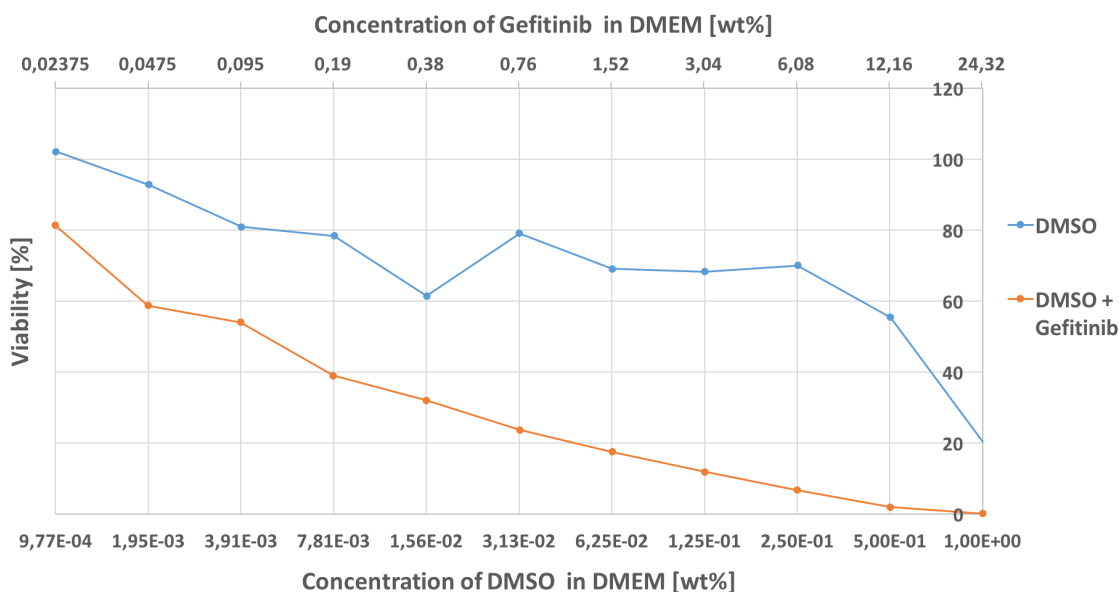
Figure 38: *The figure shows viability of cells that have been incubated for 72 hours with DMSO and DMSO with Gefitinib. The concentration of DMSO was reduced in a 2-fold serial dilution manner, with 1% DMSO as starting concentration. Gefitibib dissolved in DMSO was thus diluted to the same degree, with starting concentration of 24,5µg/ml.*

Figure 39 and 40 show the viability results of cells incubated for 24 and 72 hours with DMSO/Gefitinib-solution and NPs containing 2.5wt% Gefitinib. The concentration of Gefitinib dissolved in DMSO was 0.117wt%, and was constant in all the viability experiments with DMSO/Gefitinib solution. This concentration is the same as the total concentration of Gefitinib in a undiluted particle batch with 2.5wt% Gefitinib (concentration in the oil phase). Comparing the viability results of free and encapsulated Gefitinib can be used to verify whether the NPs themselves or Gefitinib is the most cytotoxic. In figure 39 it can be seen that after 24 hours of incubation with either loaded NPs or free Gefitinib, cells have a viability around 60-80% for low concentrations of Gefitinib in both cases. For higher concentrations, the viability decreases, especially for cells incubated with NPs.

After 72 hours of incubation with either NPs containing Gefitinib or DMSO with dissolved Gefitinib (figure 40), a decrease in viability from about 80% to 0% viability with increasing concentrations of Gefitinib can be seen for both samples. The results of incubation with the same solutions for 48 hours can be found in appendix D.1, figure 46. Viability results from all three time points show that NPs w/ Gefitinib has higher toxicity at high concentrations than DMSO w/Gefitinib, this indicates that the NPs themselves are toxic. This effect was more evident for shorter incubation times.
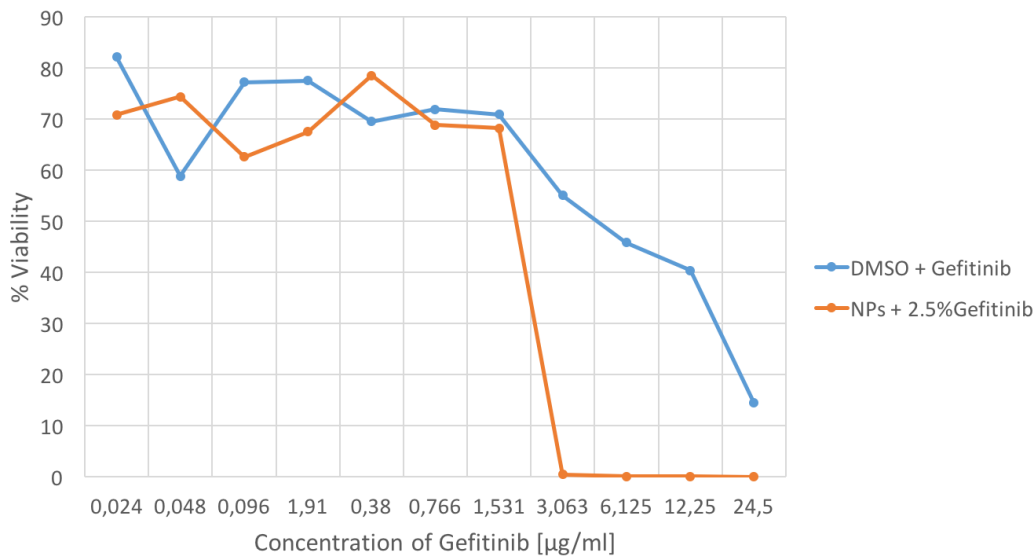
Figure 39: *Luminescence recording showing viability of cells that have been incubated for 24 hours with DMSO/Gefitinib or with nanoparticles containing Gefitinib. The starting concentration of DMSO and NPs in DMEM was 1% and 1000µg/ml, respectively. Both samples followed a 2-fold serial dilution, giving the same degree of cancentration decease for Gefitinib, DMSO and NPs. NB: notice the x-axis is not linear, but based on the concentration of Gefitinib from 2-fold serial dilution.*
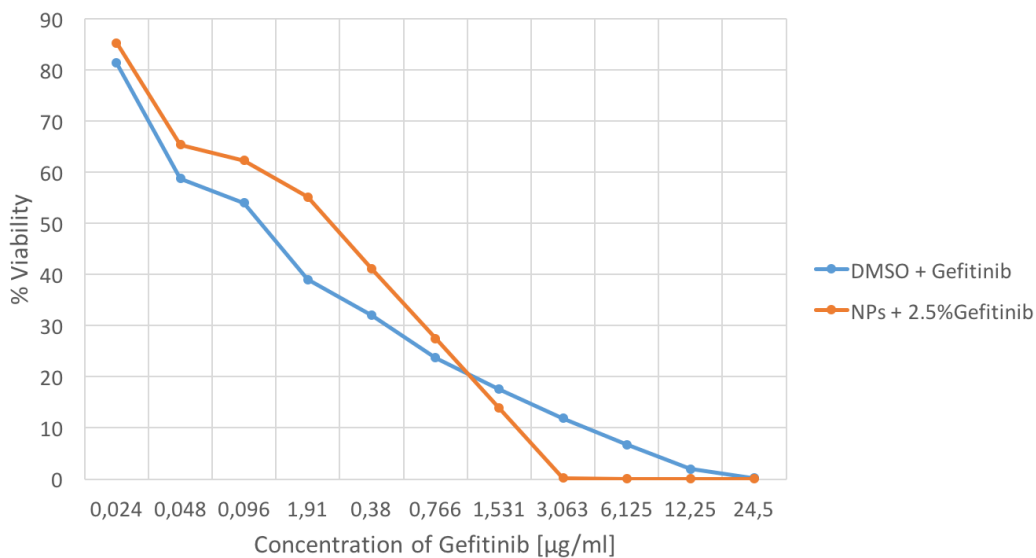
Figure 40: *Luminescence recording showing viability of cells that have been incubated for 72 hours with DMSO/Gefitinib or with NPs containg Gefitinib. The starting concentration of DMSO and NPs in DMEM was 1% and 1000µg/ml, respectively. Both samples followed a 2-fold serial dilution, giving the same degree of cancentration decease for Gefitinib, DMSO and NPs.*

68

Figure 41 shows viability of cells after 72 hours of incubation with NP encapsulating different amounts of Gefitinib (0wt%, 1wt%, 2.5wt%, 5wt%). For low concentrations of NPs, higher loading concentration with Gefitinib is shown to be more toxic. There is a steady decrease in viability for all samples with nanoparticle concentration increasing from ≈ 0 up to 62.5 μg/ml. There is zero cell viability above the NP concentration of 125 μg/ml for all samples.

What is especially important to notice from the figure is the high toxicity of empty NPs. At a concentration of about 15μg/ml NPs, the cell viability is just below 80%, and it decreases to $\approx$0% at 125μg/ml NPs.

Similar results showing high toxicity for high concentrations of NPs were observed for the same solutions incubated with cells for 24 and 48 hours, these can be found in appendix D.1, figure 47 and 48.
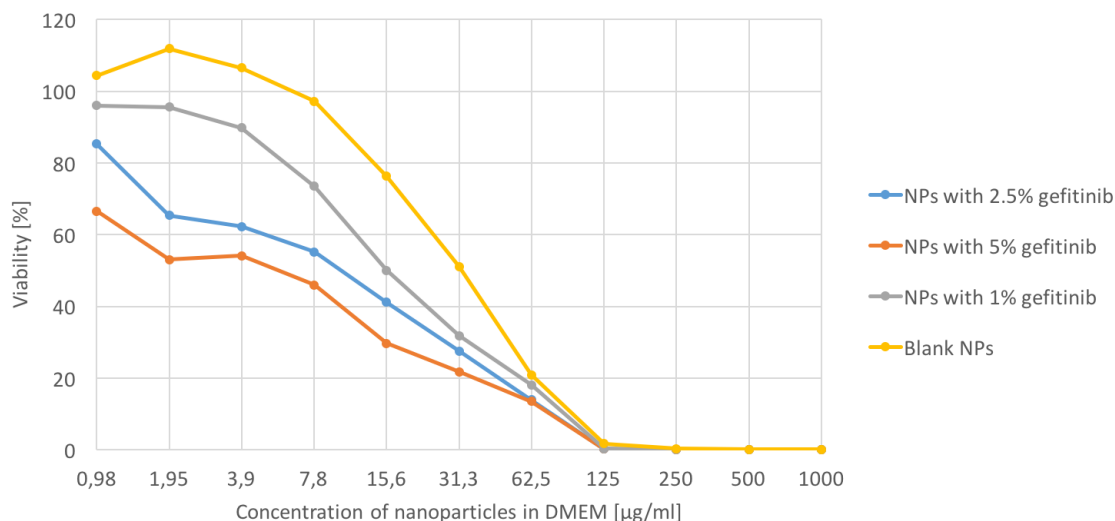
Figure 41: *Luminescence recording showing viability of cells that have been incubated for 72 hours with nanoparticlesencapsulating Gefitinib at three different concentrations. NB: notice the x-axis is not linear, but based on the concentration of nanoparticles from 2-fold serial dilution.*

In the three following figures (figure 42, 43 and 44), toxicity of NPs containing Gefitinib (1wt%, 2.5wt% and 5wt% respectively) at three different times of measurement are presented.

The results show the same tendencies for all three concentrations of loading compound, Gefitinib. It can be seen that the viability is generally significantly higher for cells incubated with NPs at concentrations between $\approx$15 and 60μg/ml for 24 hours, compared to 48 or 72 hours. After 48 and 72 hours of incubation there is a steady decrease in cell viability with increasing NP concentration. While for 24

hours of incubation, there is a sudden drop in viability with nanoparticle concentration 60-125μg/ml. There is zero cell viability above the NP concentration of 125 μg/ml for all samples, at all time points.

Figure 42: *Luminescence recording showing viability of cells that have been incubated for 24, 48 and 72 hours with nanoparticles containing 1wt%Gefitinib.*
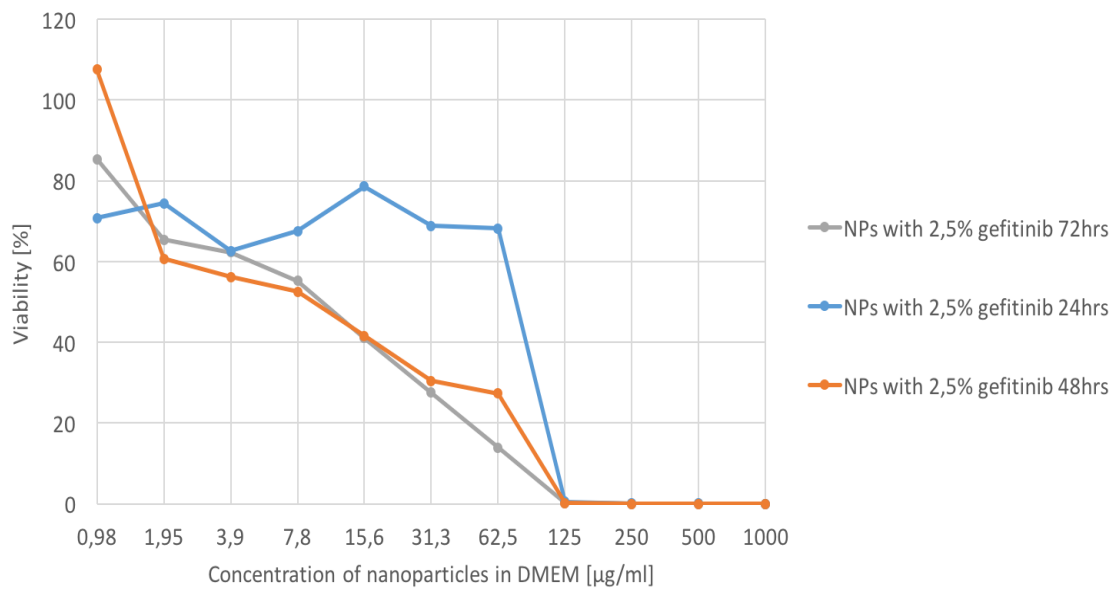
Figure 43: *Luminescence recording showing viability of cells that have been incubated for 24, 48 and 72 hours with nanoparticles containing 2.5wt%Gefitinib.*
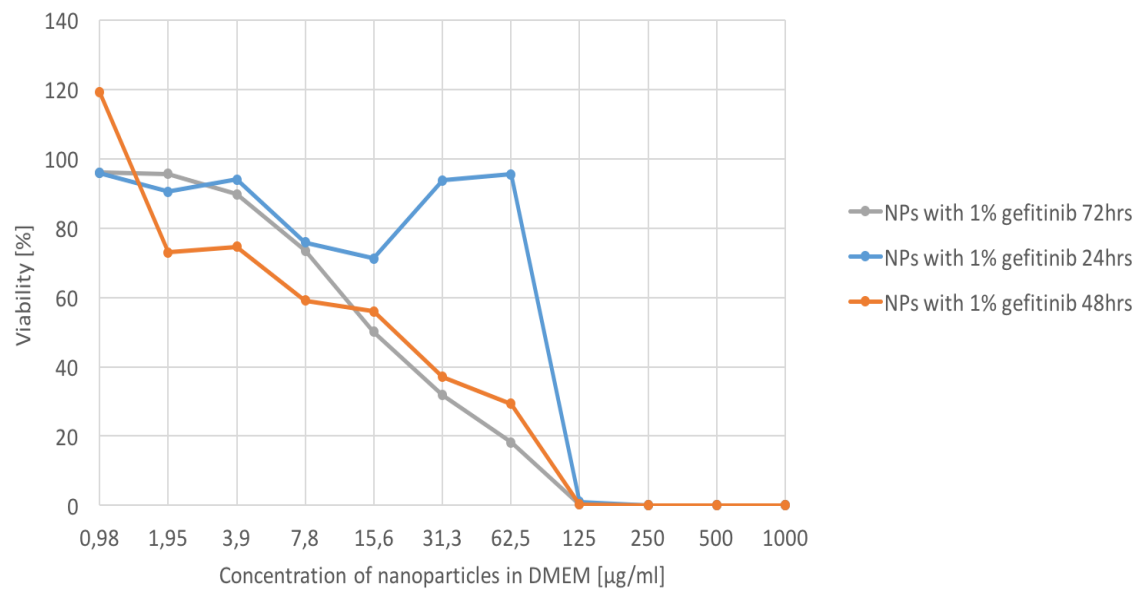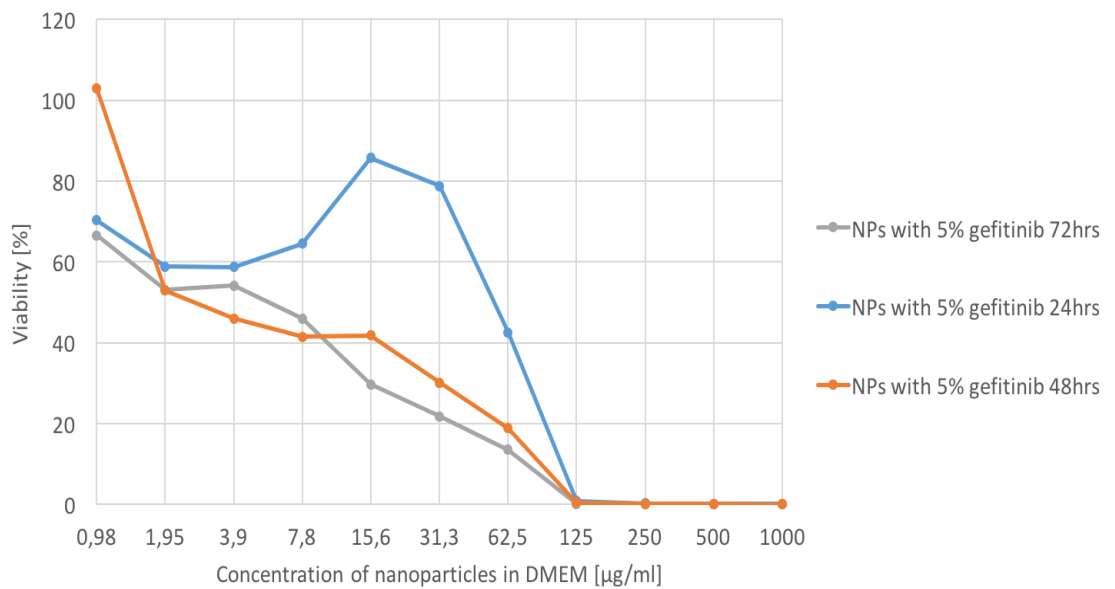

Figure 44: *Luminescence recording showing viability of cells that have been incubated for 24, 48 and 72 hours with nanoparticles containing 5wt% Gefitinib.*

5 Discussion

This thesis describes the work done in this project towards synthesizing stable lipid nanoparticles that can encapsulate chemotherapeutic drugs and fluorophores, as well as testing the toxicity and uptake of these particles in cells. The particles can potentially be applied as drug delivery systems in cancer therapy. The discussion section is divided into three parts, optimization of lipid NP stability and size (section 5.1), cellular uptake (section 5.2) and toxicity of NPs and kinase inhibitor (section 5.4).

5.1 Optimization of nanoparticle stability and size

Throughout the particle optimization process of this project, the goal has been to optimize a system where SA and IPP are always included in the particle composition, while other materials and process steps are varied. Therefore, if a change in a process step or surfactant composition does not seem compatible to SA and IPP by evaluation of ZS measurements, it is rejected.

Even though there is a large amount of literature available on SLNs, there is little on the mechanisms underlying NLC systems. Possible explanations presented in this section are therefore only attempts to justify the experimental results.

5.1.1 First generation lipid nanoparticles

In the first part of this project, lipid nanoparticles were synthesized following the particle synthesis protocol (particle synthesis protocol#1) used at Sintef Materials and Chemistry prior to development of a new protocol in this project.

The results of ZS measurements of particle batch NLP 1 and NLP 3, where the only compositional difference is presence of loading material curcumin in NLP 3, show that NPs immediately after synthesis are in the range of 230-245nm in mean particle diameter. Lipid nanoparticles produced at Sintef prior to this project have shown to be larger than the favorable particle size, as well as having limitations in stability, especially in a biological environment (unpublished results). These limitations were verified, by synthesis and ZS analysis of particle batch NLP 1 and NLP 3. Relatively monodisperse particle distribution of was found for both batches (<0.2 in PDI at all three time points). Over a time period of 48 hours the particles increased in diameter from ≈237nm to ≈272nm on average, which is a 15% size increase. The underlying mechanism of this size increase will be discussed in section 5.1.3.

5.1.2   Second generation lipid nanoparticles

As an attempt to improve nanoparticle stability and reduce particle size, systematic variations to the particle synthesis protocol were tested; amount and ratio of SA and IPP, surfactant type and concentration, and method of emulsification and cooling.

Selection of surfactant and SA:IPP ratio and amount

In particle batch PHAT 95-98 the surfactant P80H was used instead of Tween 80, and concentration and ratio of SA:IPP was varied. PHAT 96 and 98 contained twice as much lipids and surfactant as PHAT 95 and 97. ZS measurements of PHAT 96 and 98 resulted in particles with mean diameter in the same size range as the NLC#1 particles. Because there was no improvement in particle size, PHAT 96 and 98 as were discarded. Variations in ratio and amount of lipid and oil in NLCs may affect physiochemical properties of the nanoparticles, such as average diameter, particle distribution and loading efficiency [86]. High lipid content is known to result in large particles and broad particle size distributions. The phenomena is largely based on decreased efficiency of homogenization and increased agglomeration with high lipid content [87].

Lower concentration of surfactant and lipids resulted in smaller particles for batches PHAT 95 and 97. In particle batch PHAT 97, the only compositional difference from first generation lipid NPs (used in batch NLP 1) was the type of surfactant used. The change from surfactant Tween 80 to P80H resulted ≈60nm reduction in average particle diameter. It is well documented in the literature that surfactant properties can have a great effect on particle size and stability of the particle solution [88] [89]. The choice of surfactant and liquid/solid lipid ratio in particle batches PHAT 95-98 was mainly based on results presented in an article by Salminen, et al., 2014 [90], where nanostructured lipid nanocarriers of tristearine and ω- 3 fish oil with small particle size and high stability were produced. Surfactant concentration and protocol for particle synthesis with P80H was found in the paper.

Due to a slightly higher stability of PHAT 95 than PHAT 97, the formulation used in PHAT 95 was chosen for subsequent experiments with dye/model drug encapsulated. Two highly hydrophobic materials NR668 (fluorescent dye) and curcumin (model drug) were encapsulated in particle batches PHAT 99-102, at two different concentrations. All four batches resulted in ZS measurements showing slightly larger initial particle size compared to PHAT 95. The small difference in initial particle size is likely due to the presence of drug/dye in the NPs. Particle size increase over

the first 4 days was in the range of 10-23% for all four batches, indicating similar stability as empty particles (PHAT 95 had a 9% increase the first two days). PHAT 99/100 contained curcumin (0.5wt% and 1wt% respectively), while PHAT 101/102 contained NR688 (0.5wt% and 1wt% respectively).

Even though the results of zetasizer measurements for both empty and drug/dye-loaded particles (PHAT 95 and PHAT 99-102) showed a decrease in particle size and increase in stability compared to NLC#1 particles, other limitations were introduced in relation to using P80H alone, as surfactant. In the process of particle synthesis, the surfactant P80H is dissolved in water while being kept in a water bath and mixed using a magnetic stir bar. This step of surfactant dissolution is very time consuming when using only P80H as surfactant, it takes up to 90 minutes before the surfactant is properly dissolved. One of the challenges in commercializing pharmaceutical nanoparticles is to produce nanoscale systems in mass quantities, at a cheap and time-effective manner [91]. Due to these limitations in the synthesis of lipid NPs with P80H, a third surfactant, QDP was introduced to the system.

PHAT 106-109 were produced with different ratio of QDP:IPP, each batch was split into two samples and stored at 4°C and 37°C. The two particle batches with the highest content of QDP (PHAT 106/107), stored at 4°C resulted in the most promising results, with the smallest average particle size, low polydispersity, and smallest size increase over time. Shifting the focus to particles stored at 37°C, the results showed that particles were generally larger and had lower stability than particles stored at 4°C. This indicates there is a temperature dependence on destabilizing mechanisms of lipid nanoparticles in solution. Possible explanations of destabilization is discussed further in section 5.1.3.

It was found that the lower the content of P80H, the faster the process of surfactant dissolution occurred and thus the more time efficient is the overall synthesis process. Pure QDP in water at 90°C dissolved well within 10 minutes of mixing. Synthesis protocols for PHAT 106-109 were based on the experimental procedure presented in the article introduced earlier by Salminen et al. ([90]).

A mixture of two or more surfactants have been reported in literature to in some cases improve stability [51] [90]. Literature suggests that high- melting lecithins, such as P80H, do not have optimal stabilizing function on their own [90]. This may be due to a change in geometrical shape of the lecithin from a truncated cone shape to a more cylinder like shape after hydrogenation of fatty acid chains [90]. A second surfactant (QDP) helps increase the curvature of the surfactant layer on the surface of NPs. In addition, QDP can form micelles in excess concentrations and quickly

cover areas on the nanoparticle surface without surfactant coverage that are created during storage [90]. Due to low particle size, high stability and efficient particle synthesis, the formulation of PHAT 107 was chosen for subsequent experiments, and are called NLC#2 particles. This formulation has a QDP and P80H content of 0.24g and 0.06g, respectively.

Selection of method for emulsification and cooling

Method of homogenization and cooling were investigated for particle batches PHAT 115 and 116. The two tested methods of dispersing and reducing size of lipid/oil droplets in water phase to nanoscale, was ultra turrax and ultrasonication. The ultra-turraxed particle solution (PHAT 116) resulted in large particles with initial particle size in the range of 500-1400nm in mean diameter, for particles stored at 4°C. The corresponding size distribution was non-gaussian, and the particles exhibited low stability over time, indicated by high and increasingly growing PDI values (0.33-0.67).

PHAT 116, stored in at 37°C, resulted in particles that were not fit for ZS measurements due to large aggregates of lipid present in the solution This indicates an unstable dispersion. The sonicated particle batch (PHAT 115) exhibited much higher particle stability and lower particle size for both storage temperatures and at all time point of ZS measurements than the ultra-turraxed batch (PHAT 116). Rotor-stator systems, such as ultra-turraxing, often have highly distributed energy input in the stirring container, meaning regions of low and high shear, which lead to broad particle size distributions [92]. An other disadvantage is the high coalescence rate, compared to ultrasonication [92].

Ultra-turraxing as method of homogenization was tested in this project due to promising results for NLCs with respect to particle size (mean diameter 140-165nm) and stability found in the article introduced earlier by Salminen et al. [90]. Surfactant type used in the work by Salminen et al. was the same as in this project (QDP and P80H), while the solid and liquid lipids were not. The particles produced in the reference article were immediately after synthesis passed through a high pressure homogenizer, leading to further reduction in particle size. This step was not included in the protocol of particle synthesis in this project, and is most likely the main reason why particles homogenized by ultra turraxing alone did not reach as low average diameter as the particles in the reference article. Increasing the number of steps in the synthesis process is not favorable, and since ultra-turraxing alone did not result in improvement in particle size or stability, the method was discharged.

In addition to testing method of homogenization, for particle batch PHAT 115-116, method of particle cooling was also tested. For PHAT 115, hot water bath followed by room temperature cooling, and ice bath cooling resulted in particle solutions with visible particle clusters and lipid aggregates, both methods were therefore discarded. The two other solutions, cooled by tap water and in room temperature, resulted in particle solutions with no visible particles. The smallest particles size, and the highest stability was obtained for tap water-cooled particles.

5.1.3 Particle stability in various media

Size and stability of NLC#2 particles dispersed in PBS, LA Broth media, DI water, Glycine and DMEM was monitored with ZS over a time period of 48 hours.

Directly after dispersion of particles in the five medias, an increase in average particle diameter was recorded for all solutions. As mentioned in section 4.1.3, this size increase is most likely due to the choice of SOP used for ZS measurements. The same SOP was used for all measurements, difference in properties of the different medias, such as refractive index, was thus not accounted for. However, protein adsorption to nanoparticles [93] may contribute to an increase in average particles size in DMEM, which is the only out of the five solutions that contains protein serum. But since immediate increase of particle size is observed in other medias and not just the one with DMEM, protein adsorption is likely not a large contributor to the phenomena. The fact that the solution with DI water only has a small immediate particle size increase, compared to the other solutions, reinforces the theory of SOP-related size increase. The DI water solution is only a water dilution of the original particle solution, the refractive index is therefore similar.

Higher stability was observed for particles stored at 4°C, compared to the ones stored at 37°C, indicated by a lower rate of particle size increase. Stability was in the same range for all solutions stored at 4°C, as for the original particle solution (5-13% size increase over 48 hours). Ergo, there has not been any reduction i stability for NPs dispersed in media at 4°C.

A temperature and time dependence of particle mean size has been observed in batches produced throughout this project, irregardless of type or presence of loading material and media. The observed temperature dependence may be related to decrease in microviscosity at elevated temperatures [94]. The particles grow incrementally, indicating that the observed size increase can not be a consequence of aggregating particles. Possible destabilizing mechanisms are swelling of the particle core and Ostwald ripening.

Particle core swelling can occur if solution from the surrounding media penetrates

into the nanoparticles. There is little or no explanations on the underlying mechanisms of particle core swelling for NLCs in the literature. However, for bilayer lipids used in drug delivery it has been found that the packing of phospholipids on the particle surface affects its mechanical properties, including swelling [39]. And for SLNs, preservation of initial particle size includes prevention of degradation reactions on the particle surface like hydrolysis [94]. Whether these, or other mechanisms are the basis for core swelling in the NLC of this project will not be further discussed, due to lack of supporting literature.

With Ostwald ripening one can expect a linearity of the cube of the mean particle radius with time [49] [95]. The cube of the average particle radius with respect to time is plotted in figure 22 (for PHAT 122). A linear regression line is included in the figure. The equation and R-squared value that can be seen in the figure describe the regression line and how well the model fits with the experimental data, respectively. The high value of R^2 indicates that Ostwald ripening may be the destabilizing mechanism of the system. High R^2 values (in the range of 0.82-9.92) was also obtained for other particle batches, all made with particle synthesis protocol#2. These results have not been included in the thesis. Ostwald-ripening is known to be a destabilizing mechanism, limiting development of application for nano-emulsions [96], [97], [98]. However, there are only four measurement points in the plot (figure 22), so a conclusion based on sufficient statistical data can not be made. We can therefore not be sure if Ostwald ripening is the main contributor to particle destabilization.

The particles produced in this project have a liquid and a solid lipid component. But no analysis has been done towards determining the internal structure of the particles. It is uncertain if the two lipids are separated into two domains in the particles, or if there are many small pockets of liquid lipid in a continuous solid lipid crystal. The solid and liquid lipids may even be divided in separate solid and liquid nanoparticles/droplets. NPs consisting of solid lipids, can due to their small size, in fact be liquid at temperatures below their melting point. This phenomena is called supercooling. A possible destabilizing mechanism is crystallization of supercooled melts leading to drug expulsion from the lipid carrier. In SLNs, supercooled melts crystallizing results in an increase in particle surface and a decrease in loading capacity [87]. Crystallization may occur during storage and lead to decrease in particle stability. Supercooled lipids can exist as low as 30-40°C below melting point in lipid dispersions [87].

Evaluating development in particle stability was throughout this project based on visual inspection of particle solutions over time in addition to analysis of PDI values, size distributions and change in particle size obtained from ZS measurements. When comparing NLC#1 and NLC#2 particles directly, no significant change in PDI values was measured. ZS measurements resulted in PDI values <0.2, indicating relatively monodisperse particle solution for both NLC#1 and NLC#2 particles at all time points considered. However, as stated in section 4.1.4, comparison of particle solutions with NLC#1 and NLC#2 particles in various media indicated higher stability of NLC#2 particles. This was based on visual inspection of solutions and ZS size measurements for NLC#2 particles in this project, and on similar studies preformed at Sintef (unpublished results) for NLC#1 particles. NLC#1 in media particles were not even characterized with ZS due to early signs of destabilized particle solution. Thus, the stability of NLC#2 particles was considered to be higher for particles dispersed in media than for NLC#2 particles.

5.2   Uptake studies

Nanoparticles used for drug delivery must not only have small size and high stability to reach the targeted area in the body. The encapsulated drug must be released at a location where it can reach its biochemical target, usually a receptor. The TKIs that have been used in this project, inhibit growth of A431- epidermal cancer cells by intracellular binding to transmembrane bound proteins, EGFRs. For uptake studies, the highly hydrophobic fluorescent dye NR668 has been encapsulated in lipid NPs in order to study cellular uptake of NPs in A431-cells, and thus study how and where the encapsulated drug/dye is released.

5.2.1   Cellular uptake of fluorescent dye encapsulated in lipid nanoparticles

From FCM of cells cultivated with fluorescently labeled NLC#1 particles it was found that the uptake of dye was almost linear with respect to time within the duration of the experiment of 48 hours. A linear regression model with a corresponding R-squared value of ≈0,99 indicates a very high degree of linearity in uptake, see figure 26. The standard deviation from three parallels of one experiment describes the instrumental inaccuracy. Standard protocol in scientific experiments is to use three separate experiments to determine biological variation. Due to limitations in time, only one experiment with three parallels was performed in this project for all uptake and toxicity experiments.

FCM of cells cultivated with fluorescently labeled NLC#2 resulted in a ≈2.5 times higher rate of uptake compared to FCM of cells cultivated with NLC#1 particles. The uptake of dye was also for NLC#2 particles, almost linear with respect to time within the duration of the experiment of 48 hours. A linear regression model with a corresponding R-squared value of ≈0,98 indicates a very high degree of linearity in cellular uptake, see figure 28. The mechanism behind the uptake will be discussed in section 5.2.2.

In both histograms (figure 25 and 27), a population of non NP-treated cells can be seen. These are included to detect the level of autofluorescence from the cells and are used as a control sample. Any experiments resulting in higher values of fluorescence intensity than the top 3% of the cells in the control sample, means fluorescent dye or fluorescently labeled NPs have either bound to the surface of cells, or have been taken up in the cell [99]. Whether the source of the fluorescence signal originated from inside the cells or from the extracellular surface of the plasma membrane has not been determined in this project. Throughout this thesis, all fluorescence signal of higher values than autofluorescence will be referred to as cellular uptake, regardless of if its origin is on or in the cells.

A debatable issue is the possibility of difference in relative intensity of fluorescent emission from the two particle types (NLC#1 and 2). Due to differences in surfactant composition and SA:IPP ratio, one particle may have a higher fluorescent emission signal than the other, even though the concentration of fluorescent dye used is the same in both cases. This is an important source of uncertainty to the results. Fluorescence intensity is not only a matter of concentration of fluorescent probe, but also depends on the local environment. The dye NR668 is a modified version of the conventional Nile red, which is well described in the literature. Conventional Nile red may have thousandfold difference in emission intensity depending on what the local environment is [74]. Polar solvents, such as water, essentially lead to dye quenching, while the dye is intensely fluorescent in all organic solvents [74]. This subject is further addressed in spectral analysis of NR668, section 5.3.

5.2.2 Uptake mechanism

The two main endocytosis pathways, CME and CvME were inhibited by cell cultivation with Chlorpromazine and Genistein, respectively. For both experiments with endocytosis inhibitors the fluorescence intensity, shown in figure 29, is significantly higher than the cells autofluorescence. For either of the inhibited mechanisms to be the main route of cellular uptake, one would expect the resulting intensity profile to overlap to a much higher degree with the cells autofluorescence. One can therefore

conclude that neither CME or CvME is the main mechanism of cellular uptake. However, about 15-20% of the pretreated cells of each of the two pre-treated populations do not overlap with the untreated cells, indicating that the inhibitors have had some effect. Genistein is believed to inhibit not only caveolin- dependent endocytosis, but also have a broader effect on other clathrin- independent endocytosis mechanisms [66] [100] [101].

Other possible mechanisms responsible for the main uptake of dye in A431 cells are, release of NR668 from NPs outside the cells followed by passive transport the cell membrane, other endocytosis pathways than the two inhibited, and contact-mediated transfer.

Contact mediated transfer is a relatively fast process, where hydrophobic agents are transfered directly into the cytoplasm through a temporary interaction between the nanocarrier and the cell membrane. Cargo release into cytoplasm has been shown to be detected within a few minutes, and reaching a maximum cellular fluorescence intensity within a few hours of incubation with fluorescently labeled NPs [61] [34]. Results of FCM in this project shows an almost linear uptake through 48 hours of incubation, indicating contact mediated transfer is not the main uptake mechanism. Because of these results we are left with cellular uptake through passive transport or other endocytotic mechanisms than CME and CvME. The lipid NPs are too large to cross the cell membrane through passive transport, but NR668 can be taken up by extracellular release from nanoparticles followed by passive transport across the cell membrane. Release of NR668 from nanoparticles extracellularly may occur through particle degradation, diffusion of dye out of the nanoparticle matrix and into solution, or by release of dye that is loosely bound to the NP surface. Released NR668 may interact with serum proteins with hydrophobic domains in the solution [34]. The particle used in this project have not been dialyzed prior to FCM, presence of free NR668 in the particle solution is therefore possible although the dye is very hydrophobic and will favor being encapsulated in the lipid particles.

Passive transport across the cell membrane can occur either through simple or protein facilitated diffusion [102]. Diffusion rate depends on many factors, such as concentration gradient, molecular size, lipid solubility etc. [103]. The process continues until equilibrium in concentration is achieved. With free NR668, either originating from dye leakage from NPs or from non-encapsulated dye in the particle solution, one would expect a relatively rapid uptake via diffusion, that would reach a maximum uptake within much shorter time than what was observed in FCM. FCM revealed an almost linear cellular uptake within 48 hours of cultivation with NPs.

We therefore believe we can rule out leakage and rather focus on degradation of particles. If dye diffusion, as a consequence of NP degradation and dye release, is the main mechanism of cellular uptake, that means there is a continuous process of particle degradation for at least 48 hours. Whether or not this is likely is difficult to determine, but from the results of stability studies in the particle optimization part, it seems possible. NPs in DMEM at 37°C increased incrementally in size as a function of time, but even after 48 hours the solution had not separated into two phases and the mean particle size was around 357nm. If one assumes some heterogeneity in the NP population, variations in rate of degradation may be likely, leading to a continuous process of drug release over time followed by diffusion across the plasma membrane.

The part of this project involving particle optimization revealed a significant difference in stability of particles stored at 4°C and 37°C. Cell incubation at 4°C inhibits all forms of energy dependent transport, such as endocytosis. But because of the difference in particle stability, results of FCM with cells incubated at 4°C with lipid NPs can not give statistically valuable results to describe the uptake of NPs/dye in a physiological environment, at 37°C. Analysis of uptake mechanism by cultivation at 4°C, leading to inhibition of endocytosis, was therefore not performed in this project.

5.3 Spectral analysis of NR668

Analysis of the emission spectra of NR668 both free in DMEM and encapsulated in lipid NPs (NLC#2) was performed in order to see how spectral properties of NR668 change throughout the lifetime of the dye, being encapsulated and exposed to physiological environments.

The emission spectra of free NR668 in DMEM is shown in figure 31 and 32, for microplates incubated at 4°C and 37°C, respectively. The peak intensity is around 590nm in wavelength in both cases, and the recordings from different time points are almost overlapping. Ergo, there is no time dependence, or significant difference at 4°C and 37°C, observed for the emission spectra of free NR668 in DMEM. There is not much literature available on properties of NR668, but conventional Nile red is well described. Nile red is a fluorescent hydrophobic probe, meaning the excitation and emission properties of the dye is dependent on the hydrophobicity of the solvent [74]. Quenching of nile red occurs in highly polar solvents, while the dye is highly fluorescent in organic solvents and lipids [74]. NR668 is not identical to conventional nile red but is expected to have similar properties. From particle synthesis

with encapsulation of NR668 to incubation with cells and FCM, the fluorescent dye may be exposed to variations in local environment that may have an effect on its emission intensity [74]. The results of spectral recordings of free NR668 showed very little signs o time dependence or variations at 4°C and 37°C, of emission, as the local environment of the dye consisting of DMEM and small amounts of DMSO, does not change significantly for the duration of the experiment.

Emission spectra from parallel experiments of NR668 encapsulated in NPs, stored at 4°C and 37°C are shown in figure 33 and 34, respectively. A blue-shift in emission peak is observed for the particles stored at 4°C. The peak fluorescence intensity shifts from about 610nm to 600nm in wavelength. What is surprising about these results is that the results from the parallel experiments stored at different temperatures do not seem to correlate. A blue-shift is not observed for solution with NPs stored at 37°C. A physical difference between the two experiments is the state of IPP, being solid at 4°C and liquid at 37°C, how this might affect the system is uncertain. What we know about nile red, is that it becomes more blue when it is exposed to more lipophilic molecules, and becomes more red with less lipophilic molecules [74]. In particle stability studies, it was found that the lipid NPs are gradually degraded over a time period of at least 48 hours, both at 4°C and 37°C. In spectral analysis experiments, when the particles are degraded, NR668 may be released from the IPP/SA matrix and bind to more hydrophobic domains of protein in solution, thereby leading to a blue-shift. One would think that if NR668 has similar properties as Nile red, a blue-shift due to dye diffusing to more hydrophobic areas of proteins in solution should also lead to an increase in fluorescence intensity [74]. However, a decrease in fluorescence intensity was found coupled with the blue-shift. A hypothesis to explain this is as the particles are degraded and dye is released, some dye will be quenched in the aqueous solution [74], while some dye molecules will bind to hydrophobic domains of proteins that may have higher hydrophobicity than the solid matrix (at 4°C) of IPP/SA of NPs. Nile red is known to be completely quenched in water/aqueous solution [74]. This would overall lead to a decrease in number of fluorescence emitting molecules, thus intensity is affected. The suggested mechanisms are hypotheses, as there is little literature available describing the properties of NR668.

For the particles stored at 37°C an increase in fluorescence intensity is observed, while the peak of intensity remains in the same wavelength area for all five time points of emission recording. In a paper by Klymchenko et al. [40] it is shown that

in 40nm oil droplets with high concentrations of NR668 (5wt%), auto-quenching occurs. The intensity of fluorescent signal is proportional to the concentration of fluorophores in a reasonable concentration rage. Auto-quenching or self-quenching is a pheromone that occurs when the concentration of fluorophores is too high, leading to loss of fluorescence signal due to short-range interactions between fluorophore molecules [75]. Auto-quenching may be the mechanism responsible for the phenomena observed for NPs stored at 37°C, where fluorescence intensity increases with time. Auto-quenching may occur at time=0 when the concentration of NR668 inside NPs is at its highest. When the particles are degraded and dye is released, the dye is diluted, leading to decrease in auto-quenching and thus increase in fluorescence intensity. These are only suggested hypothesizes that have not been confirmed by supporting literature or extensive spectral analysis.

Figure 35 and 36 shows the emission spectra of free and encapsulated NR668, stored at 4°C and 37°C, for 1 and 48 hours respectively. The difference in intensity, and wavelength of intensity peak between free and encapsulated NR668, observed in both figures, has to do with the media surrounding the dye.

The results from NR668 spectral analysis show trends in fluorescence emission of opposing character for NPs stored under different temperature conditions. There is little literature on the underlying mechanisms of the observed phenomenas. Proposed theories presented in this section are therefore only attempts to explain the experimental results.

5.4 *In vitro* EGFR inhibition- and NP toxicity testing

5.4.1 Solubilitytesting of kinase inhibitors

Solubility testing of five different TKIs in IPP was performed to determine which of the substances was most suitable for encapsulation in lipid NPs. Gefitinib and Lapatinib reached dissolution at the highest concentration in IPP, and with the fewest process steps. The chemical structure of each of the TKI can be found in table 5 found in appendix A.1. Literature values suggest that Erlotinib, Lapatinib and Gefitinib are all practically insoluble in water (<1mg/ml at 25°C) [80]. The two other kinase inhibitors, SB6-140-06 and JH08-096, have been developed at the Department of Chemistry NTNU, and are not been described in the literature. All five TKIs generally consist of relatively unpolar groups, such as alkanes, ethers and

heteroarenes, leading to low solubility in polar solvents like water. Solubility in general follows the "like dissolves like" rule wherein polar solutes dissolve in polar solvents and nonpolar solutes dissolve in nonpolar solvents. Erlotinib has low solubility in DMSO (3mg/ml). The solubility of Gefitinib in DMSO is 89 mg/ml at 25°C, while solubility of Lapatinib in DMSO is the highest of the three commercial compounds, at 200mg/ml [80]. Based on the results of solubility testing, it is likely that solubility of the two non-commercial compounds, SB6-140-06 and JH08-096, at least have lower solubility in DMSO than Gefitinib and Lapatinib.

The method used for determining kinase inhibitor solubility in IPP was visual inspection. Exact values of solubility was not found, as the method used is not quantitative. Due to very limited amounts of kinase inhibitor available, only a few milligrams was used in each experiment. The solutions in question therefore consisted of very small volumes of kinase inhibitor/IPP, typically 0.05-0.2g in total. The small volumes made inspection of the solutions more challenging. Difference in solubility in IPP of Lapatinib and Gefitinib was therefore not observed. The literature values of solubility in DMSO would suggest Lapatinib was the most suitable compound for encapsulation in lipid NPs. However, due to cost and availability, the second most DMSO-solvable compound (Gefitinib) was used in subsequent experiments.

5.4.2 Effect of EGFR inhibitor and NPs on cell viability

Luminescent cell viability assay was used for analysis of NP and kinase inhibitor toxicity on A431- cells. The kinase inhibitor Gefitinib exhibited concentration and time dependent cytotoxicity on A431 cancer cells. Figure 37 and 38 shows the viability of cells incubated with Gefitinib dissolved in DMSO for 24 and 72 hours respectively. A reference sample with cells incubated with only DMSO was also included to determine whether cytotoxicity was a consequence of presence of Gefitinib specifically. The time dependence is evident when comparing the recordings performed after 24 and 72 hours of incubation. The difference in viability seen in these two figures also shows a time dependent DMSO toxicity. Results supporting these observations have been shown for Gefitinib in the literature. Godugu et al. ([104]) demonstrates the novel application of Gefitinib in A431 tumor cells. *In vitro* cytotoxicity testing of Gefitinib on A431 cells showed a time and concentration dependent cytotoxic effect. The results of the paper show very little increase in recorded cytotoxicity from 24 to 48 hours since kinase inhibitor treatment, but in both cases the toxicity is increasing with increasing concentrations of Gefitinib. The cytotoxicity is significantly higher at all concentrations of Gefitinib at 72 hours after treatment, and increasing toxicity with increasing concentrations of Gefitinib occurs also here. Thus, Godugu

et al. ([104]) shows a time dependence of at least 72 hours for Gefitinib's total biochemical effect. This delayed cytotoxic effect of Gefitinib may be due to the drug being dependent on cell division for mechanism of action to occur. The time before drug effect will thus depend on the rate of cell division. Zhou et al. [105] demonstrates cell arrest at checkpoint G_0/G_1 and G_2/M blockage in the cell cycle of human pancreatic cancer cells after treatment with Gefitinib (basic introduction to cell cycle and checkpoints can be found in section 2.1.1). Thus Gefitinib inhibit the proliferation of pancreatic cancer cells via cell cycle arrest.

In figure 39 and 40, cytotoxicity of free Gefitinib dissolved in DMSO and encapsulated in NPs is plotted after 24 and 72 hours of incubation. At low concentrations Gefitinib is the dominant source of toxicity, while the presence of NPs lead to an increase in toxicity at higher concentrations. This effect is more evident for the shorter incubation times.

The biological function of Gefitinib is to bind to the intracellular part of epidermal growth factor receptors located on the plasma membrane and inhibit downstream signaling, thus restraining cell growth. According to the literature, A431-cells have abnormally high expression levels of EGFRs, and should therefore be greatly affected by Gefitinib binding intracellularly. However, the level of expression of EGFRs has not been measured in this project, and it may deviate from the literature values, and thus lead to inaccuracy in measured effectiveness of Gefitinib.

Cytotoxicity of NPs with different amounts drug, recorded 72 hours after treatment, is shown in figure 41. For low concentrations of NPs, the amount of Gefitinib encapsulated is the dominant source of cell toxicity. The higher the concentration of Gefitinib encapsulated in the NPs, the higher the toxicity. For higher concentrations of NPs ($>30\mu$g/ml), cell viability is drastically reduced, regardless of the amount of loading compound. The high cytotoxicity is a consequence of high concentration of NPs, illustrating that the particles themselves are toxic.

A toxic effect of NPs alone can be observed for empty NPs at concentrations above $\approx 10\mu$g/ml. At a concentration of about 15μg/ml NPs, the cell viability is just below 80%, and it decreases to $\approx 0\%$ at 125μg/ml NPs.

Astrid Hyldbakk, a Mater's student at NTNU, has performed toxicity tests with both lipid nanoparticles NLC#1 and NLC#2 on cell lines HEP G2 and LLC-PK1 (unpublished results). The results showed significantly higher cytotoxicity, in both cell lines, for nanoparticles made with the new protocol (NLC#2) than the old particle type (NLC#1). For LLC-PK1 cells incubated with 0.6μg/mL NPs, the viability was around 50% and 70% for new and old particle formulations, respectively. Increasing the particle concentration above 1.2μg/mL led to total cell death for

LLC-PK1 cells incubated with NLC#2 particles, while the viability is still around 65% for cells incubated NLC#1 particles. The cytotoxicity of NLC#1 particles on A431-cells has not been measured, but it is expected to have the same tendencies as found by Astrid Hyldbakk for two other cell lines, being lower toxicity than the new lipid particle type (NLC#2).

Neither in the toxicity studies in this project, nor in the studies performed by Astrid Hyldbakk, was the various particle solutions dialyzed prior to incubation with cells. Excess surfactant in the solution may lead to increase in cytotoxic effect, this can be avoided by removal of excess surfactant by dialysis.

5.5 Conclusive remarks and further work

This thesis have been focused on developing and analyzing lipid nanoparticles that can potentially be used as drug carriers in cancer treatment based on drug delivery. In addition, cell experiments related to uptake and toxicity of such particles has been investigated. But still, a lot remains unknown. In light of the work presented in this thesis, I will make a few remarks on what can be learned from this work in order to further develop the presented lipid nanocarriers.

There are some loose ends from this work that should be further investigated. Not much is known about the internal structure of the lipid nanoparticles and the underlying mechanisms of destabilization. It would therefore be suggested that the structure of the NP lipid matrix is investigated further to determine whether there exists separate liquid and solid nanoparticles in particle solution, or if there are pockets of liquid lipids in a continuous matrix of solid lipid, or if the solid lipid is in fact liquid due to supercooling [106] [107]. Knowledge of such structures can be used for improving effectiveness of drug encapsulation and to understand what destabilizing mechanism that may affect the particles. This may be possible to do using CARS microscopy (Coherent Anti-Stokes Raman Scattering). The main advantages of CARS microscopy is that is a dye-free method that images structures based on intrinsic vibrational contrasts of the structure's subcomponents. It is popular for imaging lipid structures. This instrument will be available at NTNU during fall 2016 or spring 2017, and has therefore not been used in this project. To further investigate destabilizing mechanisms, zeta potential can be measured using a zeta-sizer. The measurement of zeta potential allows for predictions about the storage stability of the particle solution. In general, charged particles (high zeta potential) leads to low degree of aggregation due to electric repulsion [87]. However, this rule is not directly applicable to particle solutions containing surfactants, as such steric

stabilizers lead to decrease in zeta potential [87]. In addition, the stability of lipid NPs in this thesis was only been monitored for up to 6 days per particle batch. Storage over longer time periods followed by ZS measurements would provide further insight to the physical stability of the particles.

The NPs developed throughout this project showed high degree of cytotoxicity in A431-cancer cells. When developing nanoparticles for drug delivery, keeping toxicity of the particles themselves as low as possible to avoid harming healthy cells is important. As described earlier in section 5.4.2, toxicity studies of first generation lipid particles (NLC#1) resulted in much higher viability than the second generation particles (NLC#2). The compositional difference between these two particle types is mainly type of surfactant used. As an attempt improve viability of cells incubated with empty NPs (NLC#2), the particle solutions can be dialyzed, prior to cultivation with cells, to remove excess surfactant.

FCM was in this project used to quantify the uptake of fluorescently labeled NPs and free NR668 in A431-cells. The rate of uptake was found to be significantly higher for NLC#2 particles compared to first generation particle (NLC#1). However, the location of the origin of the detected fluorescent signals has not been determined. CLSM (confocal laser scanning microscopy) can be used to verify whether the fluorescent signal originated from inside the cells or from the plasma membrane. If the dye or drug is not actually transported to the inside of the cell, a intra-cellularly located protein target is not reached, and thus the pharmaceutical effect is lost.

To evaluate the effectiveness of kinase inhibitor delivered by lipid NPs to A431 cells, the level of expression of EGFRs should be measured in the cells. This value may deviate from literature values, and may therefore give misconceiving results of the effectiveness of the drug.

6 Conclusions

This study has been divided into three main parts that all revolve around development and testing of lipid nanoparticles for use in cancer treatment as drug carriers. In the first and largest part of the thesis, numerous small experiments and measurements with the overall goal of producing lipid nanoparticles with improved properties in size and stability were performed. This involved trying out variations in procedure for particle synthesis, systematic variation in nanoparticle composition and interpreting results obtained by visual inspection and Zetasizer measurements. Optimization led to promising results for particles composed of 5% lipid matrix with 4:1 ratio of stearic acid and isopropyl palmitate, and 1.5% surfactant with 4:1 ratio of Andean QDP Ultra and Phospholipon 80H. The optimized formulation demonstrated high physical stability and significantly reduced particle size at 4°C upon 5-6 days storage, and a slightly lower stability and increase in particle size at higher temperatures (37°C). An increase in particle size was also observed for particles dispersed in various media. Incremental increase in size over time was observed with zetasizer measurements, which the underlying mechanism still remains unclear, but Ostwald ripening stands out as a possible growth mechanism.

For the second part of the thesis cellular uptake of fluorescently labeled lipid nanoparticles was investigated using FCM. The rate of uptake of NR668 in A431 cells was increased by a factor of ≈ 2.5 from first generation lipid NPs (NLC#1) to the particle formulation developed in this project (NLC#2). Mechanisms of uptake was mainly attributed to passive uptake of fluorescent dye after release from NPs during particle degradation. The uptake was found to be almost linear within the duration of the experiment, indicating that lipid particle degradation is a continuous process within at least 48 hours of cultivation with cells. Cellular uptake was found to be reduced to some degree (17-20%) by pretreatment with endocytosis inhibitors, indicating some NPs are internalized by endocytosis.
In addition, spectral analysis of the fluorescently labeled NPs, revealed opposite behavior of fluorescent signal over time for particles stored at 4°C and 37°C. The underlying mechanism of the observed decrease in fluorescence intensity coupled with a blue-shift at 4°C, and increase in fluorescence intensity at 37° over time, was hypothesized to be due to competing processes of change in hydrophobicity of the local environment and fluorescence quenching.
Lastly, cytotoxicity of the optimized lipid nanoparticles and a kinase inhibitor was in-

vestigated with CellTiter Glo Luminescence viability assay and a microplate reader. The NPs (NLC#2) were found to be very cytotoxic. Through results of viability studies and comparison with unpublished results found by colleagues at Sintef, it was found that surfactant composition had a significant influence on the cell viability after NP exposure. NLC#1 particles, with Tween 80 as surfactant, were considerably less cytotoxic than NLC#2 particles with Andean QDP Ultra and Phospholipon 80H as surfactant. The cytotoxic effect of kinase inhibitor Gefitinib showed time and concentration dependence, but was in general overshadowed by the toxicity of NLC#2 NPs.

References

[1] Bernard W. Stewart and Christopher P. Wild, editors. *World cancer report.* WHO, World Health Organization, International Agency for Research on Cancer, 2014.

[2] Rajesh Singh and James W Lillard. Nanoparticle-based targeted drug delivery. *Experimental and molecular pathology*, 86(3):215–223, 2009.

[3] Jun Fang, Hideaki Nakamura, and Hiroshi Maeda. The epr effect: unique features of tumor blood vessels for drug delivery, factors involved, and limitations and augmentation of the effect. *Advanced drug delivery reviews*, 63(3):136–151, 2011.

[4] Srinivas Ganta, Harikrishna Devalapally, Aliasgar Shahiwala, and Mansoor Amiji. A review of stimuli-responsive nanocarriers for drug and gene delivery. *Journal of Controlled Release*, 126(3):187–204, 2008.

[5] James D Byrne, Tania Betancourt, and Lisa Brannon-Peppas. Active targeting schemes for nanoparticle systems in cancer therapeutics. *Advanced drug delivery reviews*, 60(15):1615–1626, 2008.

[6] RH Müller, Wolfgang Mehnert, J-S Lucks, Cora Schwarz, A Zur Mühlen, H Meyhers, Chrysantha Freitas, and D Rühl. Solid lipid nanoparticles (sln): an alternative colloidal carrier system for controlled drug delivery. *European Journal of Pharmaceutics and Biopharmaceutics*, 41(1):62–69, 1995.

[7] Gang Wang, JunJie Wang, Wei Wu, Shing Shun Tony To, HuaFu Zhao, and Jing Wang. Advances in lipid-based drug delivery: enhancing efficiency for hydrophobic drugs. *Expert opinion on drug delivery*, 12(9):1475–1499, 2015.

[8] RH Müller, M Radtke, and SA Wissing. Nanostructured lipid matrices for improved microencapsulation of drugs. *International journal of pharmaceutics*, 242(1):121–128, 2002.

[9] National Cancer Institute. Targeted cancer therapies. www.cancer.gov, 2014. Accessed:2016-06-02.

[10] I.S. Jorstad. Characterization of nanoparticles and nanoparticle-stabilized microbubbles. Project thesis, NTNU, The Norwegian University of Science and Technology, Department of Chemical Engineering, December 2015.

[11] Jeff Hardin, Gregory Bertoni, and Lewis J Kleinsmith. *Becker's World of the Cell*. Benjamin Cummings, 2012.

[12] Manash K Paul and Anup K Mukhopadhyay. Tyrosine kinase-role and significance in cancer. *Int J Med Sci*, 1(2):101–115, 2004.

[13] Stevan R Hubbard and W Todd Miller. Receptor tyrosine kinases: mechanisms of activation and signaling. *Current opinion in cell biology*, 19(2):117–123, 2007.

[14] Nicola Normanno, Antonella De Luca, Caterina Bianco, Luigi Strizzi, Mario Mancino, Monica R Maiello, Adele Carotenuto, Gianfranco De Feo, Francesco Caponigro, and David S Salomon. Epidermal growth factor receptor (egfr) signaling in cancer. *Gene*, 366(1):2–16, 2006.

[15] Sreenath V Sharma, Daphne W Bell, Jeffrey Settleman, and Daniel A Haber. Epidermal growth factor receptor mutations in lung cancer. *Nature Reviews Cancer*, 7(3):169–181, 2007.

[16] Amit Arora and Eric M Scholar. Role of tyrosine kinase inhibitors in cancer therapy. *Journal of Pharmacology and Experimental Therapeutics*, 315(3):971–979, 2005.

[17] Henning Bier, Thomas Hoffmann, Inge Haas, and Anke van Lierop. Anti-(epidermal growth factor) receptor monoclonal antibodies for the induction of antibody-dependent cell-mediated cytotoxicity against squamous cell carcinoma lines of the head and neck. *Cancer Immunology, Immunotherapy*, 46(3):167–173, 1998.

[18] Nature Education. Rtk. http://www.nature.com/scitable/topicpage/rtk-14050230. Accessed:2016-04-05.

[19] Felleskatalogen. Erlotinib. http://www.felleskatalogen.no/medisin/tarceva-roche-564418. Accessed:2016-04-05.

[20] Felleskatalogen. Gefitinib. http://www.felleskatalogen.no/medisin/iressa-astrazeneca-560272. Accessed:2016-04-05.

[21] Felleskatalogen. Lapatinib. http://www.felleskatalogen.no/medisin/tyverb-glaxosmithkline-564901. Accessed:2016-04-05.

[22] John R Goffin and Kevin Zbuk. Epidermal growth factor receptor: pathway, therapies, and pipeline. *Clinical therapeutics*, 35(9):1282–1303, 2013.

[23] William C Dewey, Clifton C Ling, and Raymond E Meyn. Radiation-induced apoptosis: relevance to radiotherapy. *International Journal of Radiation Oncology* Biology* Physics*, 33(4):781–796, 1995.

[24] Loren K Mell, Amit K Mehrotra, and Arno J Mundt. Intensity-modulated radiation therapy use in the us, 2004. *Cancer*, 104(6):1296–1303, 2005.

[25] Karen A Kurdziel, Joseph D Kalen, Jerry I Hirsch, John D Wilson, Harry D Bear, Jean Logan, James McCumisky, Kathy Moorman-Sykes, Stephen Adler, and Peter L Choyke. Human dosimetry and preliminary tumor distribution of 18f-fluoropaclitaxel in healthy volunteers and newly diagnosed breast cancer patients using pet/ct. *Journal of Nuclear Medicine*, 52(9):1339–1345, 2011.

[26] Sintef Materialer og Kjemi. Dreper kreftceller med superlim. wwww.sintef.no, Februar 2014. Accessed 10.06.2016.

[27] Barbara Haley and Eugene Frenkel. In vitro drug sensitivity predicts response and survival after individualized sensitivity-directed chemotherapy in metastatic melanoma: a multicenter phase ii trial of the dermatologic cooperative oncology group. In *Urologic Oncology: Seminars and original investigations*, volume 26, pages 57–64. Elsevier, 2008.

[28] Sara M Weis and David A Cheresh. Tumor angiogenesis: molecular pathways and therapeutic targets. *Nature medicine*, 17(11):1359–1370, 2011.

[29] Susan K Hobbs, Wayne L Monsky, Fan Yuan, W Gregory Roberts, Linda Griffith, Vladimir P Torchilin, and Rakesh K Jain. Regulation of transport pathways in tumor vessels: role of tumor type and microenvironment. *Proceedings of the National Academy of Sciences*, 95(8):4607–4612, 1998.

[30] Fabienne Danhier, Olivier Feron, and Véronique Préat. To exploit the tumor microenvironment: passive and active tumor targeting of nanocarriers for anticancer drug delivery. *Journal of Controlled Release*, 148(2):135–146, 2010.

[31] Carl-Henrik Heldin, Kristofer Rubin, Kristian Pietras, and Arne Östman. High interstitial fluid pressure—an obstacle in cancer therapy. *Nature Reviews Cancer*, 4(10):806–813, 2004.

[32] Katsuyoshi Hori, March Suzuki, Shigeru Tanda, and Sachiko Saito. Characterization of heterogeneous distribution of tumor blood flow in the rat. *Japanese journal of cancer research*, 82(1):109–117, 1991.

[33] Marian Löbler, HW Rohm, K-P Schmitz, AH Johnston, TA Newman, S Ranjan, R Sood, and PKJ Kinnunen. Drug delivery by nanoparticles—facing the obstacles. In *4th European Conference of the International Federation for Medical and Biological Engineering*, pages 2335–2338. Springer, 2009.

[34] Sofie Snipstad, Sara Westrøm, Yrr Mørch, Mercy Afadzi, Andreas KO Åslund, and Catharina de Lange Davies. Contact-mediated intracellular delivery of hydrophobic drugs from polymeric nanoparticles. *Cancer nanotechnology*, 5(1):1–18, 2014.

[35] B Mishra, Bhavesh B Patel, and Sanjay Tiwari. Colloidal nanocarriers: a review on formulation technology, types and applications toward targeted drug delivery. *Nanomedicine: Nanotechnology, biology and medicine*, 6(1):9–24, 2010.

[36] Sheva Naahidi, Mousa Jafari, Faramarz Edalat, Kevin Raymond, Ali Khademhosseini, and P Chen. Biocompatibility of engineered nanoparticles for drug delivery. *Journal of controlled release*, 166(2):182–194, 2013.

[37] Betty YS Kim, James T Rutka, and Warren CW Chan. Nanomedicine. *New England Journal of Medicine*, 363(25):2434–2443, 2010.

[38] Anu Puri, Kristin Loomis, Brandon Smith, Jae-Ho Lee, Amichai Yavlovich, Eliahu Heldman, and Robert Blumenthal. Lipid-based nanoparticles as pharmaceutical drug carriers: from concepts to clinic. *Critical Reviews^{TM} in Therapeutic Drug Carrier Systems*, 26(6), 2009.

[39] Anthony A Attama, Mumuni A Momoh, and Philip F Builders. Lipid nanoparticulate drug delivery systems: A revolution in dosage form design and development. 2012.

[40] Andrey S Klymchenko, Emilie Roger, Nicolas Anton, Halina Anton, Ievgen Shulov, Julien Vermot, Yves Mely, and Thierry F Vandamme. Highly lipophilic fluorescent dyes in nano-emulsions: towards bright non-leaking nano-droplets. *RSC Advances*, 2(31):11876–11886, 2012.

[41] Neda Naseri, Hadi Valizadeh, and Parvin Zakeri-Milani. Solid lipid nanoparticles and nanostructured lipid carriers: Structure, preparation and application. *Advanced pharmaceutical bulletin*, 5(3):305, 2015.

[42] A Gabizon and F Martin. Polyethylene glycol-coated (pegylated) liposomal doxorubicin. *Drugs*, 54(4):15–21, 1997.

[43] Mousa Jafari, Bahram Zargar, M Soltani, N Karunaratne, Brian Ingalls, and P Chen. Intelligent drug delivery systems for cancer therapy. *Biomedical materials and diagnostic devices, John Wiley & Sons, Inc., Hoboken, NJ, USA*, pages 1173–76, 2012.

[44] Yechezkel Barenholz. Liposome application: problems and prospects. *Current opinion in colloid & interface science*, 6(1):66–77, 2001.

[45] David Lembo and Roberta Cavalli. Nanoparticulate delivery systems for antiviral drugs. *Antiviral Chemistry and Chemotherapy*, 21(2):53–70, 2010.

[46] S Mukherjee, S Ray, RS Thakur, et al. Solid lipid nanoparticles: a modern formulation approach in drug delivery system. *Indian journal of pharmaceutical sciences*, 71(4):349, 2009.

[47] Rainer H MuÈller, Karsten MaÈder, and Sven Gohla. Solid lipid nanoparticles (sln) for controlled drug delivery–a review of the state of the art. *European journal of pharmaceutics and biopharmaceutics*, 50(1):161–177, 2000.

[48] S Weber, A Zimmer, and J Pardeike. Solid lipid nanoparticles (sln) and nanostructured lipid carriers (nlc) for pulmonary application: a review of the state of the art. *European Journal of Pharmaceutics and Biopharmaceutics*, 86(1):7–22, 2014.

[49] Veronique M Sadtler, Pascal Imbert, and Edith Dellacherie. Ostwald ripening of oil-in-water emulsions stabilized by phenoxy-substituted dextrans. *Journal of colloid and interface science*, 254(2):355–361, 2002.

[50] Ltd CycloChemBio Co. www.cyclochem.com, 2011. Accessed 10.06.2016.

[51] Rainer H Müller, Magdalene Radtke, and Sylvia A Wissing. Solid lipid nanoparticles (sln) and nanostructured lipid carriers (nlc) in cosmetic and dermatological preparations. *Advanced Drug Delivery Reviews*, 54:S131–S155, 2002.

[52] Surajit Das and Anumita Chaudhury. Recent advances in lipid nanoparticle formulations with solid matrix for oral drug delivery. *AAPS PharmSciTech*, 12(1):62–76, 2011.

[53] VB Patravale, RM Kulkarni, et al. Nanosuspensions: a promising drug delivery strategy. *Journal of pharmacy and pharmacology*, 56(7):827–840, 2004.

[54] Paul C Hiemenz and Raj Rajagopalan. *Principles of Colloid and Surface Chemistry, revised and expanded*, volume 14. CRC press, 1997.

[55] Jesse V Jokerst, Tatsiana Lobovkina, Richard N Zare, and Sanjiv S Gambhir. Nanoparticle pegylation for imaging and therapy. *Nanomedicine*, 6(4):715–728, 2011.

[56] Malvern Instruments. www.pharmaceuticalonline.com, July 2005. Accessed 10.06.2016.

[57] Rohan Shah, Daniel Eldridge, Enzo Palombo, and Ian Harding. *Lipid nanoparticles: Production, characterization and stability*. Springer, 2015.

[58] Kewal K Jain. *The handbook of nanomedicine*. Springer Science & Business Media, 2012.

[59] Gregory M Lanza, Xin Yu, Patrick M Winter, Dana R Abendschein, Kerry K Karukstis, Michael J Scott, Lori K Chinen, Ralph W Fuhrhop, David E Scherrer, and Samuel A Wickline. Targeted antiproliferative drug delivery to vascular smooth muscle cells with a magnetic resonance imaging nanoparticle contrast agent implications for rational therapy of restenosis. *Circulation*, 106(22):2842–2847, 2002.

[60] Ralph Weissleder. *Molecular imaging: principles and practice*. PMPH-USA, 2010.

[61] Daniel Hofmann, Claudia Messerschmidt, Markus B Bannwarth, Katharina Landfester, and Volker Mailänder. Drug delivery without nanoparticle uptake: delivery by a kiss-and-run mechanism on the cell membrane. *Chemical Communications*, 50(11):1369–1371, 2014.

[62] Kathryn C Partlow, Gregory M Lanza, and Samuel A Wickline. Exploiting lipid raft transport with membrane targeted nanoparticles: a strategy for cytosolic drug delivery. *Biomaterials*, 29(23):3367–3375, 2008.

[63] Hervé Hillaireau and Patrick Couvreur. Nanocarriers' entry into the cell: relevance to drug delivery. *Cellular and Molecular Life Sciences*, 66(17):2873–2896, 2009.

[64] Lucas Pelkmans and Ari Helenius. Endocytosis via caveolae. *Traffic*, 3(5):311–320, 2002.

[65] Gary J Doherty and Harvey T McMahon. Mechanisms of endocytosis. *Annual review of biochemistry*, 78:857–902, 2009.

[66] Dries Vercauteren, Roosmarijn E Vandenbroucke, Arwyn T Jones, Joanna Rejman, Joseph Demeester, Stefaan C De Smedt, Niek N Sanders, and Kevin Braeckmans. The use of inhibitors to study endocytic pathways of gene carriers: optimization and pitfalls. *Molecular Therapy*, 18(3):561–569, 2010.

[67] Robert J Lee and Philip S Low. Delivery of liposomes into cultured kb cells via folate receptor-mediated endocytosis. *Journal of Biological Chemistry*, 269(5):3198–3204, 1994.

[68] Malvern Instruments Ltd., Engima Buisness Park, Grovewood Road, Mavern, Worcestershire, WR14 1XZ, United Kingdom. *Zetasizer Nano Series User Manual*, 2.1 edition, July 2004.

[69] Encyclopædia Britannica. Rayleigh scattering. http://global.britannica.com. Accessed 29.02.2016.

[70] University of Iowa. http://www.chem.uiowa.edu. Accessed:2016-02-10.

[71] John H Seinfeld and Spyros N Pandis. *Atmospheric chemistry and physics: from air pollution to climate change.* John Wiley & Sons, 2012.

[72] Malvern Instruments Limited. Dynamic light scattering common terms defined. Technical Report MRK1764-01, Malvern Instruments worldwide, Grovewood Road, Malvern, Worcestershire, UK. WR14 1XZ, 2011. Accessed: 2016-02-29.

[73] John T Edward. Molecular volumes and the stokes-einstein equation. *Journal of Chemical Education*, 47(4):261, 1970.

[74] Phillip Greenspan, Eugene P Mayer, and Stanley D Fowler. Nile red: a selective fluorescent stain for intracellular lipid droplets. *The Journal of cell biology*, 100(3):965–973, 1985.

[75] Thermo Fisher Scientific. Fluorescence tutorials. http://www.thermofisher.com. Accessed:2016-03-29.

[76] Semrock. Filters for flow cytometry. https://www.semrock.com. Accessed:2016-02-29.

[77] Molecular Devices. http://www.moleculardevices.com. Accessed:2016-04-28.

[78] Biocompare. http://www.biocompare.com. Accessed:2016-04-28.

[79] Promega Corporation, 2800 Woods Hollow Road Madison, WI 53711-5399 USA. *CellTiter-Glo Luminescent Cell Viability Assay*, 2015. Accessed: 2016-05-06.

[80] Sigma Aldrich. http://www.sigmaaldrich.com. Accessed:2016-02-18.

[81] Lara Yildirimer, Nguyen TK Thanh, Marilena Loizidou, and Alexander M Seifalian. Toxicology and clinical potential of nanoparticles. *Nano today*, 6(6):585–607, 2011.

[82] M Nassimi, C Schleh, HD Lauenstein, R Hussein, K Lübbers, G Pohlmann, S Switalla, K Sewald, M Müller, N Krug, et al. Low cytotoxicity of solid lipid nanoparticles in in vitro and ex vivo lung models. *Inhalation toxicology*, 21:104, 2009.

[83] Jau-Song Yu and Shiaw-Der Yang. Tyrosin dephosphorylation and concurrent inactivation of protein kinase fa/gsk-3α by genistein in a431 cells. *Journal of cellular biochemistry*, 56(1):131–141, 1994.

[84] Palmer A Orlandi and Peter H Fishman. Filipin-dependent inhibition of cholera toxin: evidence for toxin internalization and activation through caveolae-like domains. *The Journal of cell biology*, 141(4):905–915, 1998.

[85] Bruce J Berne and Robert Pecora. *Dynamic light scattering: with applications to chemistry, biology, and physics*. Courier Corporation, 1976.

[86] Yaowaporn Sangsen, Punsupang Laochai, Pravara Chotsathidchai, and Ruedeekorn Wiwattanapatapee. Effect of solid lipid and liquid oil ratios on properties of nanostructured lipid carriers for oral curcumin delivery. In *Advanced Materials Research*, volume 1060, pages 62–65. Trans Tech Publ, 2014.

[87] Wolfgang Mehnert and Karsten Mäder. Solid lipid nanoparticles: production, characterization and applications. *Advanced drug delivery reviews*, 47(2):165–196, 2001.

[88] Annette zur Mühlen, Cora Schwarz, and Wolfgang Mehnert. Solid lipid nanoparticles (sln) for controlled drug delivery–drug release and release mechanism. *European journal of pharmaceutics and biopharmaceutics*, 45(2):149–155, 1998.

[89] T Helgason, TS Awad, K Kristbergsson, D Julian McClements, and Jochen Weiss. Effect of surfactant surface coverage on formation of solid lipid nanoparticles (sln). *Journal of Colloid and Interface Science*, 334(1):75–81, 2009.

[90] Hanna Salminen, Susanne Aulbach, Bruno H Leuenberger, Concetta Tedeschi, and Jochen Weiss. Influence of surfactant composition on physical and oxidative stability of quillaja saponin-stabilized lipid particles with encapsulated omega-3 fish oil. *Colloids and Surfaces B: Biointerfaces*, 122:46–55, 2014.

[91] Laura Mazzola. Commercializing nanotechnology. *Nature biotechnology*, 21(10):1137–1143, 2003.

[92] Jochen Weiss. Emulsion processing homogenization. www.people.umass.edu, November 2008. Accessed:2016-05-31.

[93] TM Göppert and RH Müller. Adsorption kinetics of plasma proteins on nanoparticles for drug targeting. *International journal of pharmaceutics*, 302(1):172–186, 2005.

[94] Cand Freitas and RH Müller. Correlation between long-term stability of solid lipid nanoparticles (sln™) and crystallinity of the lipid phase. *European Journal of Pharmaceutics and Biopharmaceutics*, 47(2):125–132, 1999.

[95] German Urbina-Villalba, Ana Forgiarini, Kareem Rahn, and Aileen Lozsán. Influence of flocculation and coalescence on the evolution of the average radius of an o/w emulsion. is a linear slope of r [combining macron] 3 vs. t an unmistakable signature of ostwald ripening? *Physical Chemistry Chemical Physics*, 11(47):11184–11195, 2009.

[96] JM Gutiérrez, C González, A Maestro, I Sole, CM Pey, and J Nolla. Nanoemulsions: New applications and optimization of their preparation. *Current Opinion in Colloid & Interface Science*, 13(4):245–251, 2008.

[97] Ilya M Lifshitz and Vitaly V Slyozov. The kinetics of precipitation from supersaturated solid solutions. *Journal of physics and chemistry of solids*, 19(1-2):35–50, 1961.

[98] P Taylor. Ostwald ripening in emulsions. *Advances in colloid and interface science*, 75(2):107–163, 1998.

[99] António J Almeida and Eliana Souto. Solid lipid nanoparticles as a drug delivery system for peptides and proteins. *Advanced drug delivery reviews*, 59(6):478–490, 2007.
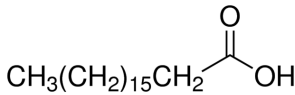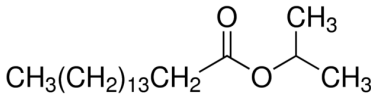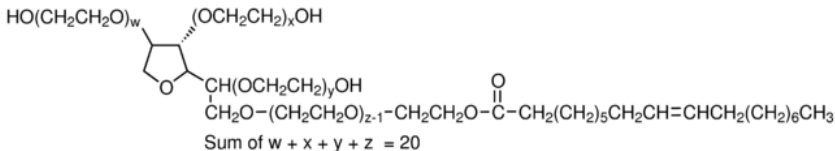
[100] Joanna Rejman, Alessandra Bragonzi, and Massimo Conese. Role of clathrin- and caveolae-mediated endocytosis in gene transfer mediated by lipo-and polyplexes. *Molecular Therapy*, 12(3):468–474, 2005.

[101] Kanagaraj Palaniyandi, Barbara A Pockaj, Sandra J Gendler, and Xiu-Bao Chang. Human breast cancer stem cells have significantly higher rate of clathrin-independent and caveolin-independent endocytosis than the differentiated breast cancer cells. *Journal of cancer science & therapy*, 4(7):214.

[102] Rick Ng. *Drugs: from discovery to approval.* John Wiley & Sons, 2015.

[103] TE Peck, SA Hill, and Mark Williams. Drug passage across the cell membrane.

[104] Chandraiah Godugu, Ravi Doddapaneni, Apurva R Patel, Rakesh Singh, Roger Mercer, and Mandip Singh. Novel gefitinib formulation with improved oral bioavailability in treatment of a431 skin carcinoma. *Pharmaceutical research*, 33(1):137–154, 2016.

[105] Xiaohua Zhou, Maqing Zheng, Fang Chen, Yunxia Zhu, Wei Yong, Haiyan Lin, Yujie Sun, and Xiao Han. Gefitinib inhibits the proliferation of pancreatic cancer cells via cell cycle arrest. *The Anatomical Record*, 292(8):1122–1127, 2009.

[106] Hilde A Rinia, Koert NJ Burger, Mischa Bonn, and Michiel Müller. Quantitative label-free imaging of lipid composition and packing of individual cellular lipid droplets using multiplex cars microscopy. *Biophysical journal*, 95(10):4908–4914, 2008.

[107] Michiel Müller and Juleon M Schins. Imaging the thermodynamic state of lipid membranes with multiplex cars microscopy. *The Journal of Physical Chemistry B*, 106(14):3715–3723, 2002.

[108] U.S. National Library of Medicine National Center for Biotechnology Information. http: //www.pubchem.ncbi.nlm.nih.gov/. Accessed:2016-02-18.

[109] Santa Cruz Biotechnology. http://www.scbt.com/index.html. Accessed:2016-02-18.

[110] Joint FAO-WHO Expert Committee Report on Food Additives, editor. *Quillaia extracts type 1 and type 2 chemical and technical assessment (CTA)*, volume 65. FAO-WHO, 2005.

Appendix A

A.1   Materials

Table 5: *Chemical structure and properties of materials [80] [108] [90] [40] [109] [110]*

Materials	Structure
Stearic acid, solid lipid Molecular weight = 284.48g/mol Melting point = 69-71°C	
Isopropyl palmitate, liquid lipid Molecular weight = 298.5g/mol Melting point = 13.5°C	
Tween 80, surfactant Molecular weight = 604.8g/mol HLB=15 CMC=0.012mM 	
Phospholipon 80 H, surfactant High-melting lecithin Composed of hydrogenated phosphatidylcholine and hydrogenated lysophosphatidylcholine No structure available	

Andean QDP Ultra, surfactant

Quillaja extract. High molecular weight, surface-active glycosides composed of hydrophilic sugar moieties and a hydrophobic triterpene or steroid aglycon
No structure available

Nile Red 668 (NR668)
Hydrophobic fluorescent dye
Molecular weight = 558.8g/mol
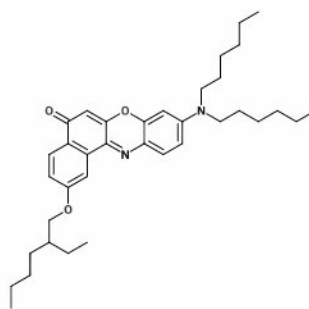
Curcumin, drug
Molecular weight = 368.4g/mol
Melting point = 183°C
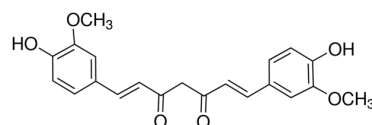
Erlotinib-HCl, drug (TKI)
Molecular weight = 429.90g/mol
Melting point =223-225°C
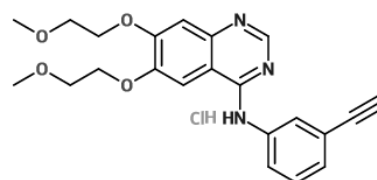
Gefitinib, drug (TKI)
Molecular weight = 446.91g/mol
Melting point =193-194 °C
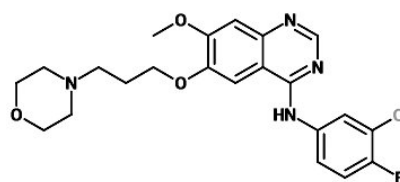
Lapatinib, drug (TKI)
Molecular weight = 581.06g/mol
Melting point = 137-139°C
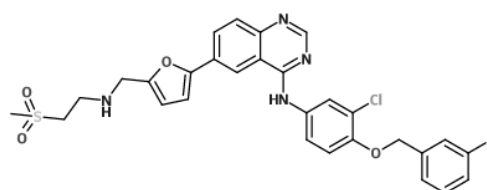
SB6-140-06 (BS-BL), drug (TKI)

Molecular weight = 407.49g/mol

Melting point = 183-185°C
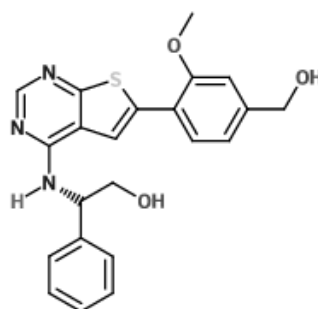
JH08-096, drug (TKI)

Molecular weight = 390.44g/mol

Melting point = 189-191°C
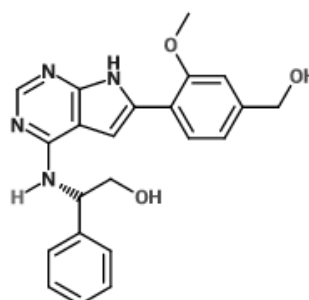
Chlorpromazine,

drug/endocytosis inhibitor

Molecular weight = 318.86g/mol

Melting point = ≈ 60°C
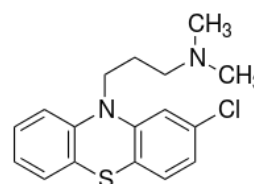
Genistein, drug/endocytosis inhibitor

Molecular weight = 270.24g/mol

Melting point = ≈300°C
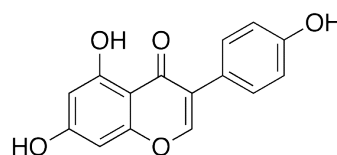
Appendix B

B.1 Nanoparticles used in this project and their composition

Table 6: *Nanoparticles used and their composition*

Sample ID	SA [g]	IPP [g]	Loading compound and concentration [wt%]*	Surfactant type and concentration [wt%]**	Comments or process specifications
NLP 1 (NLC#1)	[0.6]	[0.4]	-	Tween 80, [1.23]	-
NLP 3 (NLC#1)	[0.6]	[0.4]	Curcumin, [0.5]	Tween 80, [1.23]	-
PHAT 95	[0.8]	[0.2]	-	P 80H, [1.5]	-
PHAT 96	[1.6]	[0.4]	-	P 80H, [3]	-
PHAT 97	[0.6]	[0.4]	-	P 80H, [1.5]	-
PHAT 98	[1.2]	[0.8]	-	P 80H, [3]	-

PHAT 99	[0.8]	[0.2]	Curcumin [0.5]	P 80H, [1.5]	-
PHAT 100	[0.8]	[0.2]	Curcumin [1]	P 80H, [1.5]	-
PHAT 101	[0.8]	[0.2]	NR668 [0.5]	P 80H, [1.5]	-
PHAT 102	[0.8]	[0.2]	NR668 [1]	P 80H, [1.5]	-
PHAT 106	[0.8]	[0.2]	-	QDP [1.5]	Batch split in 2, one part stored at 4°C, one at 37°C
PHAT 107 (NLC#2)	[0.8]	[0.2]	-	QDP: P 80H, [1.2:0.3]	Batch split in 2, one part stored at 4°C, one at 37°C
PHAT 108	[0.8]	[0.2]	-	QDP: P 80H, [1.5:1.5]	Batch split in 2, one part stored at 4°C, one at 37°C

PHAT 109	[0.8]	[0.2]	-	QDP: P 80H, [0.3:1.2]	Batch split in 2, one part stored at 4°C, one at 37°C
PHAT 115 (NLC#2)	[0.8]	[0.2]	-	QDP: P 80H, [1.2:0.3]	After sonication batch split in 4, cooled in 4 ways. Each sample split again in 2, one part stored at 4°C, one at 37°C
PHAT 116	[0.8]	[0.2]	-	QDP: P 80H, [1.2:0.3]	Ultraturrax instead of sonication, batch split in 4, cooled in 4 ways. Each sample split again in 2, one part stored at 4°C, one at 37°C
PHAT 122 (NLC#2)	[0.8]	[0.2]	-	QDP: P 80H, [1.2:0.3]	Batch used for stabilitytesting in various media
PHAT 128 (NLC#2)	[0.8]	[0.2]	NR668 [0.5]	QDP: P 80H, [1.2:0.3]	-

PHAT 130 (NLC#2)	[0.8]	[0.2]	NR668 [0.5]	QDP: P 80H, [1.2:0.3]	-
PHAT 132 (NLC#2)	[0.8]	[0.2]	NR668 [0.5]	QDP: P 80H, [1.2:0.3]	-
PHAT 133 (NLC#1)	[0.6]	[0.4]	NR668 [0.5]	Tween 80 [1.23]	-
PHAT 135 (NLC#2)	[0.8]	[0.2]	Gefitinib [5]	QDP: P 80H, [1.2:0.3]	-
PHAT 136 (NLC#2)	[0.8]	[0.2]	Gefitinib [2.5]	QDP: P 80H, [1.2:0.3]	-
PHAT 137 (NLC#2)	[0.8]	[0.2]	Gefitinib [1]	QDP: P 80H, [1.2:0.3]	-
PHAT 138 (NLC#2)	[0.8]	[0.2]	-	QDP: P 80H, [1.2:0.3]	-

Appendix C

C.1 Zetasizer measurement results

Table 7: *Results of zetasizer particle size and PDI measurements of batches NLP1 and NLP2 in which tween 80 is surfactant and SA:IPP ratio is 6:4.*

Sample ID	Storage temperature [°C]	Variations in composition	Time since synthesis [days]	PDI	Average diameter
NLP 1 (NLC#1)	4	Empty	0	0.105	243.3
			1	0.016	277.1
			2	0.132	279.5
NLP 3 (NLC#1)	4	Curcumin loaded (0.5wt%)	0	0.132	231.7
			1	0.164	293.5
			2	0.075	263.7

Table 8: *Results of zetasizer particle size and PDI measurements of batches PHAT 95-PHAT98 in which amount of phospholison 80H, SA and IPP has been varied.*

Sample ID	Storage temperature [°C]	Amount of SA [g], IPP [g], P80H [wt%]	Time since synthesis [days]	PDI	Average diameter
PHAT 95	4	0.8, 0.2, 1.5	0	0.198	204.0
			1	0.193	208.9
			2	0.182	222.4
			3	0.217	227.1
			6	(0.221)	(240.2)
PHAT 96	4	1.6, 0.4, 3	0	0.185	247.1
			1	0.193	267.1
			2	0.204	269.9
			3	0.211	276.0
			6	(0.328)	(338.4)
PHAT 97	4	0.6, 0.4, 1.5	0	0.188	179.0
			1	0.204	206.5
			2	0.194	203.6
			3	0.197	204.6
			6	0.239	210.6
PHAT 98	4	1.2, 0.8, 3	0	0.190	239.4
			1	0.235	254.9
			2	0.237	267.8
			3	0.324	321.4
			6	0.237	279.2

Table 9: *Results of zetasizer particle size and PDI measurements for batches PHAT 99-102, where P80H is surfactant, SA:IPP ratio is 6:4, and two concentrations of curcumin and NR668 as loading material are incorporated*

Sample ID	Storage temperature [°C]	Loading material [wt%]	Time since synthesis [days]	PDI	Average diameter
PHAT 99	4	Curcumin 0.5%	0	0.187	208.8
			1	0.155	216.9
			4	0.213	247.6
PHAT 100	4	Curcumin 1%	0	0.236	210.9
			1	0.153	214.2
			4	0.195	236.2
PHAT 101	4	NR668 0.5%	0	0.220	213.0
			1	0.172	220.3
			4	(0.167)	(240.1)
PHAT 102	4	NR668 1%	0	0.195	214.2
			1	0.171	214.6
			4	0.138	235.1

Table 10: *Results of zetasizer particle size and PDI measurements of batches PHAT106-109 where ratio of QDP:P80H was varied, while SA:IPP ratio was constant, 4:1.*

Sample ID	Storage temperature [°C]	QDP:IPP [g]	Time since synthesis [days]	PDI	Average diameter
	4	0.3:0	0	(0.164)	(191.2)
			1	0.108	193.5
			2	0.045	198
			5	0.03	209.5
PHAT 106					
	37	0.3:0	1	0.1	243.9
			2	0.05	239.6
			5	(0.047)	(237.3)
	4	0.24:0.06	0	0.184	182.8
			1	0.142	206.0
			2	0.081	201.5
			5	0.110	219.3
PHAT 107					
	37	0.24:0.06	1	0.092	285.6
			2	0.158	295.7
			5	0.097	310.5
	4	0.15:0.15	0	0.180	196.1
			1	0.152	247.7
			2	0.169	267.0
			5	0.156	287.5
PHAT 108					
	37	0.15:0.15	1	0.125	334.9
			2	0.138	330.9
			5	0.159	364.8

	4	0.06:0.24	0	0.187	256.9
			1	0.146	281.1
			2	(0.202)	(288.2)
PHAT 109			5	(0.158)	(294.8)
	37	0.06:0.24	1	0.215	340.6
			2	(0.209)	(369.7)
			5	0.239	433.9

Table 11: *Results of zetasizer measurements of PHAT 122 in various media*

Media	Storage temperature [°C]	Time since dilution in media [hours]	PDI	Average diameter
Original particle solution	4	-24*	0.172	183.5
		0	0.135	194.0
		24	0.040	211.2
		48	0.134	212.3
PBS	4	0	0.054	222.3
		3	0.136	223.6
		5	0.118	227.4
		24	0.085	230.4
		48	0.100	233.8
	37	1	0.061	225.4
		2	0.038	231.3
		3	(0.086)	(239.2)
		5	0.126	251.5
		24	0.158	283.3
		48	(0.153)	(299.7)

LA	4	0	0.115	217.2
Broth		3	0.128	227.2
		5	0.098	216.1
		24	0.098	227.0
		48	0.057	229.8
	37	1	0.070	226.1
		2	0.081	230.0
		3	0.151	245.4
		5	0.111	260.9
		24	0.137	269.3
		48	0.111	267.5
DI	4	0	0.099	210.7
water		3	0.116	211.4
		5	0.080	205.7
		24	0.119	210.5
		48	0.223	229.0
	37	1	0.060	205.4
		2	0.106	202.0
		3	0.051	203.5
		5	0.137	226.6
		24	0.085	223.4
		48	0.032	227.8

Glycine	4	0	0.166	248.0
		3	0.152	230.2
		5	0.139	232.4
		24	0.125	249.6
		48	0.169	281.3
	37	1	0.085	266.2
		2	0.178	278.0
		3	0.174	285.8
		5	0.215	310.2
		24	0.118	295.4
		48	0.09	305.2
DMEM	4	0	0.158	232.8
		3	0.05	221.2
		5	0.065	226.3
		24	0.0134	248.5
		48	0.154	248.7
	37	1	0.073	232.3
		2	0.128	237.7
		3	0.172	260.2
		5	0.228	285.9
		24	0.279	(321.3)
		48	(0.360)	(357.4)

* Particles were diluted in various media after 24 hours of storage in a refrigerator at 4°C, the first measurement of particles in no media was performed immediately after synthesis, time of measurement is therefore set to -24 hours relative to time of dispersion in medias.

Table 12: *Results of zetasizer particle size and PDI measurements of PHAT 128,130 and PHAT 132-138. Particle batches used for FCM and viability studies.*

Sample ID	SA:IPP ratio, surfactant, load	Time since synthesis [days]	PDI	Average diameter
PHAT 128 (NLC#2)	0.8:0.2 QDP, P80H NR668 0.5%	0	0.183	186.8
PHAT 133 (NLC#1)	0.6:0.4 Tween 80 NR668 0.5%	0	0.210	276.6
PHAT 130 (NLC#2)	0.8:0.2 QDP, P80H NR668 0.5%	0	0.134	190
PHAT 132 (NLC#2)	0.8:0.2 QDP, P80H NR668 0.5%	0	0.183	188
PHAT 135 (NLC#2)	0.8:0.2 QDP, P80H Gefitinib 5%	0	0.182	209.3
PHAT 136 (NLC#2)	0.8:0.2 QDP, P80H Gefitinib 2.5%	0	0.140	169.9
PHAT 137 (NLC#2)	0.8:0.2 QDP, P80H Gefitinib 1%	0	0.159	182.3
PHAT 138 (NLC#2)	0.8:0.2 QDP, P80H Empty	0	0.069	187.4

Appendix D

D.1 Viability studies
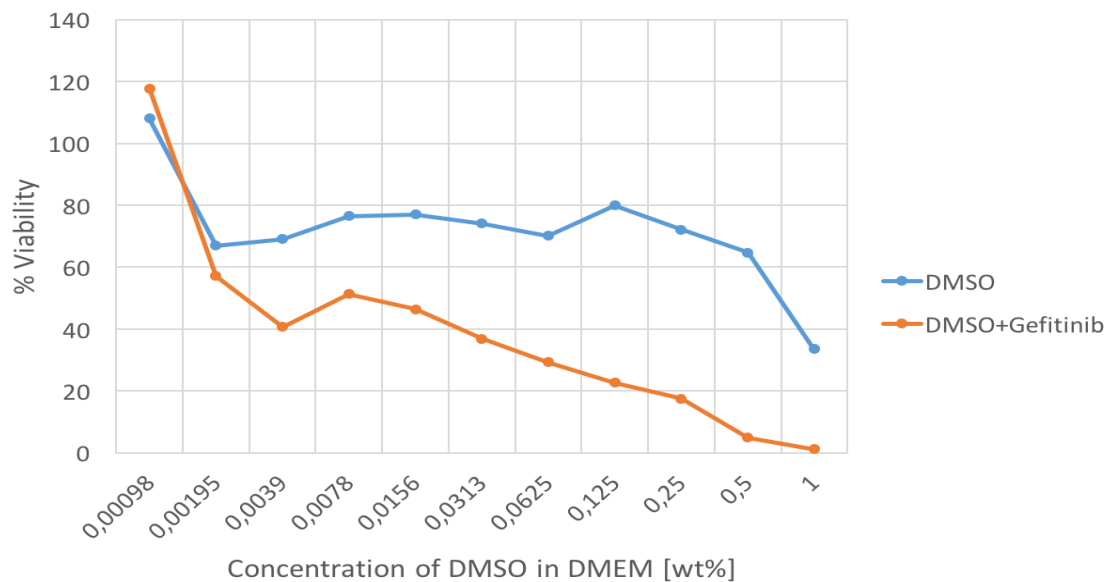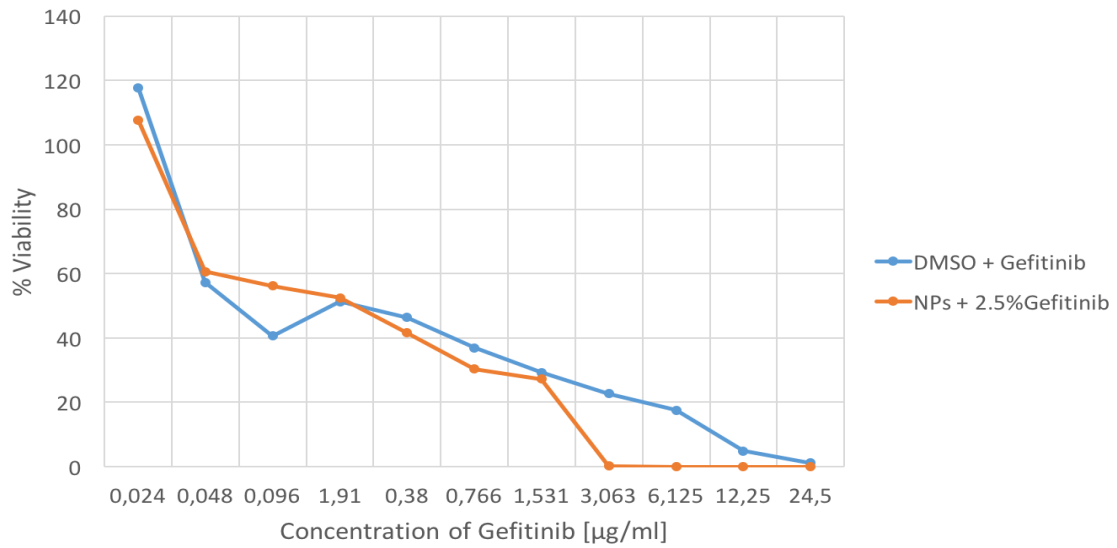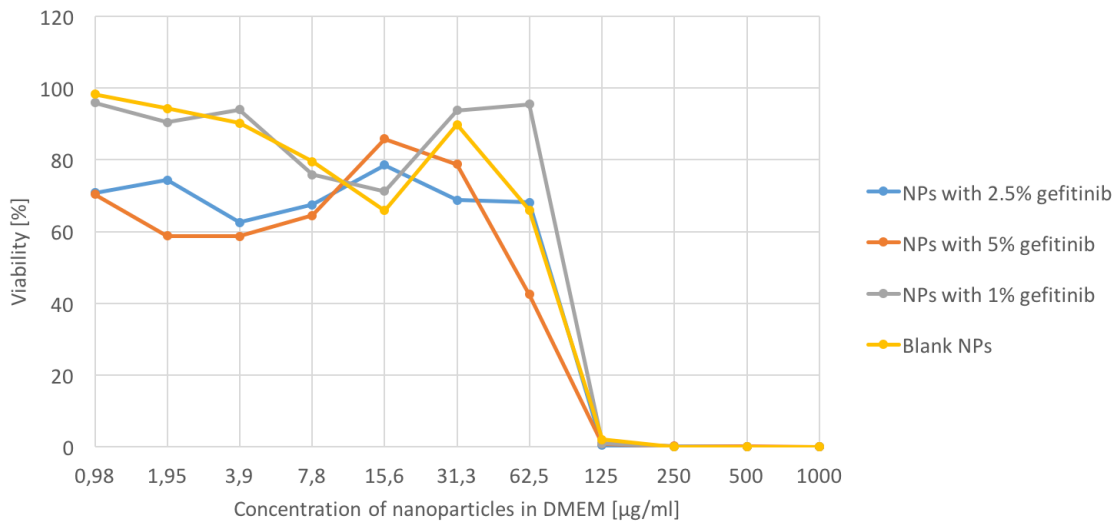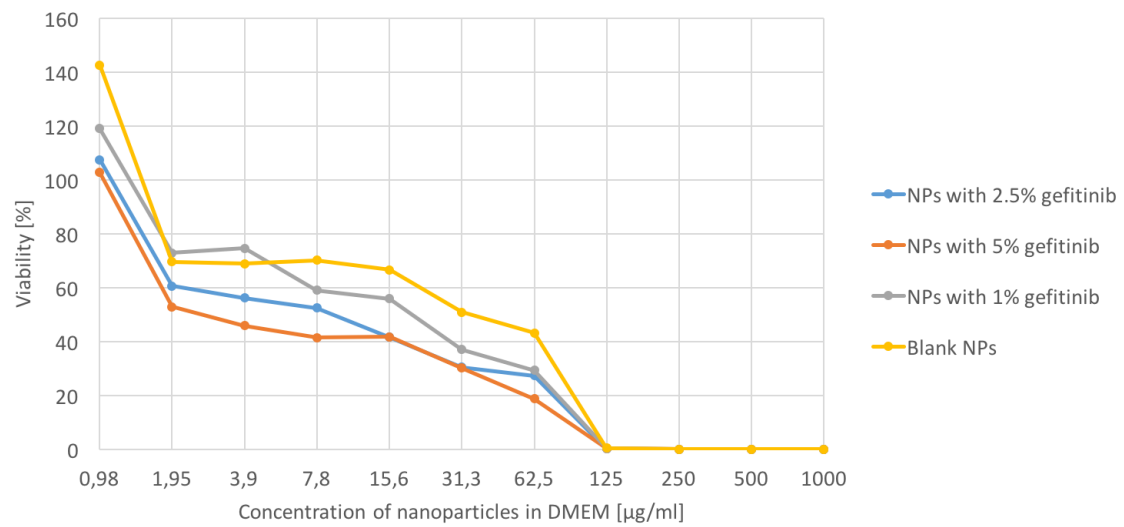

Figure 45: *Viability of cells that have been incubated for 48 hours with DMSO or DMSO and Gefitinib. The graph show that viability of cells incubated with only DMSO in DMEM is in the range of ≈30-100% with decreasing concentrations of DMSO, while cells incubated with DMEM, DMSO and Gefitinib has a decreasing viability from 100% to ≈2% for increasing concentrations of DMSO/Gefitinib*

Figure 46: *Viability of cells that have been incubated for 48 hours with DMSO and Gefitinib or with nanoparticles containing Gefitinib. The graphs show that samples of cells incubated with DMSO+Gefitinib and NPs w/Gefitinib both have a almost linear decrease in viability with increasing concentrations of Gefitinib.*

Figure 47: *Viability of cells that have been incubated for 24 hours with nanoparticles with different concentrations of Gefitinib. For low concentrations of nanoparticles, higher loading concentration with Gefitinib is shown to be more toxic. There is a drastic increase in toxicity of nanoparticles (regardles of nanoparticle content) for NP concentration above 62.5 µg/ml*

116

Figure 48: *Viability of cells that have been incubated for 48 hours with nanoparticles with different concentrations of Gefitinib. For low concentrations of nanoparticles, higher loading concentration with Gefitinib is shown to be more toxic. There is a drastic increase in toxicity of nanoparticles (regardles of nanoparticle content) for NP concentration above 62.5 µg/ml*

Table 13: *Viability results for cell plate incubated for 24 hours with NPs, NPs w/Gefitinib, DMSO w/ Gefitinib and DMSO.*

	1	2	3	4	5	6	7	8	9	10	11	12
Blank NPs, high →low concentration	0.053	0.041	3.218	68.28	104.7	85.22	103.2	100.2	117.1			130.1*
NPs 1% gef, high →low concentration	0.026	0.033	1.001	63.69	74.91	62.85	73.84	77.28	88.47	79.43		119.9*
Blank NPs, high →low concentration	0.053	0.053	1.027	71.26	93.45	75.89	93.98	90.42	95.86			112.7*
NPs 2.5% gef, high →low concentration	0.053	0.059	0.610	82.00	67.94	70.91	66.40	71.75	66.40			93.67*
NPs 2.5% gef, high →low concentration	0.013	0.079	0.345	54.35	69.67	63.62	64.07	58.71	76.94			83.08*
NPs 5% gef, high →low concentration	0.087	0.125	0.868	42.52	78.72	85.77	64.49	58.68	58.78	70.35		75.89*
DMSO+ gef, high →low concentration	14.42	40.39	45.85	55.07	70.89	71.87	69.50	77.52	77.22	58.84	82.11	98.68*
DMSO, high →low concentration	101.9	112.2	130.7	101.3	83.73	92.79	92.93	90.26	77.86	78.56	92.32	85.99*

*The last column only contains cells with DMEM, no NPs, Gefitinib or DMSO has been added.

**The values of viability enlisted in the table are based on comparison with the average amount of living cells in the last column, where no additions of solutions have been made (except growth medium) to the cell population.

Table 14: *Viability results for cell plate incubated for 48 hours with NPs, NPs w/Gefitinib, NPs w/Gefitinib, DMSO w/ Gefitinib and DMSO.*

Blank NPs, high →low concentration	0.016	0.005	0.016	0.635	39.35	49.62	61.95	60.05	62.87	62.92	136.9	105.4
Blank NPs, high →low concentration	0.016	0.013	0.029	0.221	47.08	52.09	71.42	80.32	74.86	76.28	148.6	100.9
NPs 1% gef, high →low concentration	0.008	0.008	0.008	0.238	29.31	37.01	55.97	59.11	74.64	72.99	119.2	90.60
NPs 2.5% gef, high →low concentration	0.021	0.016	0.026	0.159	29.02	27.74	42.93	47.09	58.03	61.80	106.0	89.86
NPs 2.5% gef, high →low concentration	0.021	0.026	0.021	0.205	25.55	33.06	40.29	57.92	54.27	59.50	109.1	91.01
NPs 5% gef, high →low concentration	0.021	0.037	0.063	0.355	18.81	30.13	41.82	41.51	45.92	52.90	102.9	111.9
DMSO + gef, high →low concentration	1.211	4.849	17.50	22.69	29.29	36.88	46.42	51.24	40.65	57.19	117.7	104.8
DMSO, high →low concentration	33.50	64.64	72.11	79.89	70.10	74.04	77.04	76.48	69.05	67.01	108.08	105.5

*The last column only contains cells with DMEM, no NPs, Gefitinib or DMSO has been added.

**The values of viability enlisted in the table are based on comparison with the average amount of living cells in the last column, where no additions of solutions have been made(except growth medium) to the cell population.

Table 15: *Viability results for cell plate incubated for 72 hours with NPs, NPs w/Gefitinib, DMSO w/ Gefitinib and DMSO.*

Sample												
Blank NPs, low →high concentration	0.025	0.053	0.190	1.816	18.25	51.92	75.64	88.92	105.1	107.0		100
Blank NPs, high →low concentration	0.025	0.025	0.380	1.472	23.44	50.35	76.97	105.6	107.9	118.7		100
NPs 1% gef, high →low concentration	0.036	0.033	0.064	0.332	18.12	31.85	50.03	73.48	89.78	95.56	96.01	100
NPs 2.5% gef, high →low concentration	0.020	0.041	0.020	0.263	16.88	31.20	44.32	57.05	65.62	70.98	86.91	100
NPs 2.5% gef, high →low concentration	0.008	0.016	0.032	0.093	10.85	23.83	37.85	53.35	58.99	59.77	83.65	100
NPs 5% gef, high →low concentration	0.012	0.036	0.45	0.125	13.45	21.78	29.68	45.98	54.13	53.08	66.56	100
DMSO+ gef, high →lowconcentration	0.170	1.937	6.727	11.86	17.54	23.69	32.04	39.02	54.00	58.77	81.39	100
DMSO, high →low concentration	20.33	55.41	70.04	68.29	69.12	79.11	61.42	78.39	80.87	92.86	102.1	100

*The last column only contains cells with DMEM, no NPs, Gefitinib or DMSO has been added.
**The values of viability enlisted in the table are based on comparison with the average amount of living cells in the last column, where no additions of solutions have been made (except growth medium) to the cell population.